NASA Contractor Report 159311

Airframe Noise Reduction Studies and Clean-Airframe Noise Investigation

M.R. Fink
D.A. Bailey

NASA

National Aeronautics and
Space Administration

Langley Research Center
Hampton, Virginia 23665

TABLE OF CONTENTS

SUMMARY

Acoustic wind-tunnel tests were conducted of a wing model with modified leading-edge slat and trailing-edge flap. The modifications were intended to reduce the surface pressure response to convected turbulence and thereby reduce the airframe noise without changing the lift at constant incidence. Both a porous bulk material and a perforated skin backed with a bulk absorber were used with the trailing-edge flap. Tests were conducted at 70.7 and 100 m/sec airspeeds, with Reynolds numbers of 1.5×10^6 and 2.1×10^6. Considerable reduction of noise radiation from the side edges of a single-slotted flap deflected 40° was achieved when either modification was applied to the side edge regions or the leading edge region of the flap panel. Total far-field noise was reduced 2 to 3 dB over several octaves of frequency. When these panels were installed as the aft panel of a double-slotted flap deflected 40°, a 2 dB noise reduction was achieved. Modifications to the trailing-edge region of the trailing-edge flap were ineffective for noise reduction.

Use of a perforated trailing-edge region on a leading-edge slat achieved about 2 dB noise reduction. A serrated trailing edge was ineffective for reducing slat noise. The reductions of noise source strength obtained with a modified leading-edge slat and trailing-edge flap tested individually were retained when these components were installed together.

Artificially tripping the boundary layer of a wing model without high-lift devices at a Reynolds number of 2.1×10^6 had essentially no effect on noise radiation from the trailing edge. At sufficiently high frequencies, use of sand grain roughness produced an additional noise located at the grains. Use of thin serrated tape as a boundary-layer trip either eliminated this noise or moved it to frequencies higher than those examined.

Turbulence within the viscous core of a wing-tip vortex was found to produce a concentrated noise source as it convects past the wing trailing edge. The strength of this noise source increases with increasing lift coefficient below stall. For wing aspect ratios and lift coefficients of practical interest for aircraft with high-lift devices retracted, this additional noise source is several dB weaker than conventional trailing-edge noise caused by convection of the wing boundary layer past the trailing edge along the entire span.

INTRODUCTION

Airframe noise imposes a lower limit on noise level at aircraft noise certification conditions. As noted in reference 1, airframe noise levels predicted by the method of reference 2, for a range of aircraft sizes during landing approach, are 5 to 10 dB below the current (1980) certification levels. Future reductions of propulsive-system noise might bring such noise down closer to the predicted level of airframe noise during approach. Therefore, it is useful to know whether airframe noise at approach could be significantly reduced. Acoustic wind-tunnel tests on model-airframe configurations (reference 3) have led to an improved understanding of noise-generation processes for various airframe components. Noise radiation from leading-edge slats and trailing-edge flaps at approach flight deflections was found to comprise the major portion of such noise. Techniques exist for reducing several types of surface-radiated noise by modifying the pressure response at the surface due to convected turbulence. If such techniques can be applied to the appropriate lifting surfaces of airframe components without adverse effects on aerodynamic performance, structural weight, and maintenance cost, then airframe noise could be reduced below the levels predicted in reference 1.

Also, some investigations into the fundamental behavior of airframe noise for aerodynamically clean airframes have raised questions about effects neglected in the noise prediction method of reference 2. These include the effects of boundary-layer-transition location and the method of producing a turbulent boundary layer (references 4 and 5), and the effects of spanwise variations in flow properties near a lifting wing tip. Such noise generally is too weak to be measured accurately with conventional microphones because its strength is similar to that of acoustic wind-tunnel background noise. Use of a directional microphone (reference 6) can provide a quantitative measure of local noise source strength distribution. This device would be used in measurements of airframe noise source strength reduction and could also be applied to these other basic noise source studies.

The objectives of the investigation reported herein were to (1) evaluate the possibility of reducing airframe-noise radiation from trailing-edge flaps and leading-edge slats at approach-flight deflections, (2) determine the effects of artificially fixed boundary-layer transition on noise radiation from a lifting two-dimensional airfoil, and (3) evaluate the noise source strength distribution near the tip of a lifting wing.

DESCRIPTION OF EXPERIMENT

Acoustic Wind Tunnel

The acoustic wind tunnel, designed specifically for aerodynamic noise research and described in reference 7, is of the open-circuit, open-jet type (Eiffel configuration). Use of an open circuit and a muffling section upstream of the tunnel fan reduces fan-generated noise to low levels for frequencies above which the chamber surrounding the test section is anechoic. The open jet is contained within a 5.5 m (18 ft) long, 6.7 m (22 ft) wide, and 4.9 m (16 ft) high sealed anechoic chamber. The test section area and shape can be varied by use of interchangeable tunnel nozzles. The maximum tunnel speed is in excess of 200 m/sec (660 ft/sec) for the 53x79 cm (21x31 in.) cross section used in this test program and in excess of 90 m/sec (300 ft/sec) for a 1.07 m (42 in.) diameter cross section. The rectangular test section was installed with its larger dimension (test section height) horizontal. Reflection-free conditions for broadband noise have been experimentally verified at frequencies above 200 Hz. Data are corrected for refraction at the shear layer by the method of references 8 and 9. The anechoic chamber and test section are shown in figure 1.

The inlet section has a contraction ratio of 16.5 for the test section used for this program. It is equipped with five turbulence suppression screens and a fine cell honeycomb section. The net effect of the contraction and turbulence suppression devices is to provide a spatially uniform, temporally steady, jet flow with a turbulence level on the order of 0.2%. The test section airflow is brought into the tunnel diffuser by a collector with anechoic treatment on its flow-impingement lip. An acoustic barrier was installed to prevent noise, radiated from the collector lip closest to the far-field microphones, from reaching those microphones. This high-frequency broadband noise is produced (reference 3) when a high-lift model configuration deflects the open jet toward that portion of the collector. The tunnel is driven by a 1500 hp variable speed motor coupled to a centrifugal fan.

Tunnel speed control and model jet pressure and temperature control have been demonstrated to be steady. This provides a statistically stationary test signal permitting sequential acquisition of data. Microphone data were amplified and then recorded on a fourteen channel FM tape recorder which at 76 cm/sec (30 ips) is capable of flat response operation to about 100,000 Hz. A real time spectrum analyzer and ensemble averager provided time-averaged narrow-band spectrum analyses, and real time third-octave bandwidth analyses, of direct and tape-recorded signals over a frequency range that exceeds the 200 to 40,000 Hz range. A correlation and probability analyzer is used to

obtain real time computation of acoustical signal auto and cross-correlation functions.

Instrumentation

Conventional Far-Field Microphones. - A top view of the acoustic wind tunnel test configuration and microphone installation is shown in figure 1. The directional microphone, with its sphere-segment reflector surface and focal point microphone on a forward support arm, was traversed along a track parallel to the nozzle centerline. Fixed conventional far-field omnidirectional microphones were mounted behind or to the side of this track at positions that did not interfere with motion of the directional microphone. Also, the fixed microphones were placed sufficiently far from the chamber acoustic wedges to be in the acoustic free field. Location of the wing pitching axis at an existing circular cutout in the horizontal side-plates (figure 1) placed a constraint on the omnidirectional microphone locations. Fixed microphone positions were chosen as 75° and 90° angular position at 3.25 m (10.66 ft) sideline distance, and 60° angular position at 3.05 m (10.0 ft) radius. All microphones were at least 10 wing chords and 5.7 wing spans away from the model. For frequencies down to 1 kHz they were at least 10 acoustic wavelengths away. Thus the microphones were in the geometric and acoustic far field.

Commercially available 0.635 cm ($\frac{1}{4}$ in.) condenser microphones were used at these three locations. These microphones were mounted at grazing incidence and were installed with protective grids. Several of these omnidirectional microphones are shown in figure 2 mounted on support posts in the anechoic chamber. Frequency response of the microphone and grid combination for this noise source direction is flat to 8 kHz 1/3 octave center frequency, increases to about 3 dB too high at 31.5 kHz, and decreases at higher frequencies. This installation was chosen because the increased response nearly compensates for atmospheric absorption along the acoustic path as calculated from reference 10. Since the sum of these two frequency-dependent corrections was less than 0.2 dB through 25 kHz center frequency, it was not necessary to apply an amplitude correction to those data.

Directional Microphone. - The directional microphone used in this test program, and the manner in which its focal point acoustic pressure are used in calculating noise radiation spectra, are described in reference 6. The reflecting surface, shown in figure 2, is a 1.067 m (42.0 in.) aperture spherical reflector with 1.346 m (53.0 in.) radius of curvature. A low-power laser mounted at the back of the reflector permits aiming the system and aligning the focal point microphone. The polished reflecting surface is used to align the laser with the reflector axis by optical autocollimation techniques. A

spherical reflector was used instead of a parabolic reflector in order to attain reasonable depth of field with reduced focal point aberration. Spatial discrimination (response of the directional microphone to off-axis noise sources) is controlled by diffraction. As shown in reference 6, measured response to very small off-axis noise sources at frequencies from 1 to 50 kHz closely matched the prediction by Fraunhofer diffraction theory for a circular aperture. This spectral resolution is shown in figure 3 for the frequencies used herein. Measured gain of the directional microphone system (ratio of mean square acoustic pressure at the focal point microphone to that of an omnidirectional microphone having the same acoustic path length) was shown to nearly follow the behavior calculated from diffraction theory. This gain measured in the absence of tunnel airspeed is reduced by scattering of sound by the open jet shear layer.

The directional microphone system with its focal point microphone was mounted on a track parallel to the tunnel centerline with the reflector axis perpendicular to the test section centerline. Vertical position of the re-flector centerline was at midspan of the test section. The directional microphone could be remotely driven axially along that track or remotely tilted about a horizontal axis. Thus it could be scanned in both the stream-wise and spanwise directions. Output of the focal point microphone and the axial and angular position sensors were recorded on magnetic tape as the directional microphone system was traversed at 0.85 m/min (2.8 ft/min). For frequencies down to 1 kHz, below which spatial resolution would be relatively poor, amplitudes obtained at this low traverse velocity are identical to those measured with the reflector stationary.

Airframe Models

Airframe Component Model. - The model used in most of these tests was an unswept constant-chord NACA 23012 airfoil of 30.5 cm (12.0 in.) chord and 53.3 cm (21.0 in.) span. It was mounted between horizontal solid sidewalls, with the spanwise direction vertical. The wing was attached to a support structure that permits varying the angle of attack. As discussed in reference 3, this airfoil section was chosen because its aerodynamic performance with high-lift devices is well-documented for the test Reynolds number of $2x10^6$ obtained with this model at 100 m/sec (328 ft/sec) velocity. The basic airfoil model, shown in figure 4(a), consisted of a wing with a retracted single-slotted flap panel.

The single-slotted trailing-edge flap shape used with this model (figure 4(b)) is contour 2-i of reference 11, developed for this airfoil section. It had a chord length 25.66% of the basic airfoil. The model had been built with three flap panels having 17.8 cm (7.0 in.) span. They could be installed as a

5

full-span flap, or with the side panels mounted at zero deflection and extension and a part-span flap extending over only the central 1/3 span. For the tests described herein, the side panels were always retracted. The central panel was installed either retracted or in the 40° deflection maximum-lift position.

A double-slotted trailing-edge flap could also be mounted at the central 1/3 span. This configuration, shown in figure 4(c), had a 10% chord forward-flap panel at 20° deflection. Its aft panel, mounted at 40° deflection, was the 25.66% chord single-slotted flap.

A 1/3 span, 15% chord high-lift device could be mounted ahead of the wing at two axial positions (figure 4(d)). In its forward position it formed a 25° deflection leading-edge slat. Retracted aft with its trailing edge against the wing forward upper surface and the gap sealed with modeling clay, it formed a leading edge flap. The slat was supported by two circular rods. During the test described in reference 3, it had been found that the separated flow past these struts not only produced tones at the vortex-shedding frequency but increased the broadband noise for a large range of higher frequencies. This noise, not representative of that for full-scale leading-edge slats, was reduced by use of clay fairings on the struts.

The model also included a two-wheel landing gear, described in reference 3. It consisted of a strut, a diagonal brace between the strut and cavity, a cavity door, a door brace, and a rectangular cavity. The cavity extended over more than 1/6 the wing span, so the wheel strut could be mounted at 30% chord and either midspan or 1/3 span. Filler blocks permitted testing with the cavity either open or closed, with the landing gear extended or removed. Use of a 5.0 cm (2.0 in.) wheel diameter provided a Reynolds number of 2.4×10^5 at 70.7 m/sec (232 ft/sec) velocity. This Reynolds number matches that for a test condition in reference 12 for which the scaled data agreed with flyover data for full-scale aircraft with landing gear extended. Proportions of the landing gear had been chosen as averages of the ratios for the Boeing 727 and Douglas DC-9 main landing gear.

Modified Trailing-Edge Flap. - Noise radiation from deflected trailing-edge flaps was shown in reference 3 to come from two regions of the flap, as sketched in figure 5. At small deflections, the dominant noise source for a single-slotted trailing-edge flap was observed with a directional microphone to be concentrated near the flap leading edge. Noise spectrum amplitudes observed with a full-span trailing-edge flap were consistent with those calculated for noise radiation from an isolated airfoil in uniform turbulent flow, with turbulence intensity and scale length equal to that measured in the flap slot. For large deflections of a part-span trailing-edge flap, a strong noise source developed along the flap side edge. Cross-correlation measurements

6

given in reference 13 clearly identified this noise as being caused by convection of the flap lower surface boundary layer around the side edge to the upper surface. Additional directional microphone measurements (reference 14) have confirmed the existence of these two noise-source locations for trailing-edge flaps. Acoustic treatment therefore was needed along the leading edge and side edges of trailing-edge flaps. Since other investigations have assumed that a noise source exists along the trailing edge of a flap, treatment of that region was also investigated.

The basic idea of the flap acoustic treatment was to provide a permeable rather than a uniformly solid surface in regions where turbulence is convected. Turbulent eddies could then induce airflow in and out of the surface. It was expected that allowing the development of this low-velocity, high-frequency fluctuating flow would reduce the static pressure fluctuations on those portions of the flap surface, thereby decreasing the noise radiation associated with the pressure fluctuations. These acoustically treated regions also would have to generate the required time-average high-lift aerodynamic flow field, which includes large static-pressure differences across the flap leading-edge and side-edge regions. As with the acoustically treated externally blown flap models described in reference 15, flow from the flap high-pressure lower surface through the model and out the low-pressure upper surface was prevented by use of an internal barrier. A barrier was not used in the flap trailing-edge region because of the small internal thickness. Also, the pressure difference across that portion of the model was small so that little internal crossflow would be expected. It was necessary to evaluate the assumption that acoustically treated flaps, with the same external contour as the solid flap, would produce the same lift coefficient. Those measurements are described under "Test Conditions and Procedures".

Chordwise extent of the acoustic treatment near the flap leading edge was limited by the presence of flap mounting bracket positions aft of 20% chord. One unpublished criterion (reference 16) had predicted that reduction of trailing-edge noise by porous surfaces would occur at frequencies such that the product of angular frequency and porous length, divided by velocity, is greater than 4. Use of an acoustically treated leading-edge or trailing-edge region of 20% flap chord would then be expected to produce noise reduction above 3.0 and 4.2 kHz frequencies for 70.7 and 100 m/sec velocities. This corresponds to a noise reduction above a Strouhal number of about 3 based on flap chord. Trailing-edge-flap noise is important for at least the decade of Strouhal number above that value (reference 2). Both the forward and aft 1.5 cm (0.60 in.) of the single-slotted flap therefore were modified.

Locations of acoustic treatment on the single-slotted trailing-edge flap are shown in figure 6. The forward 20% chord of two solid flap panels was machined away except for a flow divider that extended to the leading edge. This solid divider was 0.16 cm (1/16 in.) thick. In addition to preventing airflow from passing through the flap, it provided structural support to sustain the large local airloads. The flap-surface contour was then restored by use of each of two acoustic treatments. The aft 20% of the flap also was replaced with acoustic treatment, without a flow divider. The flap sides were machined away, except for a flow divider, for an arbitrarily chosen spanwise distance of 3.0 cm (1.2 in.) corresponding to a distance of 40% chord. As shown in figure 6(b), the acoustically treated portion of each flap panel's upper and lower surfaces comprised roughly 60% of the flap planform area.

Several types of porous metals and porous ceramics were considered as acoustic treatment. A reticulated vitreous carbon material, nickel plated after machining, was chosen as a good compromise on the basis of strength, machinability, crack resistance, and surface smoothness. This material generally is used as a fluid filter and as high-temperature insulation, in addition to its use as an acoustic absorber. Such material is available over a range of densities. A density of 31.5 pores per cm (80 pores per in.) was selected to provide a specific acoustic impedance of 40 rayls based on the average material thickness. Previous tests (reference 15) of acoustically treated externally blown flaps had achieved somewhat more noise reduction for this specific impedance than for twice or half this level. This flap panel is cited later in this report as the porous flap.

The other acoustically treated flap is denoted later as the perforated flap. Its outer surface in the acoustically treated region consisted of 26 gage (0.048 cm, 0.019 in.) thickness perforated carbon steel with 18% open area. This very small thickness was needed to allow the perforated metal to be bent around the relatively small leading edge radius. The material had a staggered pattern of 0.61 mm (0.024 in.) diameter circular holes. The perforated material was tack-welded to the solid, central portion of the flap. As with models of similar construction and open area described in references 15 and 17, the spaces between the perforated skin and the internal flow divider were filled with steel wool packed to half its normal volume. This material damps out the velocity of air blown into the interior regions by turbulence and also serves as a bulk acoustic absorber. Side edges of the flaps were ribs made from the same porous material and tack-welded to the side edge of the flow divider. Use of a perforated leading edge of this type had been shown in reference 17 to provide up to 5 dB noise reduction on a simulated turbofan engine strut in turbulent flow.

A photograph of the reference solid flap and the two modified flaps is shown in figure 7. The solid flap is at the right side of the figure. The porous flap, in the center, has been covered with tape so that only its porous leading edge region is exposed to the airstream. Its internal flow divider is visible along the side edge. The perforated flap, at the left of this picture, has been taped so that only its side edge regions (extending along the entire chord) are exposed to the airflow.

The aft 20% chord of the trailing-edge flap was so thin that it was not practical to install a flow divider to prevent steady airflow into the lower surface, through the acoustic treatment, and out the upper surface. Existence of such flow would produce the effect of a negative camber on the flap, reducing the lift force. No theory is available for predicting the effect of such thru-flow on the airloads on a deflected trailing-edge flap. However, the theory given in reference 18 for isolated airfoils with porous trailing edges can be applied as a first approximation. For an airfoil having its aft 20% chord porous, and with the average properties of the porous and perforated materials used on these models, lift reductions of 7 to 9% are predicted.

It is recognized that the use of a constant-density porous material and of a constant percent open-area perforated skin is not optimum for noise reduction. Impedance of the acoustic treatment probably should increase as the solid surface is approached, so that a gradual rather than an abrupt change in flow resistance is achieved. Such optimization would best be done in tests at larger scale, rather than in this small-scale preliminary test.

The two acoustically treated flap panels were tested only as a 40° deflection single-slotted flap and as the aft panel of the 40° deflection double-slotted flap. Both of these flaps extended only over the central 1/3 span and were flanked by retracted solid flap panels.

Modified Leading-Edge Slat. - Noise radiation from a leading-edge slat was shown in reference 3 to be caused by convection of the slat boundary layer over the trailing-edge of the slat. The high local flow velocity at this position, and high turbulence levels in the slat passage caused by local flow separation on the slat lower surface, produce a strong trailing-edge noise source distributed relatively uniformly along the slat span. Reduction of such noise can use the techniques developed for reduction of trailing-edge noise radiation from upper-surface-blowing externally blown flap configurations.

One technique for reducing such noise has been the use of a porous or perforated trailing-edge region. The effects of material properties and treated length on noise radiation caused by an exhaust jet blowing along a

solid flat plate with a porous trailing edge were reported in reference 19. That data analysis validated the use of a Strouhal number given by the product of frequency and porous length divided by flow velocity. Plots of coalesced data contained a relatively sharp peak of noise reduction at a Strouhal number of about one. This result generally agrees with the prediction from reference 16 that noise reduction should occur above a Strouhal number of $2/\pi$ or about 0.64. The chordwise extent of modifications to the airframe-noise leading-edge-slat model was limited by the presence of slat support brackets at about 1.3 cm (0.5 in.) from its trailing edge. A treated length of 1.0 cm (0.4 in.), which is about 22% of the slat chord, was arbitrarily selected to maintain sufficient structural rigidity at the support attachment. Thus the data correlation of reference 19 and method of reference 16 correspond to peak noise reduction at Strouhal numbers of 1 and 5, and greater than 3, based on slat chord.

This aft portion of the solid slat contour has 0.21 cm (0.082 in.) maximum thickness, tapering to 0.025 cm (0.010 in.) at the trailing edge. Attempts to make this tapered portion from reticulated vitreous carbon porous material were unsuccessful because of the material's low strength in thin sections. Therefore, (figure 8) the trailing edge region of one slat was arbitrarily made from the 26 gage (0.048 cm, 0.019 in.) thickness, 18% open-area perforated carbon steel used for the perforated trailing-edge flap. The step change in thickness from the solid slat to its perforated aft region was faired with clay.

The other method investigated for reducing slat trailing-edge noise was a serrated trailing edge. As described in reference 20, this utilizes the prediction that trailing-edge noise should vary with cosine cubed of sweepback angle. Data were presented in reference 20 for sawtooth serrations with alternate $\pm 60^\circ$ sweepback. Turbulent eddies which interact only with the sweptback edges would be predicted to have their noise radiation decreased by 9 dB. Little or no effect would be expected on noise from eddies which interact with the serration corners. This prediction is consistent with the 6 dB reduction shown in reference 20 over a wide range of frequencies, and decreased noise reduction for the smallest serrations tested. For the leading-edge slat, use of too deep a serration would increase the edge thickness, which might produce too much bluff-body noise radiation from the blunt edges. Also, deep serrations would weaken the slat near its support brackets. The resulting leading-edge slat with a serrated trailing edge is shown in figure 8. Each serration edge has a spanwise extent of 0.50 cm (0.195 in.) which is approximately three times the calculated flat-plate boundary layer thickness at the slat trailing edge. The 18 tabs have $\pm 60^\circ$ edge sweepback and 0.86 cm (0.34 in.) indentation depth. Use of this number of tabs placed each slat support bracket in line with the center of a tab. A photograph of the basic slat and the two modified slats is presented as figure 9.

10

Part-Span Wing. - The part-span wing had been utilized in the experimental investigation reported in reference 21 and is described therein. It is a constant chord unswept wing with NACA 0012 airfoil section, 22.9 cm (9.0 in.) chord, and 26.7 cm (10.5 in.) span plus a 1.37 cm (0.54 in.) span wing tip. The half body-of-revolution wing-tip shape was generated by rotating the airfoil section about its chord line. This wing, shown in figure 10, has openings for mounting 0.635 cm ($\frac{1}{4}$ in.) diameter microphones flush with the surface at four chordwise positions. It also contains a slider at 30% chordwise position so that one flush-mounted microphone and its preamplifier can be moved to various spanwise positions. The presence of this slider produces a small discontinuity in airfoil contour. Flush-mounted microphones were not installed for the tests described herein.

The noise radiated by this wing model is documented in reference 21. For Reynolds numbers greater than 0.7×10^6 and less than 2^O angle of attack, noise produced by this model could not be detected above tunnel background noise by use of a far-field omni-directional microphone. For a Reynolds number of 2.5×10^6, corresponding to 194 m/sec (500 ft/sec) velocity, noise from the airfoil at any unstalled angle of attack also could not be detected with an omni-directional microphone. At intermediate Reynolds number, and with the slider on the wing upper surface, increasing the geometric angle of attack eventually produced discrete tone noise. For a velocity of 100 m/sec corresponding to a Reynolds number of about 1.6×10^6, this tone developed above 7° geometric angle of attack. (Corrected angle of attack for this wing chord and test-section height is about 93% of the geometric angle.) It disappeared between 17° and 18° geometric angle of attack, where the wing stalled. Occurrence of this tone was traced (reference 22) to an aeroacoustic feedback between instability waves convected downstream in the wing lower-surface laminar boundary layer and trailing-edge noise propagating forward. Increasing angle of attack produces an increasing length of favorable pressure gradient along the wing chord, causing the laminar boundary layer to persist further along the chord until it reaches the trailing edge.

Because the wing model had an uncambered airfoil section, it could also be tested with the slider on the lower surface. The resulting surface discontinuity was expected to trip the boundary layer at this test Reynolds number for all angles of attack, thereby preventing occurrence of the tone noise. During these tests, a weak tone was observed at 15° angle of attack. A boundary layer trip consisting of serrated plastic tape, described in the section entitled "Test Conditions and Procedures: Boundary-Layer-Transition Devices" was applied to the lower surface at 75% chord. This device eliminated the tone.

Test Conditions and Procedures

Test Conditions. Airframe noise generally is important only on approach to landing, when high-lift airframe components are deployed and engine thrust levels are reduced. Approach flight paths generally are flown at 1.3 times stalling speed to provide a safety margin for gusts and go-around maneuvers. This speed corresponds to flight at a lift coefficient approximately 0.6 times maximum lift coefficient. Realistic aerodynamic conditions for the noise component tests of reference 3, and for the noise reduction tests described herein, therefore were obtained by testing at 0.6 times the estimated maximum lift coefficient of each configuration at a Reynolds number of 2×10^6. These coefficients and the associated angles of attack, as affected by the open jet reduction to effective angle of attack, are listed in a following section entitled "Wind-Tunnel Corrections".

Noise reduction tests were conducted at 70.7 and 100 m/sec (232 and 328 ft/sec) wind-tunnel velocities. These speeds bracket the range of approach speeds for most commercial and business jet aircraft. Velocity scaling laws for noise amplitude and spectrum can be checked by comparison of these two sets of data. The airspeeds correspond to Mach numbers of 0.21 and 0.30, and Reynolds numbers of 1.47×10^6 and 2.08×10^6 based on wing chord. The clean-airframe noise experiments were conducted at 100 m/sec (328 ft/sec) airspeed.

Far-field 1/3-octave-band spectra were recorded on magnetic tape while the directional microphone was located at the downstream end of its track. In that position, it did not shield the fixed microphones. Output of the directional microphone was then recorded as that device was traversed streamwise and spanwise as required. The 1/3-octave spectrum from the microphone at 90° direction angle, and the directional microphone signal in the 1/3-octave band having 10 kHz center frequency, were monitored and plotted on-line.

Directional microphone traverses were taken along streamwise lines at midspan for all configurations, along the side edges of part-span high-lift devices, and along spanwise lines at the streamwise position of maximum signal strength.

All microphones were calibrated daily with a pistonphone. Air temperature and relative humidity in the anechoic chamber were recorded manually during each run, for use in calculating attenuation of acoustic signals. Air pressure in the atmospheric-inlet wind tunnel settling chamber was measured for use in determining the difference between settling-chamber stagnation pressure and tunnel inlet nozzle static pressure at the test

velocities. This pressure difference was measured by a pressure gage having a dial marked linearly in inches of water, to an estimated error less than 0.3 cm (0.1 in.) H_2O.

Tape-recorded data were played back during and after the test program, through a 1/3-octave band analyzer, to obtain 1/3-octave band spectra for the conventional microphones. Directional microphone output was passed through 1/3-octave band filters having 5 and 20 kHz center frequencies. (Data for 10 kHz had been plotted on-line.) The filtered signals were connected to an x-y plotter, along with the traverse position signal, to obtain plots of signal amplitude versus axial or spanwise distance. All acoustic pressures were normalized relative to 2×10^{-5} n/m^2 (2×10^{-4} microbar) reference pressure.

Verification of Lift Coefficient. - To evaluate the acoustic effects of noise-reduction modifications, the basic and modified configurations should be tested at the same lift coefficient. The acoustic wind tunnel was not equipped with a force balance for measuring the downwash flow angularity at midspan, one chord length behind the wing trailing edge, at four positions. These positions were 5 and 10 cm (2 and 4 in.) above and below the measured center of the wake for each unmodified configuration at its approach angle of attack. Measurements were obtained at 100 m/sec (328 ft/sec) velocity, using a remotely traversed five-hole probe. Flow angularity at these positions was measured, with the probe nulled, as less than 0.2° in downwash and yaw for the cambered wing without high-lift devices, set at its predicted zero-lift incidence.

The two modified leading-edge slats gave average flow angularities approximately 0.3° larger than that of the basic slat at the same angle of attack. This difference probably is within the measurement accuracy; the wing with basic and modified slats was assumed to be producing the same flow angularity and therefore the same nominal lift. The average value for the sine of the measured flow angle was 0.185 for the nominal lift coefficient of 1.26.

The wing with 40° deflection part-span unmodified single-slotted trailing-edge flap, at its nominal approach angle of attack, had its average sine of the flow angle equal to 0.23. This was about 25% larger than the corresponding quantity for the leading-edge slat. Expected lift coefficient for the wing with trailing-edge flap was about 25% larger than that for the wing with leading-edge slat. Measurements of flow angularity for these two basic high-lift configurations, therefore, were self-consistent.

Replacing the solid trailing-edge flap by the perforated flap, with any or all perforated regions exposed to airflow, caused negligible changes in flow angularity. Use of the porous flap with all regions exposed to the flow, or with any regions except the trailing edge covered with tape, caused 0.6 to 0.7° decrease of flow angularity. The average value of the sine of the flow angle was decreased to 0.22. Covering the porous trailing edge region with tape, independent of what other porous regions were taped, raised the flow angles to those for the hard-wall flap. These results are reasonable because porous surfaces of the flap were attached to a central impervious panel for all porous regions except the trailing-edge region. From the analysis presented in reference 18, an isolated airfoil with its aft 20% chord porous (as with this flap) would be expected to produce about 10% less lift than a solid airfoil. Increasing the wing geometric angle of attack from 5.0 to 6.0 deg, at constant deflection of the flap with untaped porous trailing edge, increased the flow angularity to greater than for the solid flap at 5.0° wing angle of attack. A 5.8° angle was chosen, by interpolation, as the wing incidence that would cause that porous flap configuration to attain the approach lift coefficient.

Boundary-Layer-Transition Devices. - Effects of artificially induced boundary-layer transition on clean-airframe noise were examined by application of two types of transition devices. One was the most commonly used device for initiating transition: distributed roughness particles sprayed onto a thin shellac layer. Commercially available sand grains were applied between 10 and 15% chord on the airfoil upper and lower surfaces. Particle size was chosen by the method of reference 22 for determining the critical roughness height to produce transition of a laminar boundary layer. Use of this critical height assures that the particles are large enough to assure transition without producing an excessively thick layer of high-turbulence boundary-layer flow. These calculations used the predicted local flow properties at the edge of the laminar boundary layers at 10% chord and lift coefficients of 0, 0.3, and 0.9. Critical roughness height was predicted to vary from about 0.35 mm (0.014 in.) to 0.51 mm (0.020 in.). Therefore a sparse distribution of 30-40 mesh sand grains, with 0.32 to 0.56 mm (0.012 to 0.002 in.) nominal diameter, was used.

The second transition device was a thin plastic tape having ±45° serrations on one edge. Tape thickness was about 0.13 mm (0.005 in.) which is about ¼ that of the distributed roughness particles. This tape was placed on the airfoil with its serrations upstream at 10% chord. Laminar boundary layers flowing over the serrations are expected to form three-dimensional vortices which are amplified and then break down into turbulence. This transition device has come into use because of its ease of repeatable installation.

14

Wind-Tunnel Corrections

Shear Layer Refraction Effects. - Sound waves generated at the model are convected downstream within the acoustic wind-tunnel airstream and are refracted as they pass through the open-jet shear layer. At moderate subsonic flow speeds, the sound waves reach far-field microphones within the anechoic chamber along paths that differ significantly from the line of sight. The associated changes in acoustic path length of the convected and transmitted sound waves, and divergence of acoustic ray tubes, produce changes to measured far-field sound pressure levels at constant far-field geometric distance. Measurement-direction angles must also be corrected appropriately. These corrections were calculated by the method of references 8 and 9, and their implications are sketched in figure 11.

Application of these corrections is discussed in reference 3. One set of corrections, indicated in figure 11(a), converts the data for each microphone outside the shear layer to a measurement system in which the microphone is fixed relative to the airframe model and a uniform flow extends from the model to the microphone. Thus it corresponds (figure 11(b)) to a flyover measurement in which both the airframe and the microphone are moving through still air on parallel paths at constant velocity. For ease in comparing acoustic wind-tunnel data with conventional predictions and flyover data, it is more convenient to use a retarded-time coordinate system. This coordinate system, shown in figure 11(c), moves the noise source downstream relative to its physical position. A sound wave would travel through still air from this retarded-time source position to the previously corrected microphone position during the time required for the model to move, at its flight speed, from the retarded-time position to its physical position. As is indicated by comparing figures 11(a) and 11(c), the corrected direction angles and path lengths differ only slightly from their initial uncorrected geometric values. For the three measurement angles and two airspeeds used in these tests, the largest corrections were 2.5° in angle and 1.8 dB in amplitude. The detailed corrections used herein are tabulated in reference 3.

Open-Jet Effect on Angle of Attack. - Lifting airfoils within an open jet induce curvature of the shear layer and deflection of the jet. The change in wing pressure distribution due to flow curvature far from the wing is equivalent to that for negative camber added to the wing in an undistorted flow. A wing model in an open-jet wind tunnel must therefore be placed at increased angle of attack, relative to its angle for zero lift, to attain its intended lift coefficient. The manner in which these angles were calculated is described in reference 3.

Expected maximum lift coefficients, approach lift coefficients, intended (corrected) approach angles of attack, and geometric (uncorrected) angles of attack are tabulated below for the noise-reduction model configuration.

Configuration	Maximum C_L	Approach C_L	Angle of Attack, deg Corrected	Geometric
Clean wing	1.52	0.91	7.5	9.6
Leading edge slat	2.10	1.26	11.5	15.2
Single slotted flap	2.67	1.60	2.0	5.0
Double slotted flap	2.95	1.77	-8.0	-3.5
LE+TE devices	3.02	1.81	1.5	6.5

The part-span wing, with its smaller chord and lower lift coefficient slope, requires considerably less correction to angle of attack. Its corrected angles of attack are estimated to be less than 4% lower than the geometric angles.

AIRFRAME NOISE REDUCTION EXPERIMENTS

Modifications to Trailing-Edge Flap

Porous Surface. - Spectra measured at the 90° microphone position for the 40° deflection part-span single-slotted flap with porous regions are plotted in figures 12 and 13. Also shown in these figures are the spectra measured for the solid flap, previously given in reference 3. Porous regions of the flap upper and lower surfaces were covered with thin plastic tape, so that selected regions could be exposed to the external flow. Spectra measured with only the porous leading-edge region (forward 20% flap chord) and with only the porous trailing-edge region (aft 20% flap chord) exposed are presented in figure 12. Data are shown for the two test airspeeds of 70.7 and 100 m/sec velocity. The flap with porous trailing edge generally produced the same spectra as the solid flap. However, the flap with porous leading edge generally achieved about 3 dB noise reduction at the lower velocity, and 2 to 3 dB reduction at the higher velocity, from 5 to 31.5 kHz center frequency. Noise reduction began at the 1/3-octave bands having 4 and 5 kHz center frequencies for the two airspeeds. These are one 1/3-octave band higher than frequencies at which this chordwise extent of acoustically treated surface was predicted by the method of reference 16 to become effective for noise reduction.

These tests were conducted at velocities that bracket the approach speeds of commercial jet transports, with a wing chord of 1/10 to 1/20 those for the full scale airplanes. Thus one would expect these benefits to extend from 250 or 500 Hz to 1.6 or 3.15 kHz full-scale center frequencies. Airframe noise from deflected trailing-edge flaps during landing approach has its strongest contributions to annoyance-weighted noise within this frequency range.

Spectra for this model with only its porous side edges exposed, and its porous leading edge and side edges exposed, are compared in figure 13 with those for the solid model. The porous sides produced 1 to 2 dB reduction over the same large frequency range for which 3 dB noise reductions were obtained with the porous leading edge. Combining those two best configurations gave 3 to 4 dB noise reduction. That is, even though the configuration with porous leading edge and sides had nearly 2.4 times the exposed porous area as that with only the porous leading edge, it was only about 1 dB quieter. Much of the total noise reduction evidently comes from the corner regions of the porous leading edge, which are exposed for both the porous leading-edge and porous side-edge configurations.

Directional microphone measurements of noise source strength for these configurations at the 1/3-octave band having 10 kHz center frequency are plotted in figures 14 and 15 for the two test velocities. These plots give the noise source strength obtained during axial traverses at midspan and at the side edge of the flap. These distributions show that the porous trailing edge provided no effect at midspan and a small noise reduction at the side edge. The flap with porous sides greatly reduced the noise radiation from the side edges of the flap. It also decreased the noise radiation from midspan, possibly by reducing the turbulence level within the flap slot. This measured level at midspan of the part-span flap corresponds to the level given in reference 3 for the corresponding position on a full-span flap.

The porous leading edge of the part-span flap produced about 3 dB decrease of noise strength at midspan and about 6 dB decrease at the side edge. This level measured at the side edge is about 3 dB below that for midspan, as would be expected if the flap noise radiation was decreased to that for a line source with constant strength per unit span. (The reflecting dish of the directional microphone would gather sound from a line extending across its field of view when the dish is focused at midspan. However, when the dish is focused at a side edge, the line source would extend only to the center of the field of view.) These decreases of apparent source strength correspond to about 6 dB decrease in far-field noise radiation, rather than the 3 dB change that was found in the 1/3-octave band spectra. Perhaps the far-field noise levels contain significant noise radiation from the flap support brackets at this large deflection angle, as was found in tests of full span slotted flaps reported in reference 13.

As shown in the lower portion of figures 14 and 15, the trailing-edge flap with porous leading edge and sides produced only about one dB less noise than did the flap with only the porous leading edge. Because this small decrease of noise was obtained with such a large increase of porous surface, use of porous sides and leading edge would be less practical in full-scale application than use of just a porous leading edge. Also, the reticulated carbon material used for these porous regions had proven to be fragile. The thin sharp corners at the junctions of the trailing edge and side edges, and the corners at the junctions of the side edges and the flap upper and lower surfaces, had become rounded by abrasion. This flap with its thick well-supported porous leading-edge region exposed to the flow, and the other porous regions taped to restore their external shape, was chosen for tests with other airframe components.

Perforated Surface. – Spectra measured at the 90° microphone for the 40° deflection part-span single-slotted flap with perforated surfaces are presented in figures 16 and 17. The perforated trailing edge (figure 16) generally caused less than 1 dB change from the spectrum measured with the solid flap. Modifying the aft portion of a trailing edge flap, whether by use of porous or perforated surfaces, therefore, does not provide significant reduction of flap noise radiation. The perforated leading edge (figure 16) produced one to 2 dB noise reduction over a small frequency range of about four 1/3 octave bands. Noise radiation was increased several dB above that for the solid flap at higher frequencies. Use of perforated sides (figure 17) produced about 2 dB noise reduction over that same frequency range. The perforated leading edge and sides produced essentially the same reduction as that for perforated sides only.

Directional microphone measurements of source strength for the wing with these trailing edge flap configurations are plotted in figures 18 and 19 for 10 kHz center frequency and the two test velocities. All of the flap-surface perforated regions produced noise reductions for this center frequency. The perforated trailing edge caused about 3 dB noise reduction at the side edge but had little effect at midspan. The perforated leading edge was more effective in reducing noise radiation from the sides and also produced several dB noise reduction at midspan. Use of perforated sides produced a little more noise reduction at the flap side edges than did the perforated leading edge but had little effect on noise radiation at midspan. Exposing both the perforated leading edge and perforated sides to the flow produced the same noise reduction at the flap side edges as occurred with only the perforated sides, and the same reduction at midspan as obtained with only the perforated leading edge. These reductions were larger than those measured with the far-field omni-directional microphone (figures 16 and 17).

Directional microphone measurements of noise source strength were examined for these flap configurations at higher frequencies, for which no noise reduction was observed with the omni-directional microphone. The peak value of relative signal strength at midspan, for the flap with perforated leading edge, was found to increase above that for the solid flap. Reductions of peak noise radiation along the flap side edge were less than those observed at lower frequencies. Although the perforated sides and perforated leading edge apparently continue to suppress the noise radiation from the flap side edge at high frequencies, they also appear to act as a noise source. This effect is largest for the perforated leading edge, where the highest local velocities occur. The additional high-frequency noise apparently is produced by airflow over the perforations. Importance of such noise at full scale could be reduced by increasing the perforation hole size by less than the model scale factor. Surface-generated noise would then be kept at high frequencies that are significantly attenuated by the atmosphere. These

model-scale data therefore give too conservative an indication of the frequency range for which perforated surfaces provide noise reduction for trailing-edge flaps.

Double-Slotted Flap. - The flap panel having its porous leading edge exposed to the flow, and the flap panel with perforated side edges, were tested as the aft panel of a 40° deflection, part-span, double-slotted flap. Measured 1/3-octave spectra at the 90° microphone are presented in figure 20 for these and the solid flap. Absolute-level spectra for the two airspeeds are given in the upper part of the figure. Both modifications produced approximately 3 dB noise reduction over a two-octave range of frequencies. The reduction extended over a wider frequency range for the perforated than for the porous modification.

Spectra for the solid and perforated-side configurations are plotted in a velocity-adjusted normalized manner in figure 20(b). Amplitudes are normalized by use of an assumed dependence on velocity raised to the sixth power. Frequency is normalized as Strouhal number, fc_F/U, where the total flap chord, c_F, is 35% of the basic wing chord. Data for the solid flap are closely coalesced on this plot. Agreement is not quite as good for the perforated flap, which achieved somewhat more noise reduction at 100 than at 70.7 m/sec velocity. In general, noise radiation from this double-slotted flap was decreased 3 dB for Strouhal numbers between 5 and 20.

Noise source strength distributions on the double-slotted flap, as measured with the directional microphone, are presented in figure 21. Separate figures are given for traverses at midspan and along the flap side edge, analyzed at 1/3-octave band center frequencies of 5, 10, and 20 kHz, at 100 m/sec velocity. At midspan, maximum noise radiation was located at the solid forward-flap panel. Perforated sides on the aft flap panel caused a narrowing of the noise source strength distribution at midspan. Suppression of flow disturbances at the side edges of the aft flap panel may have reduced the turbulence levels or amount of flow separation on the aft panel at midspan. In contrast, the porous leading edge seems to have increased the noise radiation from the trailing edge of the aft flap panel at midspan. Both modifications produced 5 to 6 dB reductions of noise radiation from the flap side edges.

Thus the strong noise source at the side edges of a double-slotted trailing-edge flap is associated with the highly deflected aft panel rather than the small-deflection forward vane. Further inboard, the noise radiation apparently is dominated by incident-turbulence noise from the forward flap vane. This vane is subjected to the high turbulence levels produced when the wing lower-surface turbulent boundary layer is convected into the open flap slot. Larger noise reductions might be achieved by use of a double-slotted

trailing-edge flap having a porous leading edge on its forward vane and perforated side edges on its aft panel.

The directivity of noise radiated by these modified trailing-edge flaps was checked by comparing with data of reference 3 for the solid flaps. Those spectra were not valid for high Strouhal numbers because of noise radiation from the test-section jet collector in tests at high lift coefficients. Directivities had been examined therein for 1/3-octave band center frequencies of 5 and 6.3 kHz at 70.7 and 100 m/sec velocities, respectively. These frequencies and velocities correspond to Strouhal numbers of approximately 5 and 8 for the single- and the double-slotted flaps, respectively.

These data for the solid flaps are compared in figure 22 with data for the two chosen modified flap panels. Measured sound pressure levels for the two modifications were within 0.4 dB for all but one of the measurement conditions; an average of the measured levels has been plotted. Within the probable experimental error, the measured directivity for the single- and double-slotted flaps having noise-reduction modifications agree with that for the solid flaps. They are given by the shape predicted for a lift dipole oriented normal to the free stream direction, adjusted for convective amplification.

Configurations Tested With Modified Trailing-Edge Flap

Leading-Edge Flap. - The configuration having a part-span leading-edge flap ahead of a part-span trailing-edge flap was identified in reference 3 as producing favorable noise interaction. The leading-edge flap alone was a weak noise source relative to the trailing-edge flap. Directional-microphone traverse data show that noise radiation from the side edges of the 40° deflection trailing-edge flap were reduced by the presence of the leading-edge flap. Resulting far-field noise levels for the combination were 3 to 4 dB less than those for the acoustic sum of spectra for the wing with each component deflected separately. In general, the side-edge noise source was not completely eliminated by this favorable interaction. A possiblity of further noise reduction thus existed.

Far-field 1/3-octave spectra measured at 90° direction for the wing with the conventional leading edge flap and the conventional and modified trailing-edge flaps are plotted in the upper part of figure 23. The conventional configuration was re-run as part of this test program. Its spectra contain a broadband hump, centered at 25 kHz frequency, that was barely noticeable in the tests reported in reference 3. The spectra for this configuration, as given in that report, would generally match those shown here for the model having a trailing-edge flap with perforated side edges. The other modified

configuration, which had a porous leading edge on its trailing-edge flap, was 1 to 2 dB quieter above 10 kHz center frequency.

Spectra for these configurations with the conventional flap and the porous flap are given in a normalized manner in the lower part of figure 23. Amplitudes were adjusted by assuming a dependence on velocity to the sixth power, and frequency was normalized as Strouhal number based on flap chord. Data for the two velocities were closely matched for the porous flap (closed symbols). For the conventional flap, agreement was good except at high Strouhal numbers. Use of the porous flap provides some noise reduction above a Strouhal number of 10.

Chordwise traverses at midspan and along the side edge for these configurations are plotted in figures 24 and 25 for three frequencies at each of the two velocities. For 5 kHz center frequency, there was essentially no difference between noise source strengths of the three configurations at the lower velocity. The model with the perforated flap was about one dB quieter than the others, both at midspan and at the side edge, for this frequency and the higher velocity. This result agreed with the difference in spectrum levels as measured with a conventional microphone (figure 23). The porous flap was 1 to 2 dB quieter than the conventional flap at both midspan and the side edge for 10 kHz center frequency and both velocities. At 20 kHz center frequency, the porous flap was indicated by the directional microphone to provide about 3 to 5 dB noise decrease at both midspan and the side edge. These results agree with the 3 to 4 dB difference measured with the conventional microphone. The trailing-edge flap with a porous leading edge therefore produces noise reduction for this configuration by decreasing the noise caused by turbulence convected into the flap slot and past the flap leading edge, over its entire span. Such noise is important for this leading-edge flap, trailing-edge flap combination because the flow field generated by the leading-edge flap suppresses noise radiation from the sides of the trailing-edge flap. For configurations which have a leading-edge flap and a double-slotted trailing-edge flap, the leading-edge region of the fore flap and the forward portion of the main flap's side edges should be made porous for noise reduction.

Leading-Edge Slat. – The configuration having a leading-edge slat and trailing-edge flap was shown in reference 3 to have its far-field spectra dominated by noise radiation from the slat. This slat model was found to produce noise that was about 5 dB higher in amplitude but reasonable in spectrum shape relative to spectrum levels scaled from aircraft flyover data. Noise from the trailing-edge flap was significant relative to that from the slat only at center frequencies of 25 kHz and greater. Therefore, one would not expect much noise reduction to be attained by this configuration with a modified trailing-edge flap. The far-field 1/3-octave data, plotted in

figure 26, indicate about 1 dB noise decrease for those cases. Directional microphone data for the two velocities are given in figures 27 and 28. Use of the modified trailing-edge flaps clearly reduced the flap noise at midspan and at the side edge. However, they did not affect the slat noise at midspan and along most of the slat span.

Landing Gear. - Acoustic data were obtained for the wing with landing gear at midspan, open gear cavity extending laterally from midspan to the position of a flap side edge, and part-span single-slotted trailing-edge flap. Far-field 1/3-octave band spectra measured at 90° direction for these configurations are plotted in figure 29. Replacing the conventional solid flap with a flap having porous or perforated regions caused about 1 dB total difference for frequencies through 12.5 and 16 kHz at 70.7 and 100 m/sec velocities, respectively. At higher frequencies, the perforated flap was about 1 dB louder and the porous flap about 1 dB quieter than the conventional flap.

This lack of significant noise reduction is disappointing. As noted in reference 3, the model landing gear and conventional flap as tested individually with the wing had approximately equal noise radiation above 5 kHz center frequency for 100 m/sec velocity. Directional microphone traverses showed several dB reductions of landing gear and cavity noise at 5 kHz, and slight reductions at 10 kHz, due to the presence of the deflected flap. This result is reasonable because the deflected flap reduces the local flow velocity at the landing gear and cavity locations. Noise radiation from the trailing edge flap downstream of the landing gear strut was increased over that for the flap alone, probably due to the strut and wheel turbulent wake. It had been hoped that the modified flaps would reduce the added flap noise, producing a configuration for which both the landing-gear noise and trailing-edge-flap noise were decreased.

Directional-microphone data for these configurations are given in figures 30 and 31 for 70.7 and 100 m/sec velocities. At both velocities and 5 kHz center frequency, the modified flaps increased the noise from the landing gear (midspan, 30% chord) by several dB while decreasing the flap side-edge noise by about the same amount. Generally, similar small changes occurred at 10 kHz frequency. For 20 kHz center frequency, the porous flap had no adverse effect on landing-gear noise and achieved 3 to 5 dB reduction of flap noise both at midspan and at the side edge. This model, with its small flap span relative to landing-gear size, had about equal noise radiation from the two airframe components. If noise from one component (the trailing edge flap) were reduced by 4 dB, only a 1.5 dB decrease of total noise would occur. Thus the measured 1 dB reduction is consistent with the favorable effect found in the directional-microphone data. It is expected that a larger noise reduction would occur for typical aircraft configurations which have large

trailing-edge-flap span relative to the landing-gear size. The portion of the trailing-edge flap's leading-edge region downstream of the landing gear would have to be made porous to reduce its acoustic response to convected turbulence.

Modifications to Leading-Edge Slat

Preliminary tests of the wing and unmodified leading-edge slat yielded higher noise levels, at high frequencies, than those previously obtained with the same model and reported in reference 3. These levels were strongly affected by the manner in which the slat support rods were streamlined. If these rods were kept as cylindrical shapes, data for the two test programs generally agreed within 1 dB. Placing clay on the aft portion of each rod to produce an airfoil shape caused about 2 dB noise reduction above a Strouhal number of 5 based on slat chord. Fairing the forward and aft portions of the rod to achieve a smaller thickness ratio caused 3 to 4 dB noise reduction over this frequency range. This configuration was 1 to 2 dB louder than the nominally identical configuration as reported in reference 3. Spanwise traverses with directional microphone identified the noise source region for the slat with cylindrical supports as a region of about 1/4 the slat span and centered at the supports. Removable airfoil-shaped fairings therefore were attached to thin cylindrical sleeves that enclosed the slat support rods. These fairings were contoured to fit against the slats and the wing. When tested with the unmodified and modified leading-edge slats, the additional noise source downstream of the supports was not observed in spanwise traverses with the directional microphone.

Far-field 1/3-octave spectra at 90° direction for the wing with the conventional and modified leading-edge slats are plotted in the upper part of figure 32. The slat having a serrated trailing edge generally was 1 to 2 dB louder than the conventional slat. However, the slat having a perforated trailing edge was about 2 dB quieter than the conventional slat over a large frequency range for 100 m/sec velocity. This benefit occurred over a limited frequency range for 70.7 m/sec velocity.

Spectra for the conventional slat and the slat with a porous trailing edge, normalized in the manner used in reference 3, are plotted in the lower part of figure 32. Amplitudes are scaled with the ratio of slat area to far-field distance squared, and with velocity to the fifth power. Frequency is scaled as Strouhal number based on wing chord. The open symbols are data for the conventional slat and the circle and triangle symbols are for the slat with a perforated trailing edge. Maximum noise reduction occcured for Strouhal numbers up to 20. The two sets of data for different velocities are consistent with each other and show about 2 dB noise reduction for the

24

modified leading-edge slat. At higher Strouhal numbers the data are not coalesced. Also shown in this figure is the spectrum of leading-edge slat noise as calculated by the method of reference 2. It lies below the data for the model conventional leading-edge slat. As with the tests reported in reference 3, the slat model was louder than was scaled from flyover tests of a large airplane with its leading-edge slat extended.

Measurements conducted with the directional microphone do not agree with the increased noise shown in these data for the slat with perforated trailing edge at high frequencies and the lower velocity. Chordwise traverses of directional-microphone signal strength at 5, 10, and 20 kHz center frequencies at midspan of these slat configurations are given in figure 33 for 70.7 m/sec velocity. They show the serrated slat as 2 to 3 dB louder, and the perforated slat the same increment quieter, than the conventional slat at 5 and 10 kHz center frequencies. All configurations had the same noise signal strength for 20 kHz frequency. The corresponding data traces at the spanwise position of the slat side edge are given in figure 34. They show less of an adverse effect for the serrated slat, and the same benefit for the perforated slat, at the lower two frequencies. Both modifications slightly increased the noise from the slat side edge at the highest frequency.

Spanwise traverses, given in figure 35, were conducted at the streamwise position that yielded maximum signal strength. For the two lower frequencies, they show constant increments along the span. The spanwise variations are consistent with a line source of constant strength per unit slat span, located at the slat trailing edge. For the highest frequency, the major noise source appears to be located at the spanwise position of the slat support strut. This noise may be caused by convection of the strut wake past the slat trailing edge. These directional microphone data are consistent with about 2 dB noise reduction for the slat with perforated trailing edge at 10 kHz center frequency, rather than the 3 dB increase shown in figure 32(a).

Corresponding directional-microphone data for the conventional and modified leading-edge slats at 100 m/sec velocity are given in figures 36 through 38. They show that the slat with perforated trailing edge was about 2 to 3 dB quieter at midspan, and 1 to 2 dB quieter at the side edge, than the conventional slat. The serrated slat was about 1 dB louder than the conventional slat. Thus the results of the conventional and directional microphones agree for 100 m/sec velocity. They indicate about 2 dB reduction of leading-edge slat noise, over a broad frequency range that scales to frequencies of practical importance at full scale, by use of a perforated trailing-edge region on the slat. This sort of modification would seem to be easily applied to existing full-scale leading-edge slats.

It is not known why the slat with a serrated trailing edge was ineffective for noise reduction. The only previous tests of serrated edges (reference 20) were for the trailing edge of a panel having flow on only one side. Perhaps additional noise was caused by flow separation at the tapered blunt bases of the serrations in the presence of flow over both the upper and lower surfaces. Also, the ratio of serration span to boundary-layer thickness may not have been in the correct range.

Modified Leading-Edge Slat and Trailing-Edge Flap

Far-field spectra beneath the wing with modified leading-edge slat and trailing-edge flap, at 70.7 and 100 m/sec velocities, are compared in figure 39 with those for the wing with conventional slat and flap. Both modified configurations had a perforated trailing-edge region on the leading-edge slat. One had perforated side regions, and the other had a porous leading-edge region, on its 40° deflection single-slotted trailing-edge flap. Both of the modified configurations produced about 2 dB noise reduction over nearly all the frequency range. Thus the combination of a modified leading-edge slat and modified trailing-edge flap provided noise reduction over a larger frequency range than either modification had produced alone.

The reason for this effectiveness can be determined from the directional-microphone measurements of noise source strength distribution. These are given in figures 40 and 41 for 70.7 and 100 m/sec velocities. At the lowest frequency for which data are shown, far-field noise of the conventional model was dominated by radiation from the slat. This noise contribution was reduced by the slat modification. At higher frequencies this modification became ineffective. However, much of the far-field noise at those high frequencies came from the flap side edges. This noise was reduced by both modifications to the trailing-edge flap. The perforated trailing-edge flap seems to have caused more high-frequency noise source reduction in the presence of the leading edge slat than it produced when tested alone. However, slat noise reduction due to its perforated trailing edge region and flap noise reduction due to its porous leading edge regions seemed unaffected by component interactions. Modifying both the slat and flap achieved noise reduction over a large frequency range by reducing the noise from each airframe component over the frequencies at which that component's noise was dominant.

CLEAN-AIRFRAME NOISE EXPERIMENTS

Effects of Boundary-Layer Transition on Clean-Airframe Noise

The purpose of this experiment was to determine whether noise radiation
from an airfoil without high-lift devices was affected by forcing transition
of the boundary layer from laminar to turbulent flow. In an earlier test
conducted elsewhere (reference 4) with an uncambered NACA 63-012 airfoil,
tripping the boundary layer increased the coherence between near-field and
far-field acoustic radiation. The maximum test Reynolds number of 2.2×10^6
for that test is close to the value of 2.1×10^6 obtained at 100 m/sec airspeed
for the tests reported herein. However, the airfoil section used in the tests
reported in reference 4 has an accelerating pressure gradient conducive to
maintaining natural laminar flow past 30% chord on both surfaces at zero
lift. Tripping the boundary layer at 6% chord would be expected to cause a
significant change in boundary-layer properties at the trailing edge. Thus
the noise caused by convection of boundary-layer turbulence past the trailing
edge could be changed.

In contrast, the cambered NACA 23012 airfoil used in the present tests
has a more realistic, more complicated pressure distribution. The pressure
distribution at the design lift coefficient of 0.3 has a favorable pressure
distribution to about 30% chord on the lower surface but only to 10% chord on
the upper surface. At zero lift, the favorable pressure gradient extends to
about 25% chord on the lower and 10% chord on the upper surfaces. For a lift
coefficient of 0.9, appropriate for approach to landing for a lightplane
having this airfoil and Reynolds number, and not equipped with high-lift
devices, the favorable pressure gradient would extend to 80% chord on the
lower surface. It was expected that the airfoil surface discontinuity at 75%
chord of the lower surface would assure boundary-layer transition for this
lift coefficient.

Two different methods were employed to insure boundary-transition
at a specified location. As one method, a sparse distribution of 0.5 mm
(0.020 in.) diameter sand grains was glued to the surface between 10% and
15% chord on the lower surface and, in a subsequent run, on both surfaces.
Sand grain size was chosen by the procedure of reference 22 as the minimum
that would assure transition. The other transition method was the use of thin
serrated plastic tape, with a thickness ¼ that of the roughness grains. It
was applied to the airfoil surfaces with the serrations facing forward and
their forward corners at 10% chord.

Traces of noise signal strength as measured during streamwise traverses of the directional microphone at midspan are presented in figure 42. Data are shown for 1/3-octave band center frequencies of 10 and 20 kHz at 0, 0.3, and 0.9 nominal lift coefficients. Peak amplitude of noise radiation for this airfoil and test condition is predicted (reference 3) to occur in the 1/3-octave band having 2 kHz center frequency. Thus the noise radiation expected at these high frequencies is considerably weaker than that for peak amplitude. For 10 kHz frequency, and also (not shown) at lower frequencies, the peak of noise radiation at lift coefficients of 0 and 0.3 came from the airfoil trailing edge. This result that an artificially thickened turbulent boundary layer should produce less rather than more trailing-edge noise may seem contrary to expectations. From the noise prediction method given in reference 2, increased boundary layer thickness would be expected to increase both the overall sound pressure level (OASPL) and maximum 1/3-octave SPL. It should also decrease the center frequency at which that maximum SPL occurs. The spectrum shape associated with trailing edge noise yields a rapid decrease of SPL amplitudes at Strouhal numbers much larger than that for peak SPL. At large measurement frequencies as with these data, increased boundary layer thickness causes reduced Strouhal number and a larger reduction of (SPL-peak SPL) than the direct increase of maximum SPL. Thus the observed decrease of SPL at constant frequency and velocity, due to an increase of boundary layer thickness at the trailing edge, is consistent with theory.

Increasing the lift coefficient to 0.9 caused about 5 dB increase of wind-tunnel background noise. There was little change in amplitude of the peak located at the trailing edge. This amplitude is a sum of noise radiated from the airfoil and from the wind-tunnel shear layer and collector. It can therefore be inferred that noise radiation from the airfoil trailing edge had decreased 1 to 2 dB when lift coefficient was increased to 0.9. This small decrease is consistent with the data of reference 4; increasing the angle of attack in those tests reduced the coherence between near-field and far-field noise.

Data taken at 20 kHz center frequency for the airfoil with natural transition and with serrated tape resemble the lower frequency data. However, the airfoils with sand grain roughness had stronger noise radiation originating from the roughness than from the trailing edge. This high frequency corresponds to a Strouhal number of about 0.1 based on grain size. That is near the expected value of 0.2 for peak noise radiation due to flow separation behind each grain. Noise radiation from the airfoil trailing edge at this frequency is predicted to be 16 dB below that for peak amplitude, so it is not unreasonable that noise radiation from sand grain roughness could be louder.

It is concluded that for the NACA 23012 airfoil at a Reynolds number of 2.1×10^6, tripping the airfoil laminar boundary layer generally causes about 1 dB reduction of airfoil noise. Use of serrated tape for tripping the boundary layer eliminates extraneous high-frequency noise caused by flow over sand grains, or displaces it to much higher frequencies.

Noise Source Distribution Near A Clean Wing Tip

The airframe noise prediction method of reference 3 does not include any representation of increased noise radiation from wing tip regions. However, flow around the tip of a lifting wing is known (e.g., reference 23) to produce a tip vortex having a thick viscous core which is convected past the trailing edge. Increased noise radiation might be expected from motion of this turbulence past the trailing edge and from movement of vorticity around the wing tip. Such noise had been observed in early tests (reference 24) of a directional microphone. Directional-microphone measurements were therefore conducted of the noise source strength distribution on an available rectangular wing with an aspect ratio of 2.33. This wing was mounted on the acoustic wind-tunnel lower sidewall. It extended to midspan of the test section, except for the half body of revolution tip cap. This wing model had an uncambered NACA 0012 airfoil section of 22.9 cm (9.00 in.) chord. Reynolds number based on wing chord was 1.56×10^6 at the 100 m/sec test airspeed. The wing had a slider in the lower surface at 30% chord, to allow placement of a flush-mounted microphone with its preamplifier at arbitrary spanwise positions (reference 21). The resulting surface discontinuity was expected to trip the pressure-surface laminar boundary layer and thereby eliminate laminar instability feedback tones at this relatively low Reynolds number. Tones were not observed in the far-field spectra measured at $0°$, $5°$, or $10°$ angle of attack. However, a weak tone was detected at $15°$ angle of attack. A serrated tape was applied to the model along the 75% chord station of the lower surface, eliminating the tone. Data were also taken with the tape on that surface at $25°$ angle of attack, well above the $18°$ to $20°$ angle at which stall would occur.

Plots of the chordwise variation of directional microphone signal strength are shown in figure 43 for two spanwise positions: along the wing tip and half a chord inboard from the tip. Data are given for the 1/3-octave band frequencies centered at 5 and 20 kHz. At the lower frequency, there was little or no difference between traces for 0 and $5°$ angles of attack. Peak signal strength occurred near the trailing edge for both spanwise locations. Measured signal strength at the tip was about 2 dB below that for the inboard location. This difference is in reasonable agreement with the 3 dB decrease that would be expected if the wing noise source distribution along the trailing edge was a line source having constant strength per unit span, as

assumed in reference 2. Further increases of angle of attack to 10° and 15° increased the peak amplitude of the trailing edge noise signal, with this increase being largest at the wing tip. A further increase to 25° caused the wing to stall. Stall did not significantly change the peak amplitude from that measured at 15° but it moved the noise source location to about 75% chord at the wing tip. Data for the higher frequency show the same trends except for increased noise from the wing tip at 5° angle of attack. These data traces are presented to show that for angle of attack at which the wing is not stalled, the only noise source location is along the trailing edge.

At each angle of attack, the directional microphone was positioned at the streamwise position that gave peak signal strength at the spanwise station half a chord inboard from the wing tip. (Changing the angle of attack changed the position of the trailing edge.) The reflector was then traversed spanwise from the sidewall to a position beyond the wing tip. The resulting spanwise variations of wing trailing-edge noise signal strength for the angles of attack tested, at 5 and 20 kHz center frequencies, are plotted in figure 44. For this directional microphone reflector, the calculated dif- fraction pattern half-power width (the apparent width of the region having signal strength within 3 dB of maximum) is about 1 chord at 5 kHz and ¼ chord at 20 kHz frequencies. Thus the data correspond to the presence of a concen- trated broadband noise source at the trailing edge near the wing tip. The width of the measured traces is consistent with a noise source having a span- wise extent of less than 10% chord. Spanwise location of this noise source cannot be directly determined because of the inherent decrease in signal strength as the tip is approach, as with the data trace at 0° angle of attack. This location is of the order of 5% to 10% chord inboard from the wing tip, and farther inboard as angle of attack is increased.

These results can be understood by examining the development of viscous flow around the tip of a thin rectangular wing. Calculated features of such a flow are given in reference 23 for 6° angle of attack and a Reynolds number of 1x10^6. Over the forward 30% chord of the wing tip, boundary-layer fluid is predicted to move from the lower surface around the wing tip and onto the upper surface. This forward portion of the wing model had a large radius of curvature, relative to the local boundary-layer thickness, so generation of edge noise due to flow around this portion of the wing tip would not be expected and was not observed. Aft of about 30% chord, the circulation associated with vorticity convected around the wing tip causes the upper-sur- face boundary layer to be directed outboard along the surface. The lower- surface boundary layer continues to flow toward the tip and is shed off the tip. However, instead of moving onto the wing upper surface, it is convected and diffused in an upward inboard direction. Thus it forms a tongue-like region of free vorticity, above and clearly distinct from the upper surface crossflow boundary layer. The center of this viscous vortex core was

30

calculated to pass the streamwise location of the trailing edge at a height 6% chord above the trailing edge and a spanwise location 1% chord inboard from the tip. Data cited therein for 12° angle of attack generally agree with this calculated behavior; the observed vortex-core location at the trailing-edge streamwise position was 9% above the trailing edge and 6% chord inboard from the tip. Thus the observed wing-tip noise radiation for an unstalled wing is consistent with the concept of trailing-edge noise generated by the viscous core of the wing-tip vortex, as its turbulence is convected past and a considerable distance above the trailing edge.

For unstalled flow, the noise per unit span decreased as inboard distance from the tip vortex was increased. This noise approached levels which varied by only several dB for the 0° to 15° angle of attack range. That small effect of angle of attack on trailing-edge noise radiation far from a wing tip was also found in the tests of a full-span wing described in the preceding section. In contrast, for stalled flow (25° angle of attack) the noise radiation was approximately constant along the span. Its amplitude generally matched the peak signal strength beneath the tip vortex at 15° angle of attack. This result is reasonable if the noise-producing turbulence for a stalled wing is assumed to be that of the shear layer which originates from the wing upper surface near its leading edge. Turbulence levels and scale lengths in this free shear layer probably are the same as in the free viscous core of the tip vortex. Both the shear layer and the vortex core move downstream over the wing in essentially the free-stream direction. Vertical displacement of the turbulent region above the wing trailing edge then is not caused by upward displacement of the turbulent regions, but by downward displacement of the wing upper surface and trailing edge relative to the separation position. Therefore both situations would be expected to produce about the same turbulence at about the same distance above the trailing edge. It is reasonable that they should cause about the same peak noise signal strength, one at only one spanwise location and the other for the entire stalled span.

The importance of this wing-tip vortex noise process can be examined relative to conventional clean-airframe noise caused by convection of the wing turbulent boundary layer past the trailing edge. Clean-airframe flyover noise data were given in reference 25 for four airplanes with retracted landing gear over a range of weights and airspeeds. Lift coefficients ranged from approximately 0.2 to 0.6, and normalized spectrum shape was not noticeably affected by this change. The low aspect ratio rectangular wing at 10° angle of attack had a lift coefficient in the upper portion of this range. From figure 44, the amplitude of the tip-vortex noise signal (regarded as from a point source) was about 5 and 8 dB above that from the portion of the trailing-edge line source viewed by the directional microphone at 5 and 20 kHz center frequencies. Adjusting for the decrease of spanwise resolving length as frequency

is increased (reference 6), tip-vortex noise would be about 3.5 and 1 dB higher than the trailing-edge noise from a spanwise distance equal to one chord length at the lower and higher frequencies, respectively. Most of the aircraft used in the flight tests reported in reference 25 had a semispan of about 5 chords. Thus the trailing-edge noise from each wing panel would be about 7 dB larger than that from a wing having a spanwise extent of one chord. Amplitude of tip-vortex noise from those airplanes at the higher lift coefficients would be 1 to 3.5 dB below the wing trailing-edge noise. Thus the presence of wing-tip vortex noise for those flights would be expected to add less than 2 dB to the flyover noise. This increment is within the expected accuracy of current airframe noise prediction methods.

For the highest unstalled angle of attack used in this test program, the measured tip-vortex noise was about 10 dB higher than trailing-edge noise from a spanwise length equal to the wing chord. Airplanes with wing aspect ratios similar to those of the typical propeller-driven commercial and business airplanes used in the flight tests would then have tip-vortex noise 3 dB above the trailing-edge noise at high lift coefficients. Flight at such conditions would then increase the total noise to about 5 dB more than that predicted for trailing-edge noise alone. This evaluation is based on the assumption that turbulence properties in the wing-tip vortex viscous core are the same for model- and full-scale Reynolds numbers.

Although wing-tip vortex broadband noise does not appear to be very important for airplane wings, this noise process may impose the broadband noise floor for thrusting propellers and helicopter rotors. The variation of relative velocity with radial distance for such devices increases the importance of a noise source located near the blade tip relative to a source distributed along the blade trailing edge.

CONCLUSIONS

1.   Noise radiation from the side edges of highly deflected trailing-edge flaps can be reduced by use of porous or perforated surfaces near those edges, producing 2 to 3 dB decrease of flap noise over a moderate frequency range.

2.   Noise radiation from leading-edge slats can be reduced by about 2 dB over a large frequency range by use of a perforated trailing edge region on the slat.

3.   Artificial thickening of the turbulent boundary layer at the trailing edge of a wing without high lift devices has essentially no effect on noise radiation.

32

4.   Noise reductions caused by modifying one high-lift component of a wing are not significantly affected by the presence of other wing components.

5.   Wing-tip noise caused by convection of the tip-vortex viscous core past the wing trailing-edge is a weak broadband noise mechanism relative to conventional wing trailing-edge noise, for moderate and high aspect ratio wings at low and moderate lift coefficients.

RECOMMENDATIONS

In these tests it was shown that porous and perforated surfaces having arbitrarily chosen physical properties and geometric extent could provide significant localized reductions of airframe noise. These design quantities should be varied, at model scale, so that near-optimum combinations can be selected for eventual validation on full-scale airframes. Model-scale tests should use a considerably larger wing so that acoustic treatment can be applied to both panels of a realistic double-slotted trailing-edge flap. This could be done by testing a 3/4 m (3 ft) chord model in a conventional closed-wall wind tunnel at low subsonic speeds, as in the experimental programs described in references 13 and 14. Noise source strength distributions would be measured with a directional microphone scanning through an open portion of the tunnel wall. If the wind tunnel is sufficiently quiet and has acous- tically treated walls, noise spectra could be measured with microphones in the tunnel airstream.

One current turbofan-engine installation noise problem is the increased noise produced when the side edge of a trailing-edge flap is deflected into the engine exhaust jet mixing region. This problem becomes more important as the need to improve aerodynamic high-lift performance and to allow larger airplanes to use existing runways conflicts with the need for improved fuel economy as achieved with higher bypass ratio turbofan engines. High-lift performance is improved by reducing the width of the trailing-edge flap cutouts; use of high-bypass ratio engines increases exhaust diameter at constant cruise thrust. It is recommended that noise prediction methods previously developed for externally blown flaps be extended for prediction of such noise, and that porous and perforated modifications to the side edges of such flaps be tested at model scale to evaluate their effectiveness in reducing this installation noise.

REFERENCES

1. Block, P. J. W.: Assessment of Airframe Noise. J. of Aircraft, Vol. 16, No. 12, Dec. 1979, pp 834-841.

2. Fink, M. R.: Airframe Noise Prediction Method. FAA-RD-77-29, Mar. 1977. Also, J. of Aircraft, Vol. 16, No. 10, Oct. 1979, pp 659-665.

3. Fink, M. R. and Schlinker, R. H.: Airframe Noise Component Interaction Studies. NASA CR 3110, Mar. 1979. Also, J. of Aircraft, Vol. 17, No. 2, Feb. 1980, pp 99-105.

4. Yu, J. C. and Joshi, M. C.: On Sound Radiation From the Trailing Edge of an Isolated Airfoil in Uniform Flow. AIAA Paper 79-0603, Mar. 1979.

5. Brooks, T. F. and Hodgson, T. H.: An Experimental Investigation of Trailing Edge Noise. NASA TM-80134, June 1979.

6. Schlinker, R. H.: Airfoil Trailing Edge Measurements with a Directional Microphone System. AIAA Paper 77-1269, Oct. 1977.

7. Paterson, R. W., Vogt, P. G., and Foley, W. M.: Design and Development of the United Aircraft Research Laboratories Acoustic Research Tunnel. J. of Aircraft, Vol. 10, No. 7, July 1973, pp 427-433.

8. Amiet, R. K.: Correction of Open-Jet Wind-Tunnel Measurements for Shear Layer Refraction. Aeroacoustics: Acoustic Wave Propagation, Aircraft Noise Prediction: Aeroacoustic Instrumentation, Vol. 46, Progress in Aeronautics and Astronautics, M.I.T. Press, Cambrige, MA., 1976, pp 259-280. Also, AIAA Paper 75-532, Mar. 1975.

9. Amiet, R. K.: Refraction of Sound by a Shear Layer. J. of Sound and Vibration, Vol. 58, No. 4, June 1978, pp 467-482.

10. Shields, F. D. and Bass, H. E.: Atmospheric Absorption of High Frequency Noise and Application to Fractional-Octave Bands. NASA CR-2760, June 1977.

11. Wenzinger, C. J. and Harris, T. A.: Wind-Tunnel Investigation of an NACA 23012 Airfoil With Various Arrangements of Slotted Flaps. NACA Report No. 664-1939.

REFERENCES (Continued)

12. Heller, H. H. and Dobrzynski, W. M.: Sound Radiation From Aircraft Wheel-Well/Landing Gear Configurations. J. Aircraft, Vol. 4, No. 8, Aug. 1977, pp 768-774.

13. Ahtye, W. F., Miller, W. R., and Meecham, W. C.: Wing and Flap Noise Measured by Near-Far Field Cross-Correlation Techniques. AIAA Paper 79-0667, Mar. 1979.

14. Kendall, J. M. and Ahtye, W. F.: Noise Generation by a Lifting Wing/ Flap Combination at Reynolds Numbers to 2.8×10^6. AIAA Paper 80-0035, Jan. 1980.

15. Pennock, A. P., Swift, G., and Marbert, J. A.: Static and Wind Tunnel Tests for the Development of Externally Blown Flap Noise Reduction Techniques. NASA CR-134675, Feb. 1975.

16. Howe, M. S.: Attenuation of Aerodynamic Sound by a Porous Airfoil. Oral Presentation at NASA Langley Research Center under Contract NAS1-14611-21, July 1978.

17. Fink, M. R.: A Method for Calculating Strut and Splitter Plate Noise in Exit Ducts - Theory and Verification. NASA CR-2955, Mar. 1978.

18. Ventres, C. S. and Barakat, R.: Aerodynamics of Airfoils With Porous Trailing Edges. Aeronautical Quarterly, Vol. 30, Part 2, May 1979, pp 387-399.

19. Bohn, A. J.: Edge Noise Attenuation by Porous-Edge Extensions. AIAA Paper 76-80, Jan. 1976.

20. Filler, L.: Swept Edge to Reduce the Noise Generated by Turbulent Flow Over the Edge. J. Acoust. Soc. Am., Vol. 59, No. 3, Mar. 1976, pp 697-699.

21. Paterson, R. W., Vogt, P. G., Fink, M. R., and Munch, C. L.: Vortex Shedding Noise of an Isolated Airfoil. United Aircraft Research Laboratories Report K910867-6, Final Report Under U. S. Army Research Office-Durham Contract No. DAHC04-69-C-0089, Dec. 1971.

REFERENCES (Concluded)

22. Braslow, A. L. and Knox, E. C.: Simplified Method for Determination of
    Critical Height of Distributed Roughness Particles for Boundary-Layer
    Transition at Mach Numbers From 0 to 5.   NACA TN 4363, Sept. 1958.

23. Shamroth, S. J. and Briley, W. R.: A Viscous Flow Analysis for the Tip
    Vortex Generation Process.   NASA CR-3184, Oct. 1979.

24. Kendall, J. M.: Measurements of Noise Produced by Flow Past Lifting
    Surfaces.   AIAA Paper 78-239, Jan. 1978.

25. Healy, G. J.: Measurement and Analysis of Aircraft Far-Field
    Aerodynamic Noise.   NASA CR-2377, Dec. 1974.
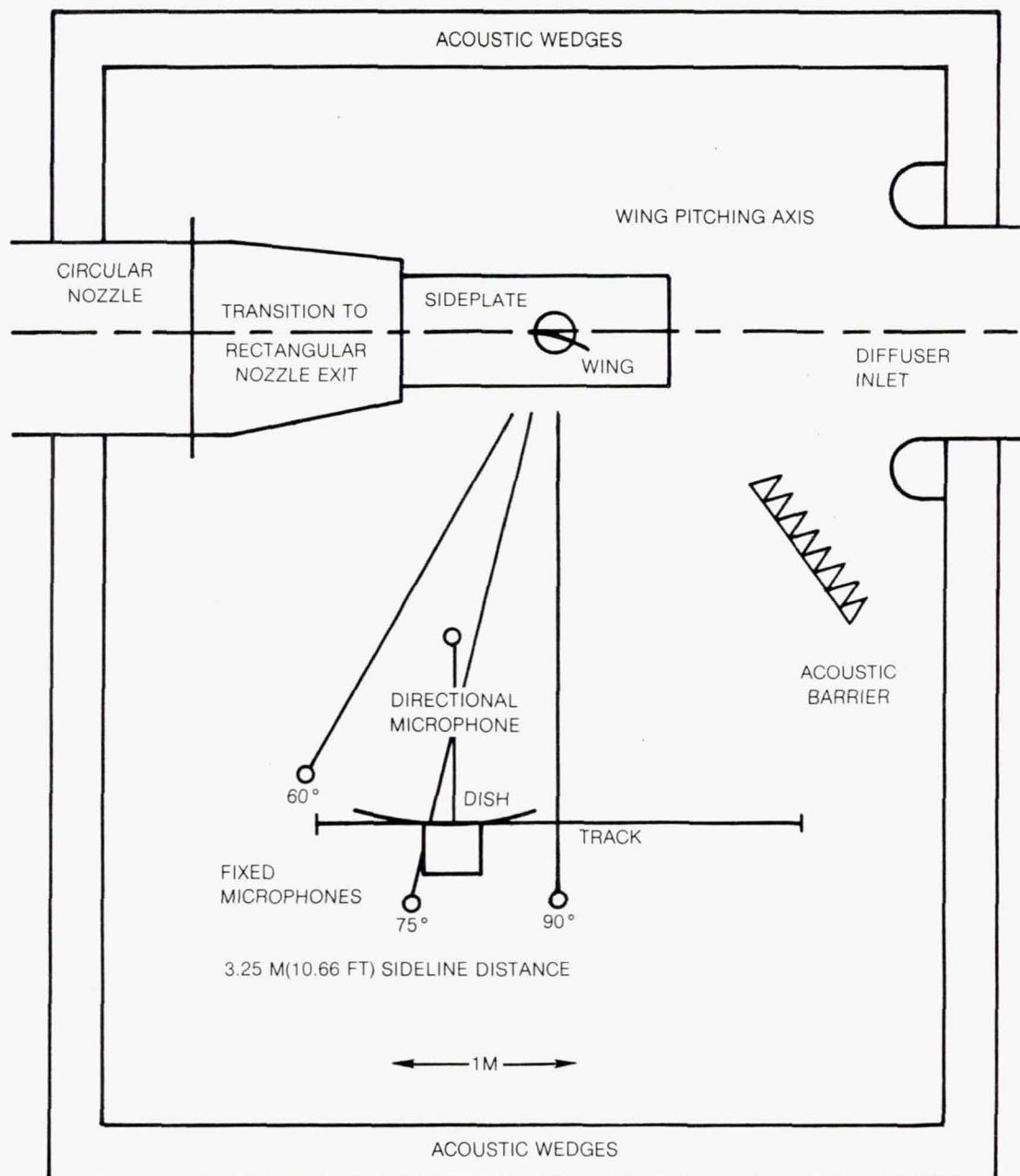
Figure 1 Sketch of Acoustic Wind Tunnel Configuration and Microphone Installation
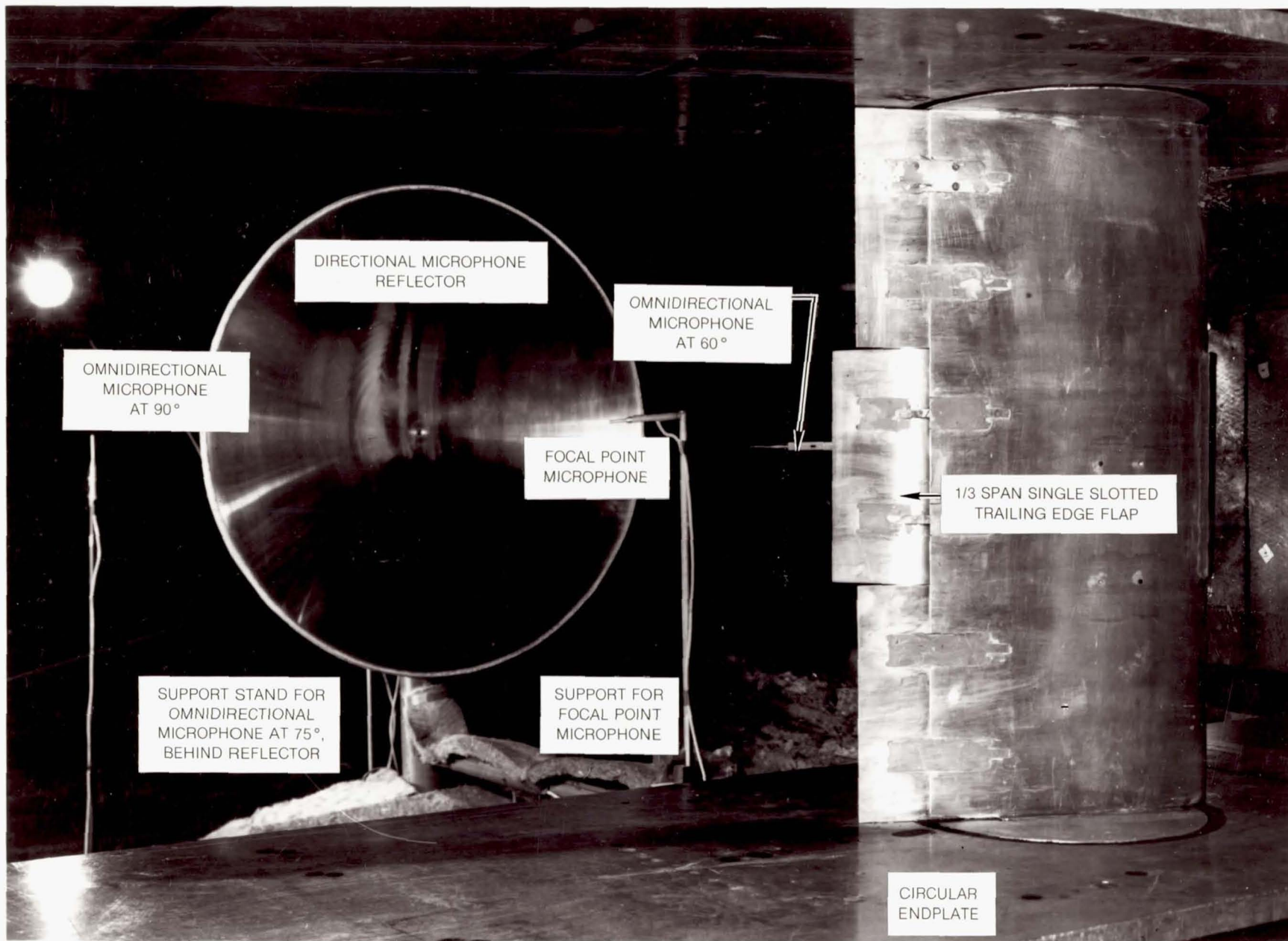
Figure 2 Airframe Noise Model and Far Field Microphones
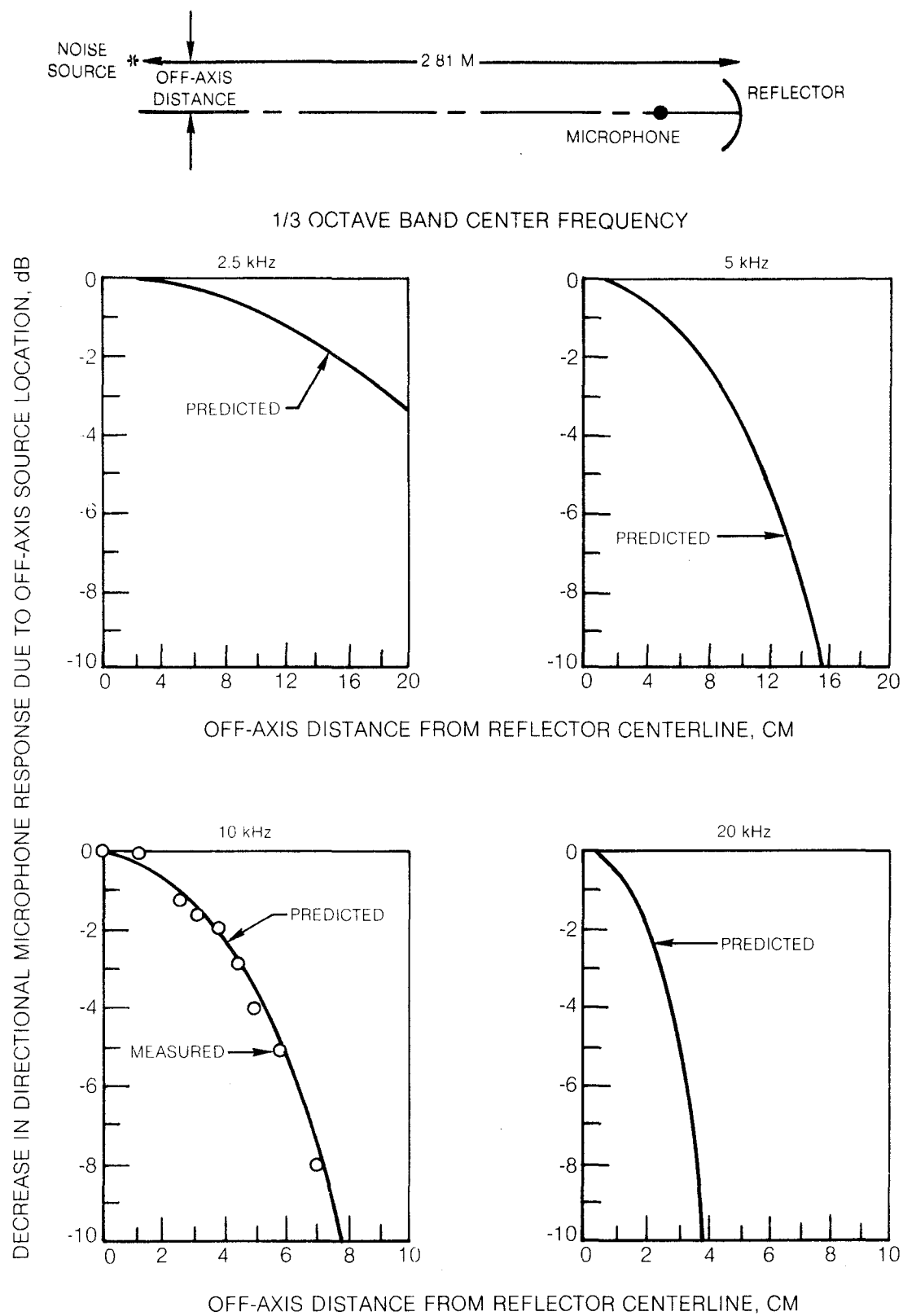
Figure 3 Spatial Discrimination of UTRC Directional Microphone
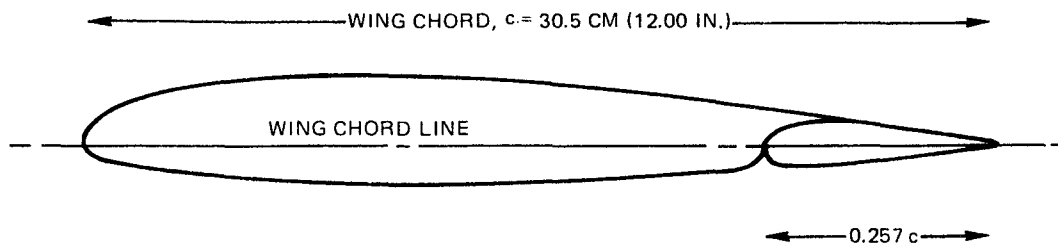
(a) WING AND 25% CHORD SINGLE SLOTTED TRAILING EDGE FLAP IN RETRACTED POSITION
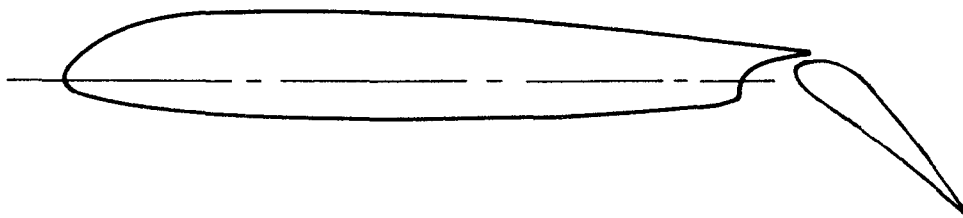
(b) WING AND 25% CHORD SINGLE SLOTTED TRAILING EDGE FLAP AT 40° DEFLECTION
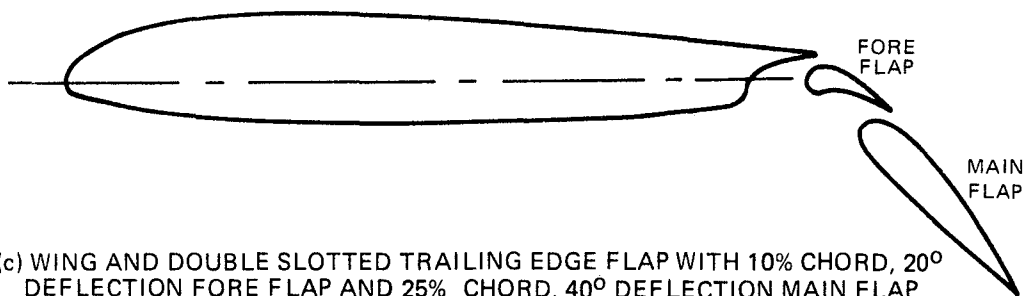
(c) WING AND DOUBLE SLOTTED TRAILING EDGE FLAP WITH 10% CHORD, 20° DEFLECTION FORE FLAP AND 25% CHORD, 40° DEFLECTION MAIN FLAP
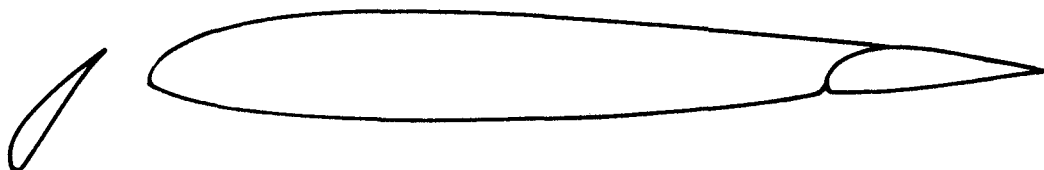
(d) WING AND 15% CHORD, 25° DEFLECTION SLAT

Figure 4 Airfoil Sections of Wing Model and High-Lift Devices

40

LIFT DIPOLE DISTRIBUTED ALONG FLAP SPAN

FLAP SLOT
FREE SHEAR
LAYER

WING

WING LOWER SURFACE
TURBULENT BOUNDARY LAYER

FLAP VANE LOWER SURFACE
TURBULENT BOUNDARY LAYER
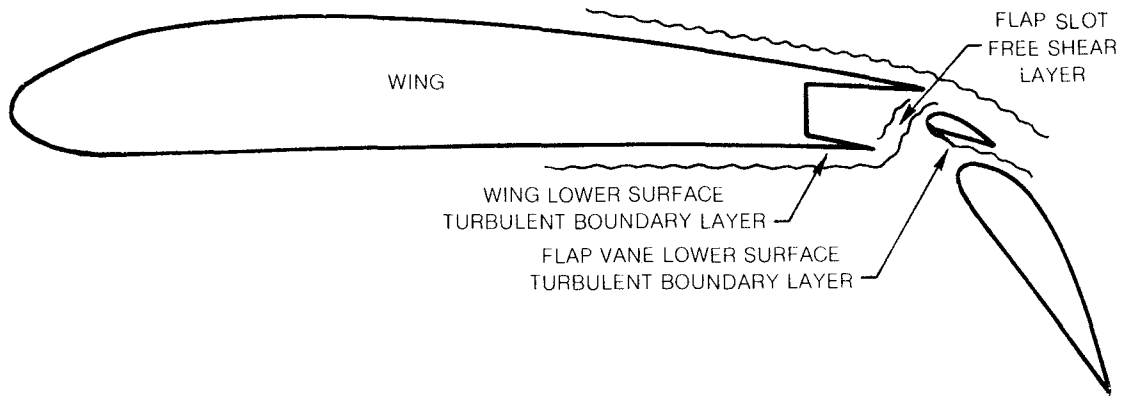
LIFT DIPOLE DISTRIBUTED ALONG FLAP SIDE EDGES
(WING AND FLAP VIEWED FROM REAR)

WING UPPER SURFACE

FLAP VANE

WING
TRAILING
EDGE

WING LOWER
SURFACE

AFT PANEL OF
TRAILING EDGE FLAP

FLAP TRAILING EDGE

FLAP LOWER SURFACE TURBULENT
BOUNDARY LAYER CONVECTED AROUND
SIDE EDGE AND PAST TRAILING EDGE
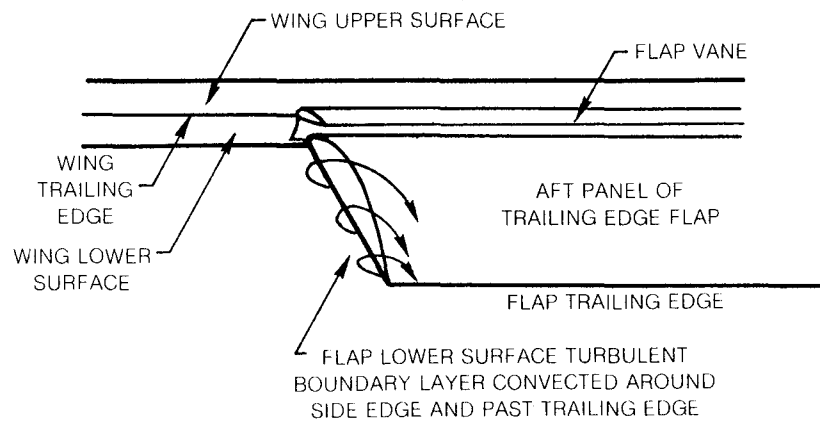
Figure 5 Trailing Edge Flap Noise Generation Processes

WING

ACOUSTIC MATERIAL ALONG
LEADING EDGE

AIRFOIL CHORD LINE

40° DEFLECTED FLAP

FLOW DIVIDER AT
LEADING EDGE

FLOW DIVIDER
AT SIDE EDGE

ACOUSTIC MATERIAL ALONG SIDE EDGE

ACOUSTIC MATERIAL
AT TRAILING EDGE
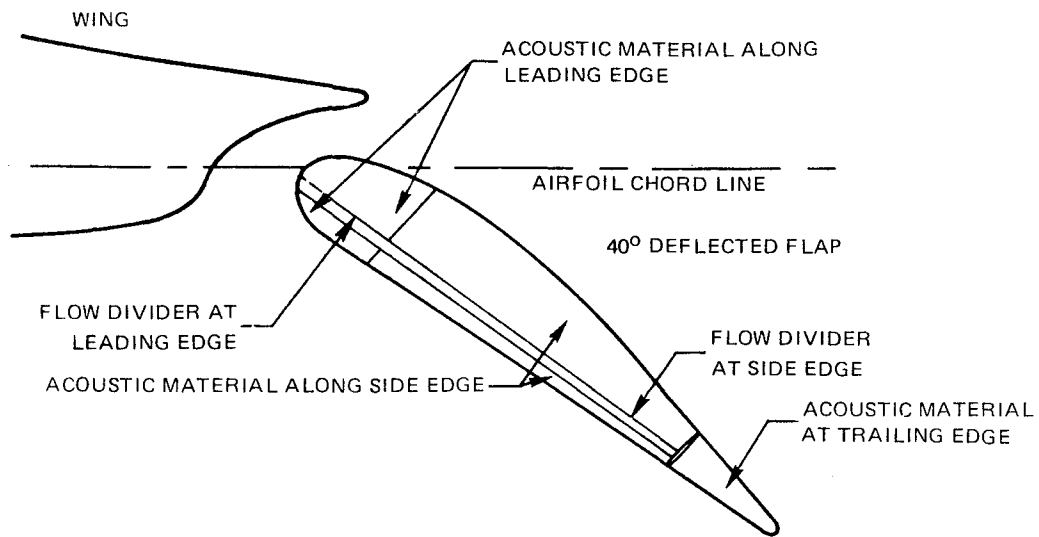
a) CROSS SECTION OF ACOUSTICALLY TREATED TRAILING EDGE FLAP (FULL SCALE)

WING

JUNCTION OF FLAP SLOT
AND WING UPPER SURFACE

RETRACTED FLAP

RETRACTED FLAP

SOLID PORTION OF
DEFLECTED FLAP

ACOUSTICALLY TREATED LEADING, TRAILING,
AND SIDE EDGES
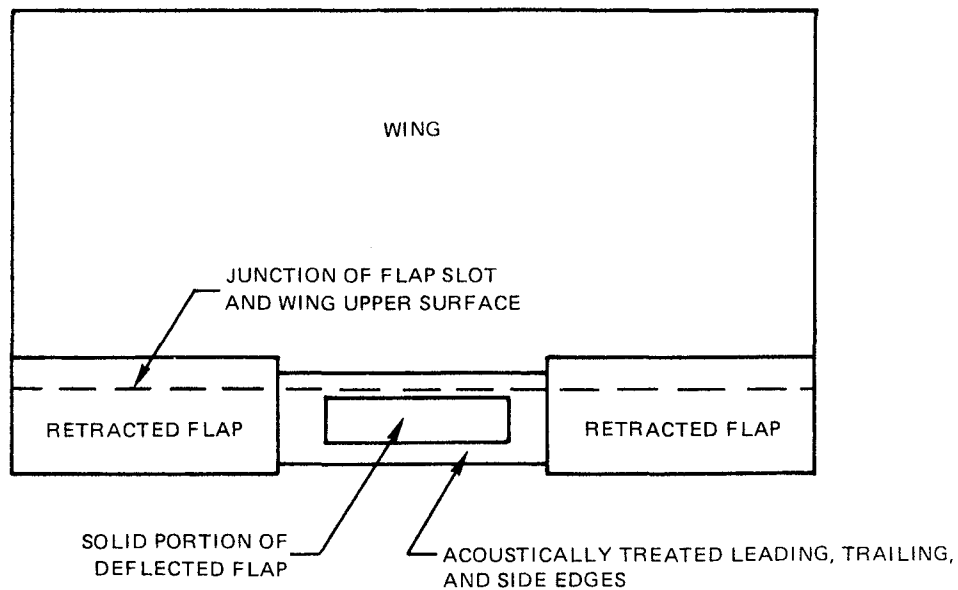
b) ACOUSTICALLY TREATED REGIONS OF PART SPAN TRAILING EDGE FLAP,
VIEWED FROM BELOW (1/5 SCALE)

Figure 6 — Acoustically Treated Trailing Edge Flap

PERFORATED SIDE EDGE REGIONS   POROUS LEADING EDGE REGION   CONVENTIONAL SOLID FLAP

cm 2   4   6   8   10   12   14   16   18   20
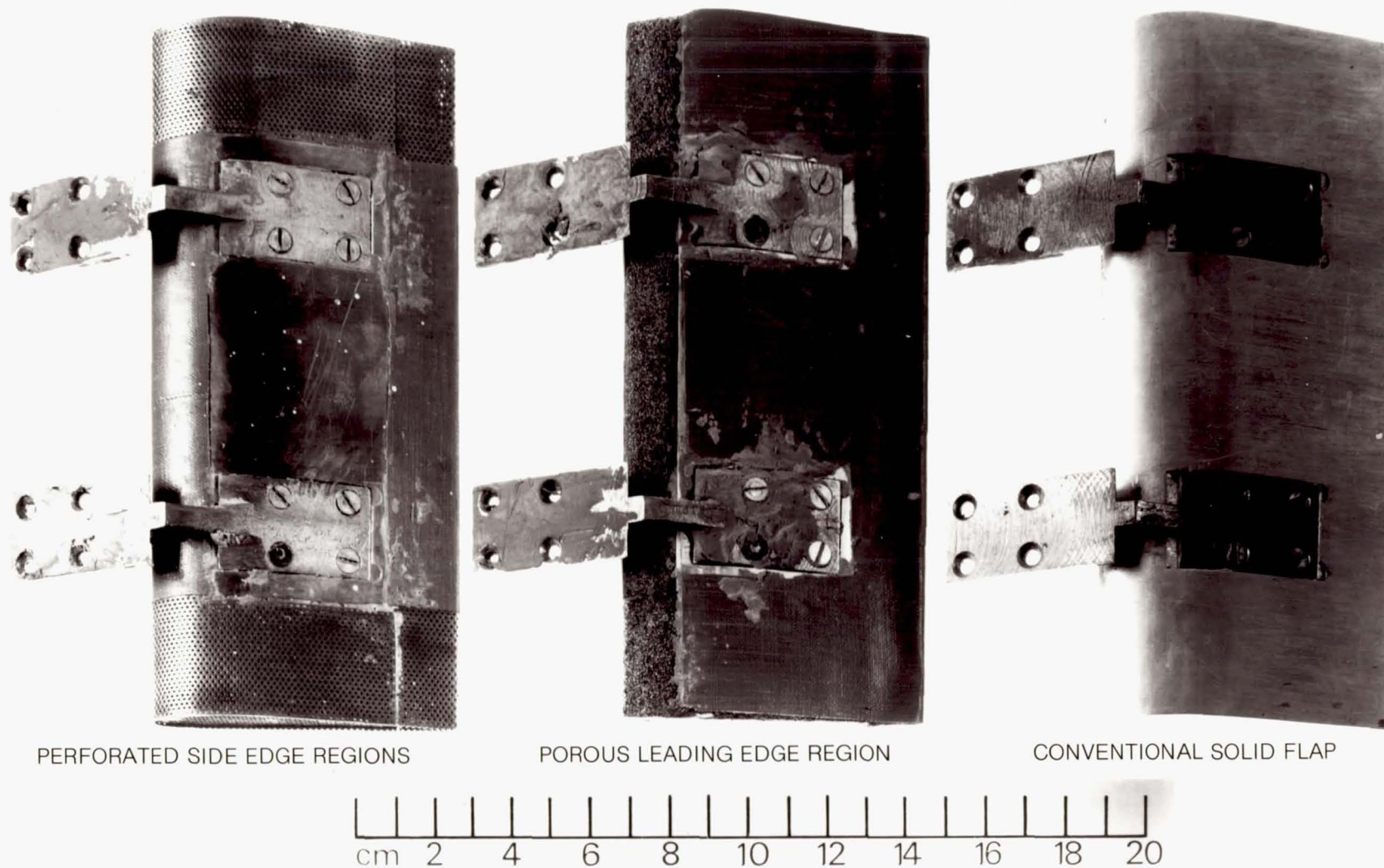
Figure 7 — Conventional and Modified Trailing Edge Flaps

PERFORATED

1.0

4.6

LEADING EDGE SLAT
(FULL SCALE)

SLAT

TOP VIEW OF WING WITH PART
SPAN LEADING EDGE SLAT

0.86

60°

0.49

DETAIL OF SLAT TRAILING EDGE
SERRATIONS (TWICE SCALE)

4.62

17.78

TOP VIEW OF LEADING EDGE SLAT WITH
SERRATED TRAILING EDGE (HALF SCALE)
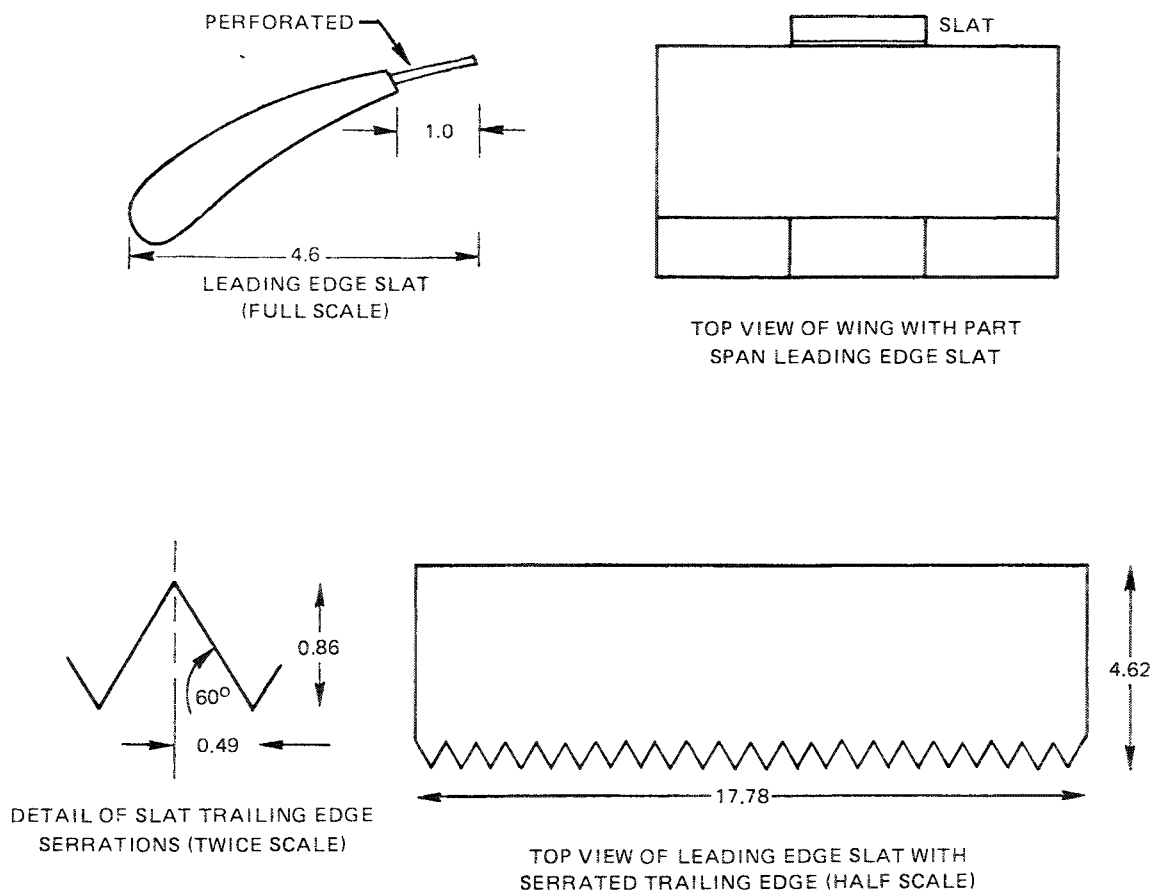
Figure 8 Part-Span Leading Edge Slats with Porous and Serrated Trailing Edges,
All Dimensions in Centimeters

POROUS TRAILING EDGE REGION   SERRATED TRAILING EDGE   CONVENTIONAL SOLID SLAT

cm 2   4   6   8   10   12   14   16   18   20
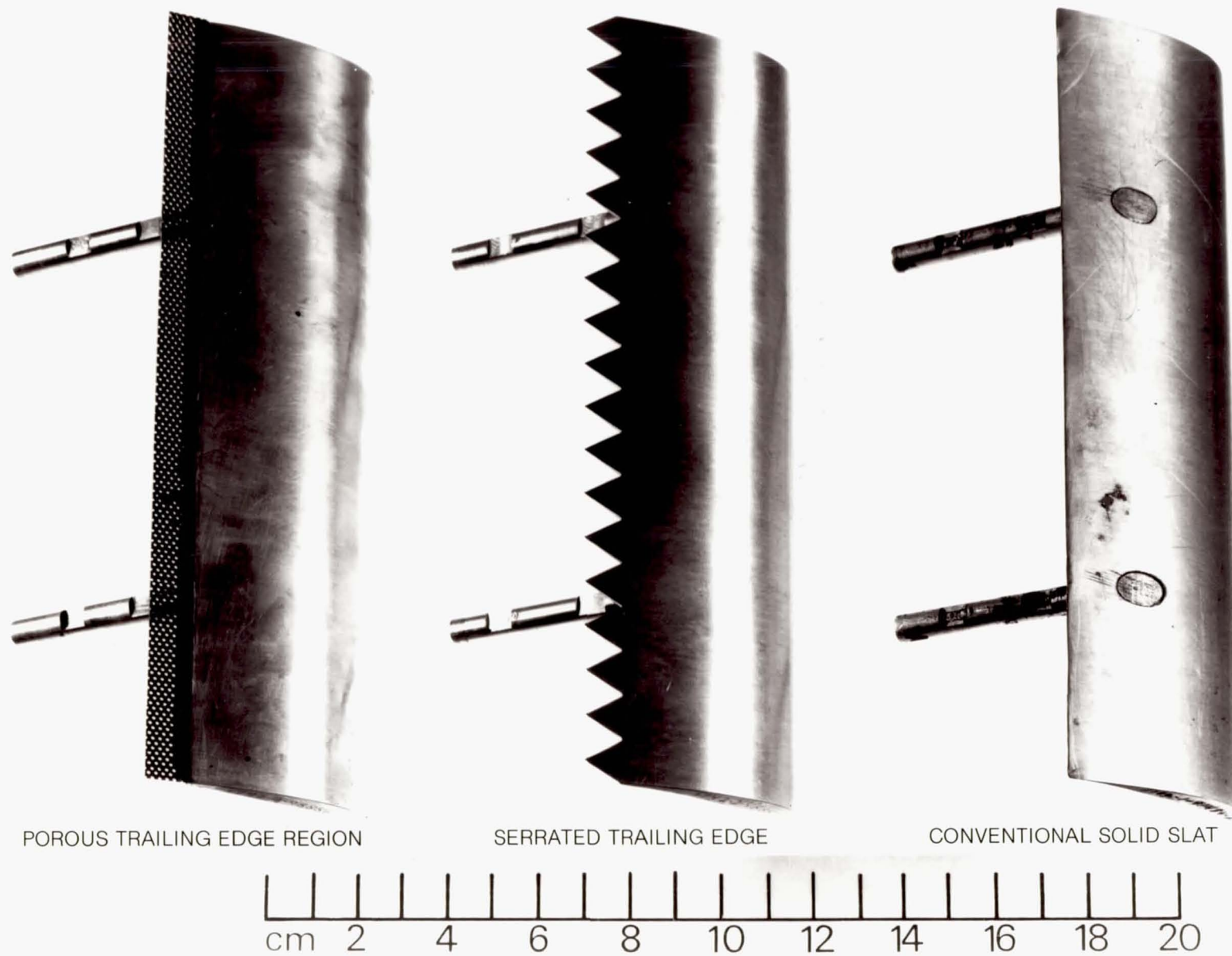
Figure 9 Conventional and Modified Leading Edge Slats

0.280

0.267

SLIDER AT 30% CHORD

NACA 0012 AIRFOIL

0.229
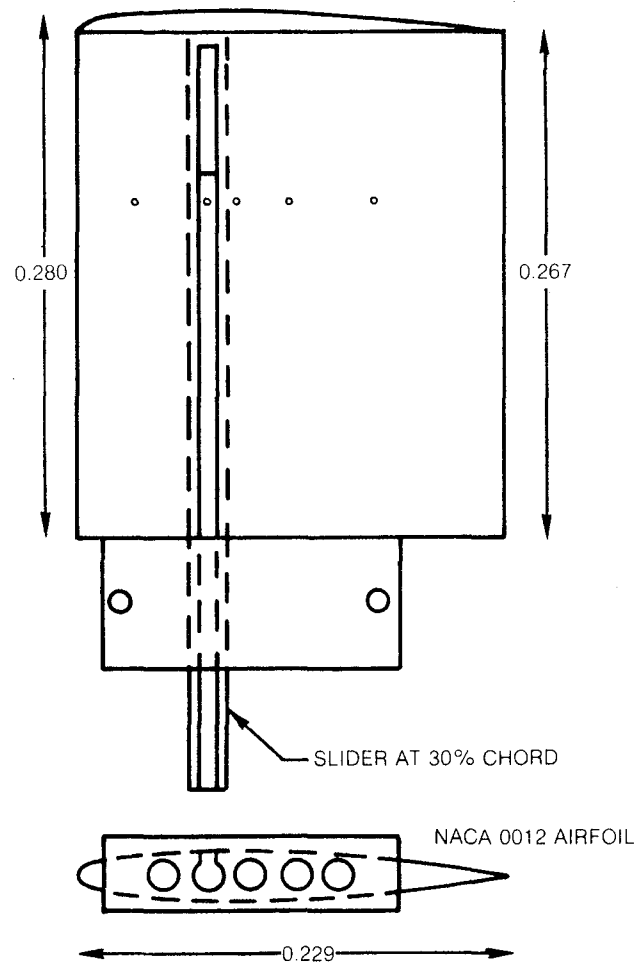
Figure 10 Part-Span Wing. One-Quarter Scale Drawing, All Dimensions in Meters
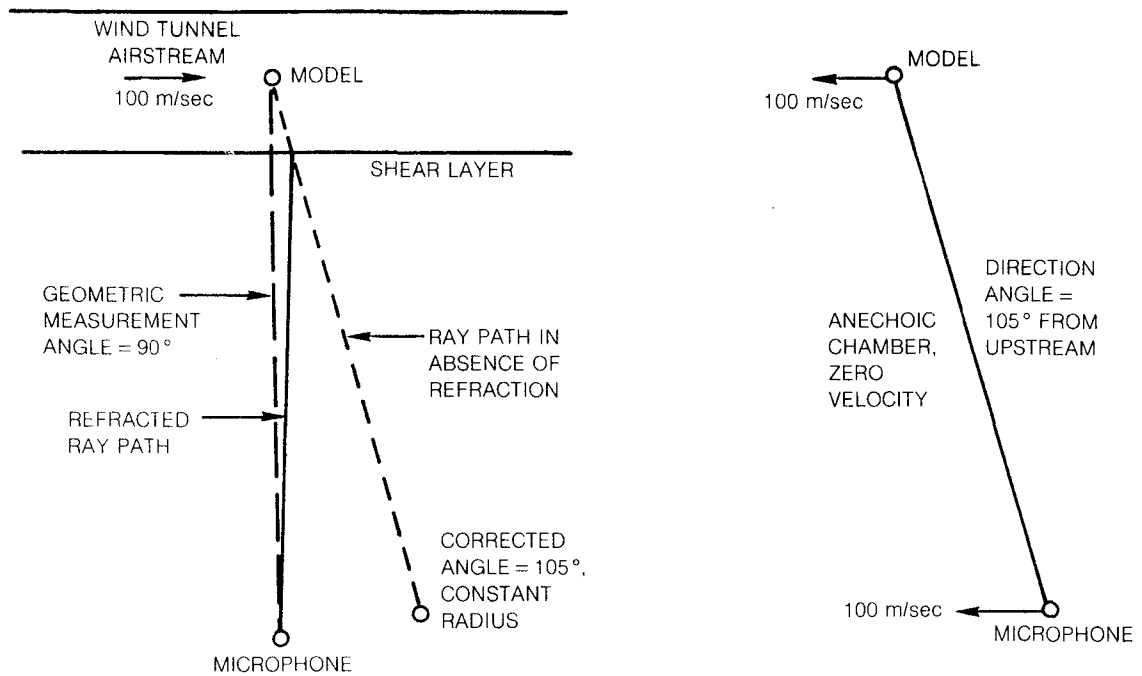
a) CORRECTION FROM WIND TUNNEL
MEASUREMENT SYSTEM

b) EQUIVALENT OF CORRECTED
MEASUREMENT SYSTEM
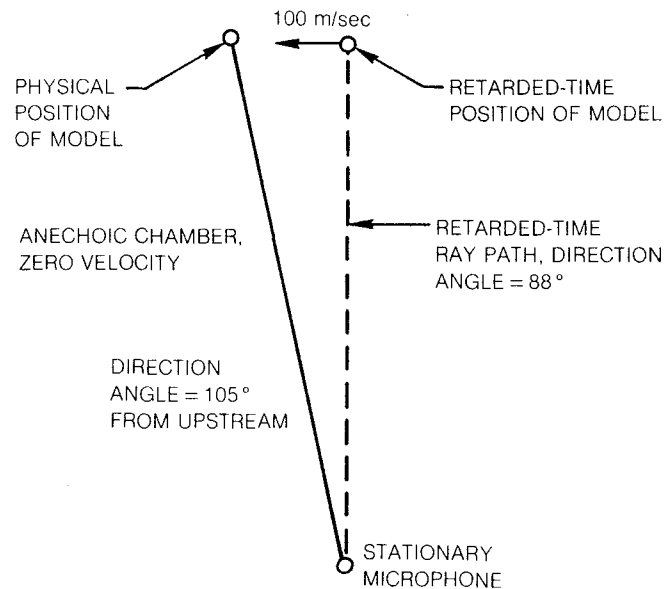
c) TRANSFORMATION TO RETARDED-TIME COORDINATE SYSTEM

Figure 11 Corrections to Acoustic Measurement Coordinate System Due to Shear Layer Refraction and Retarded Time
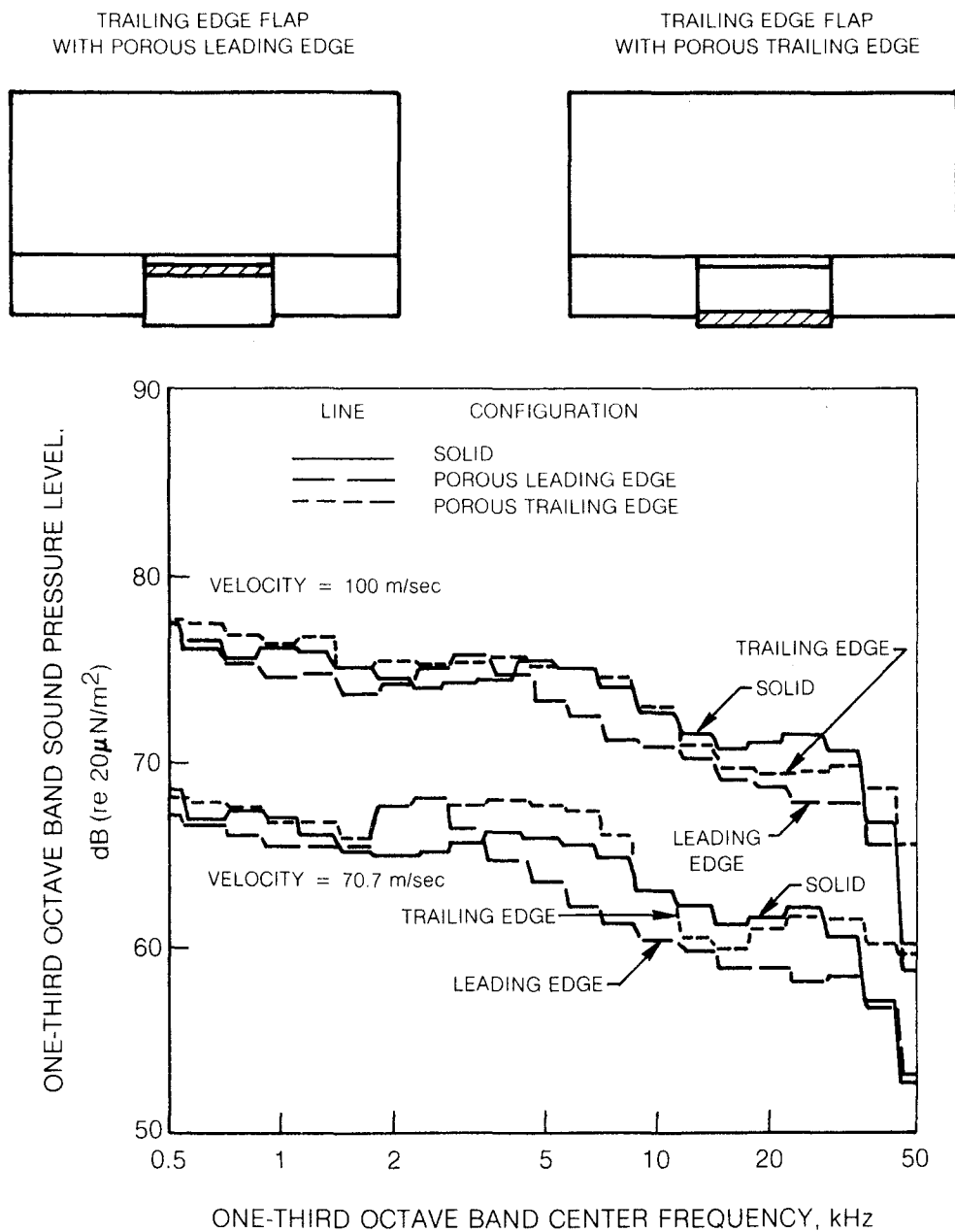
Figure 12 Effect of Porous Leading Edge and of PorousTrailing Edge on Noise Radiation Directly Below a 40° Deflection Part Span Single Slotted Trailing Edge Flap
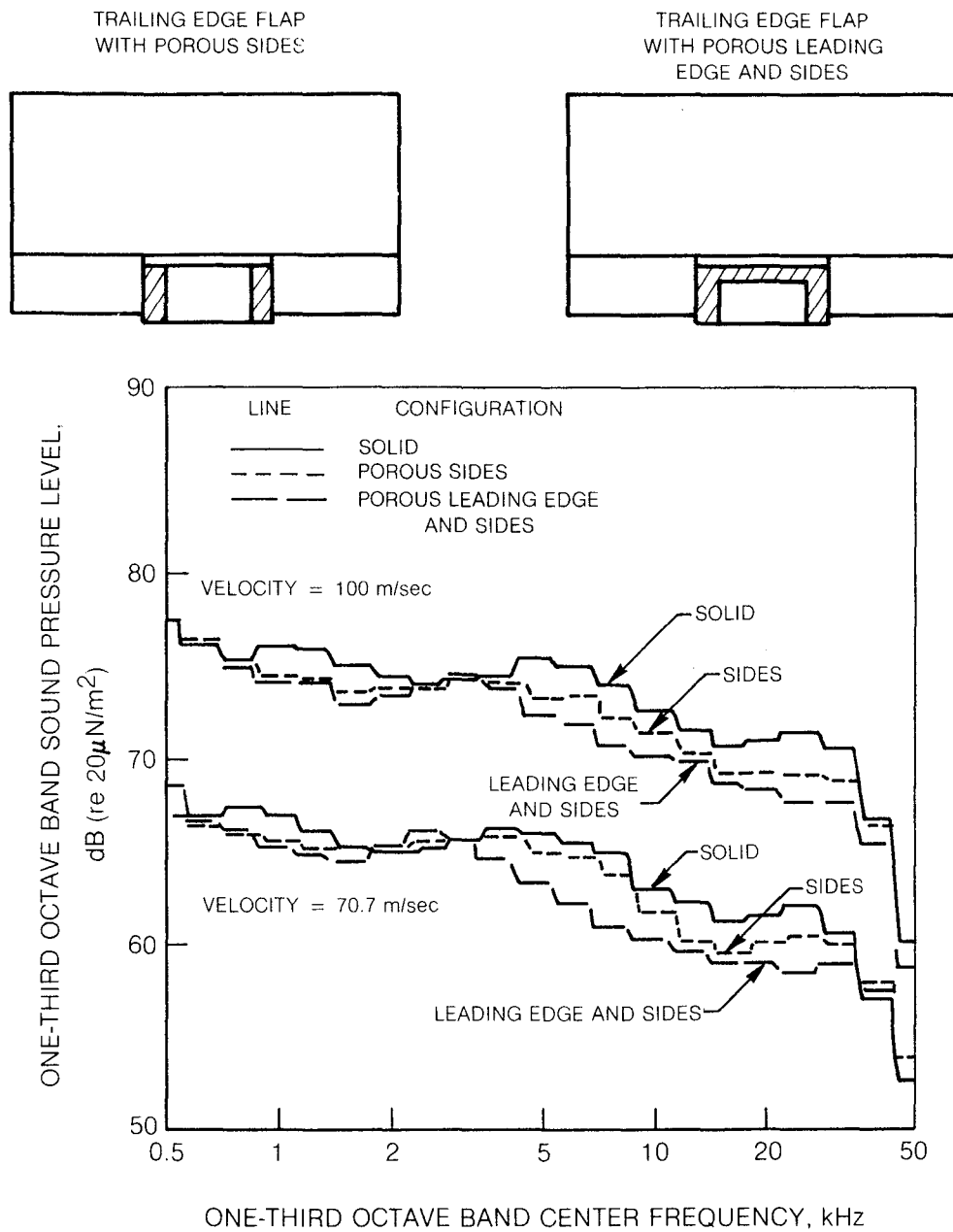
Figure 13 Effect of Porous Sides, and Porous Leading Edge and Sides, on Noise Radiation Directly Below a 40° Deflection Part Span Single Slotted Trailing Edge Flap
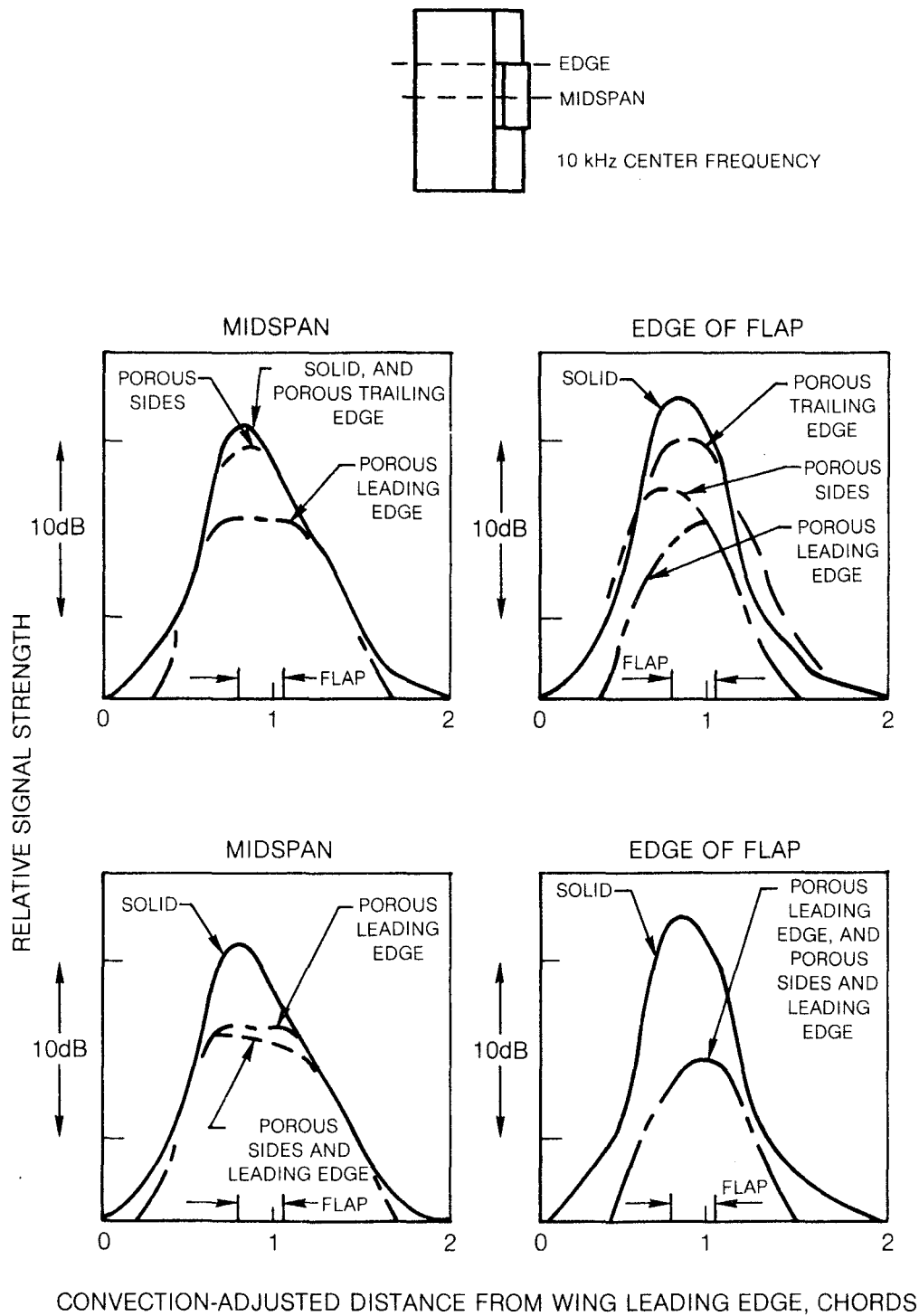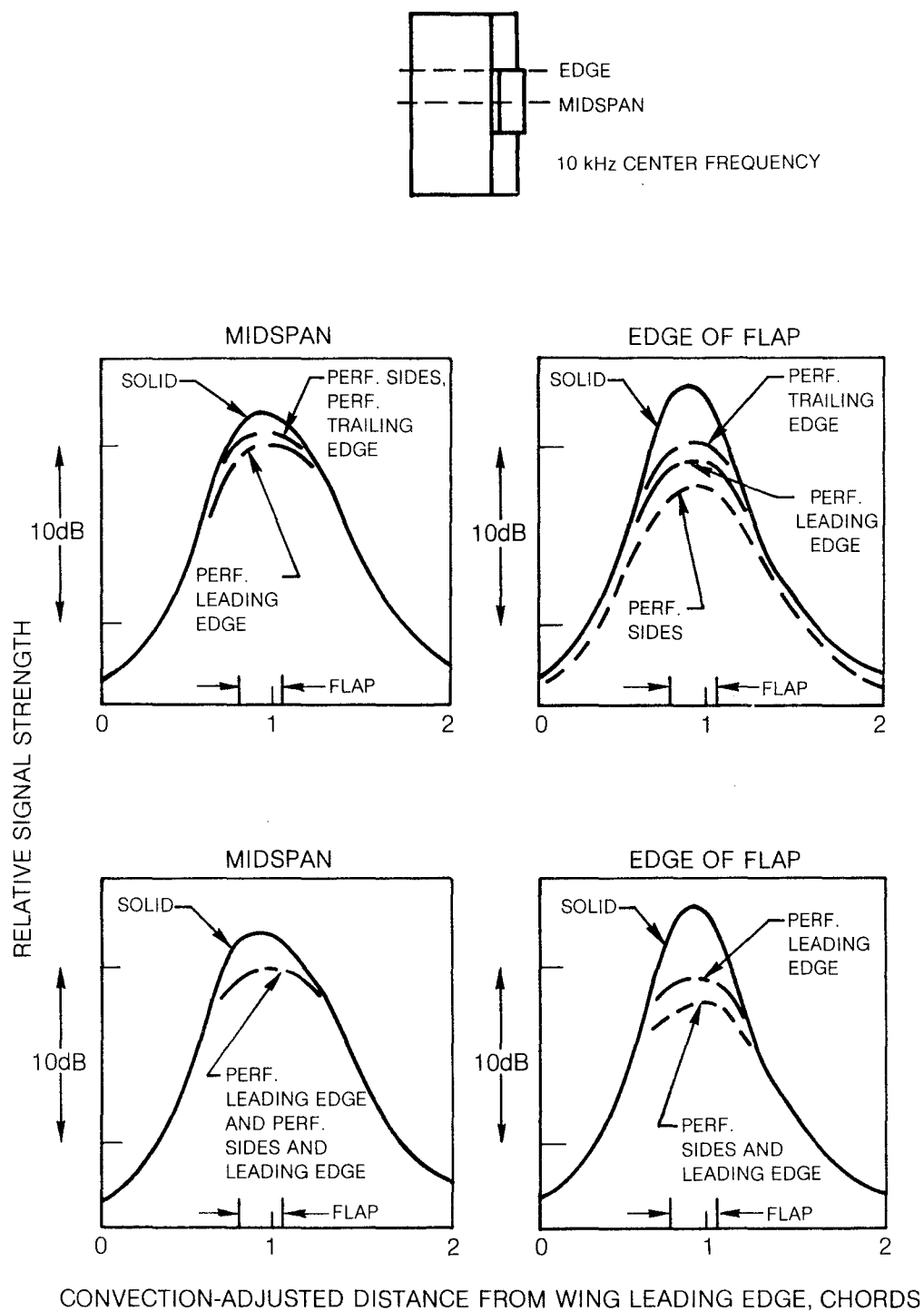
Figure 14 Effect of Porous Trailing Edge Flap Surface on Noise Source Strength
Distribution for 40° Deflection Part Span Single Slotted Trailing Edge
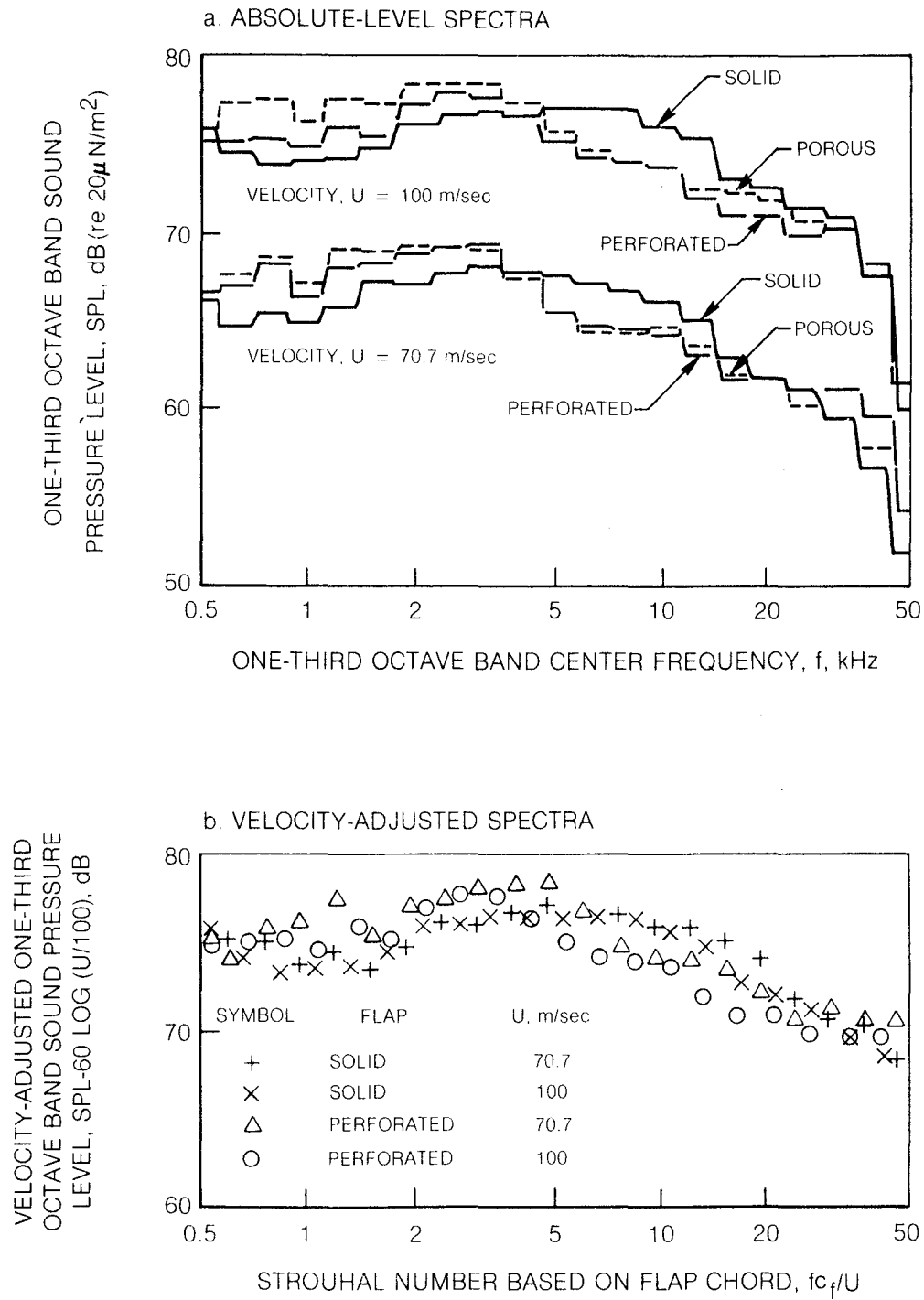Flap at 70.7 M/sec Velocity

50
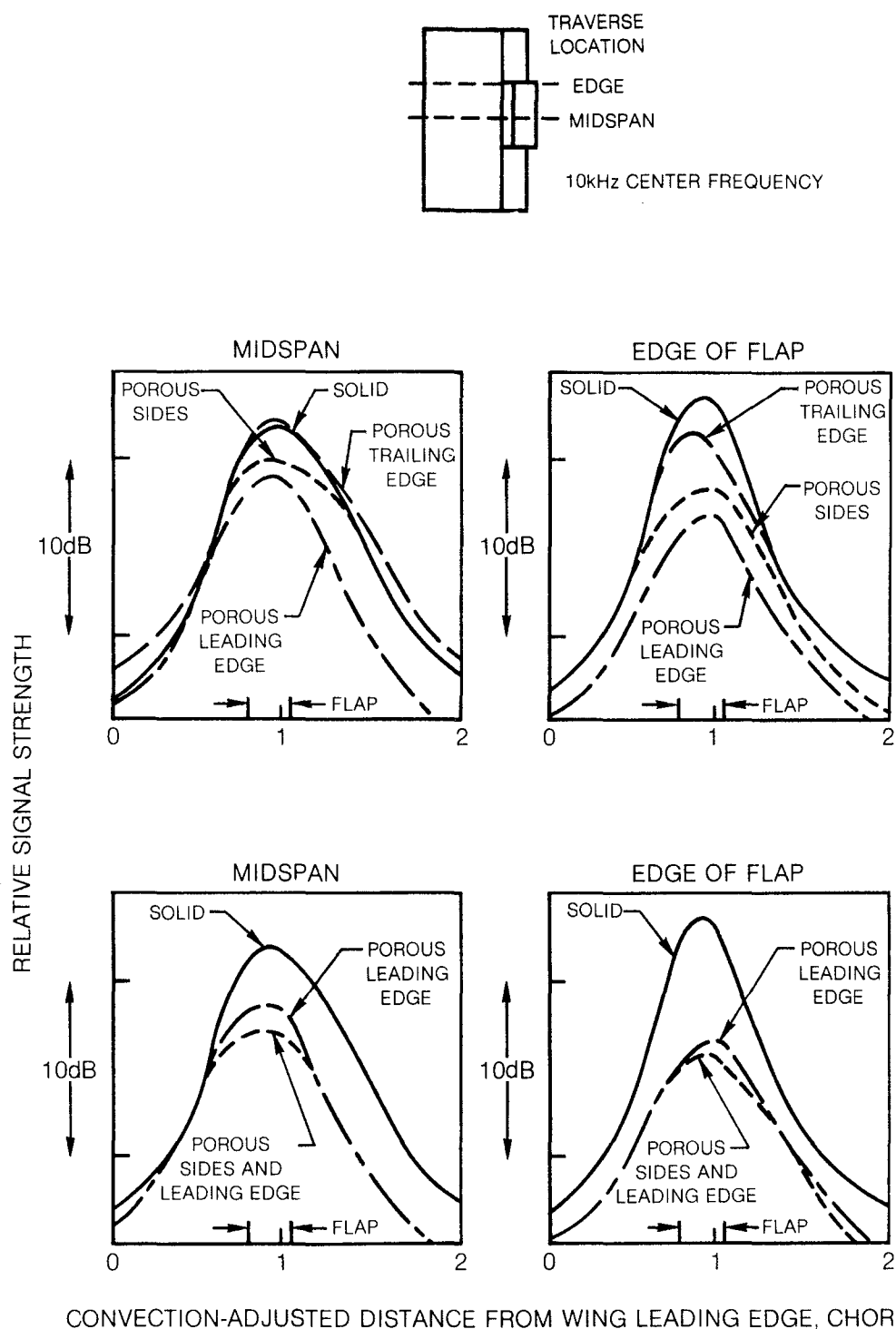
Figure 15 Effect of Porous Trailing Edge Flap Surface on Noise Source Strength Distribution for 40° Deflection Part Span Single Slotted Trailing Edge Flap at 100 M/sec Velocity

TRAILING EDGE FLAP
WITH PERFORATED
LEADING EDGE

TRAILING EDGE FLAP
WITH PERFORATED
TRAILING EDGE
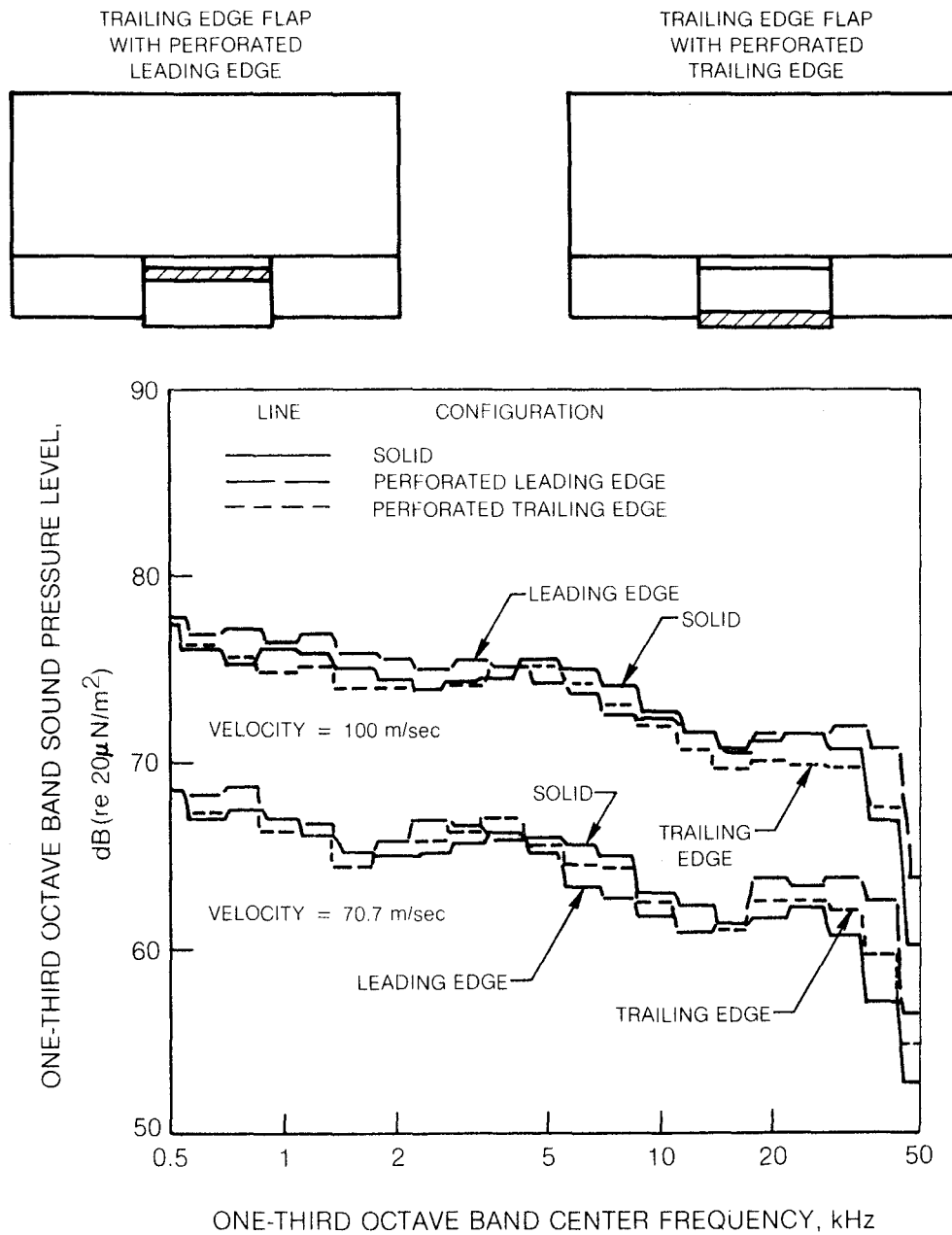
Figure 16   Effect of Perforated Leading Edge and of Perforated Trailing Edge on Noise Radiation Directly Below a 40° Deflection Part Span Single Slotted Trailing Edge Flap
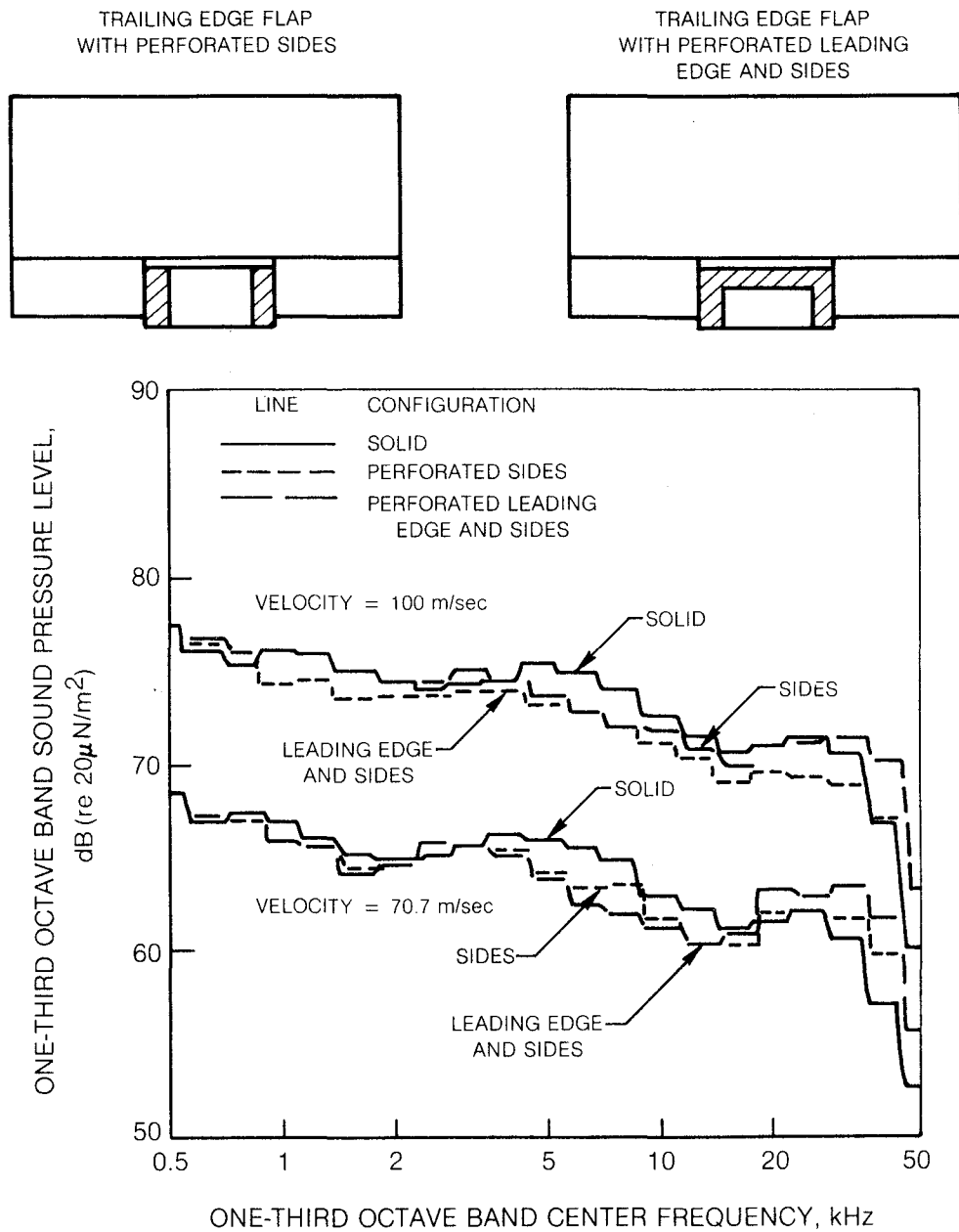
Figure 17 **Effect of Perforated Sides, and Perforated Leading Edge and Sides on Noise Radiation Directly Below a 40° Deflection Part Span Single Slotted Trailing Edge Flap**

CONVECTION-ADJUSTED DISTANCE FROM WING LEADING EDGE, CHORDS
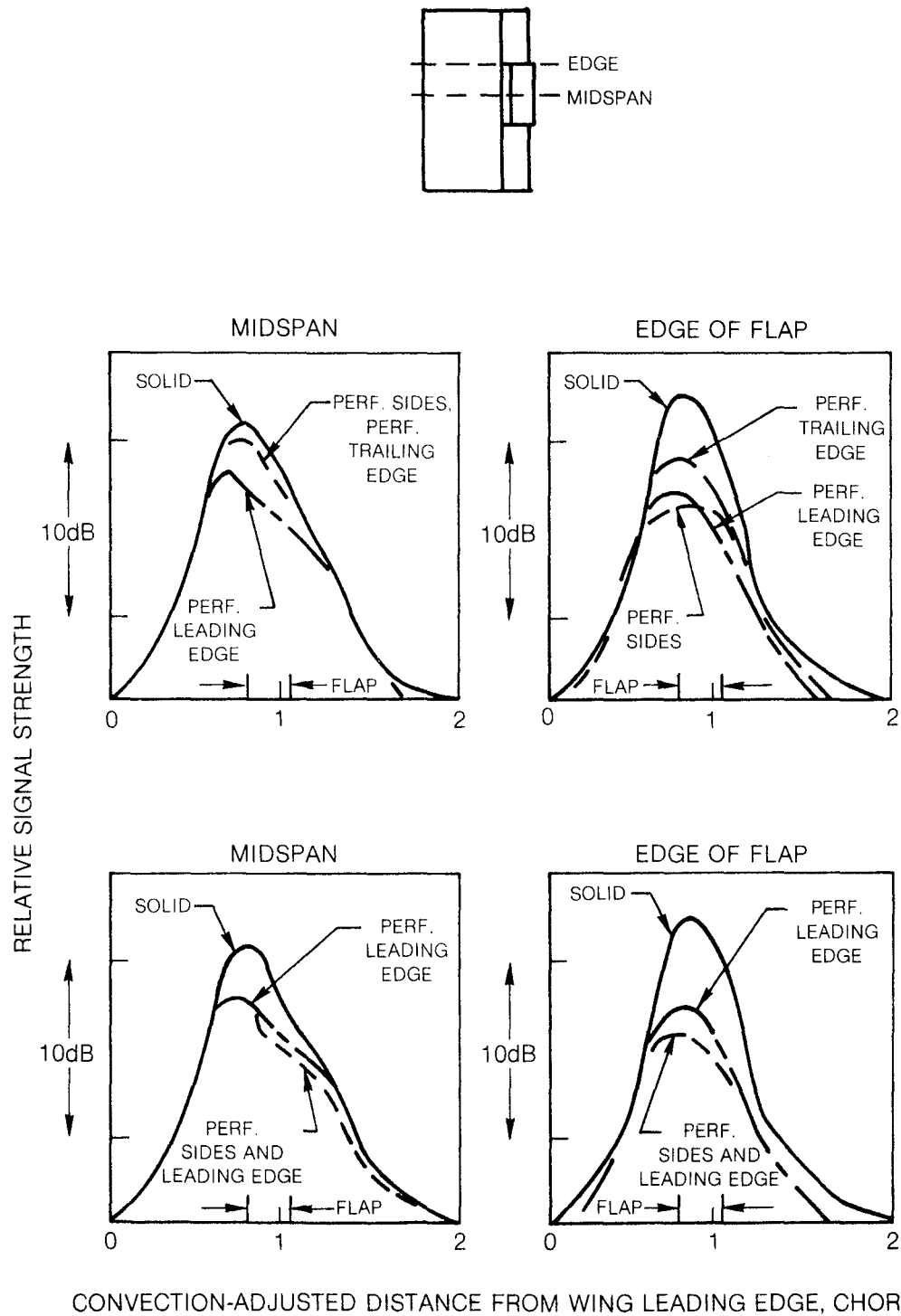
Figure 18 Effect of Perforated Trailing Edge Flap Surface on Noise Source
Strength Distribution for 40° Deflection Part Span Single Slotted
Trailing Edge Flap at 70.7 M/sec Velocity

Figure 19 Effect of Perforated Trailing Edge Flap Surface on Noise Source Strength Distribution for 40° Deflection Part Span Single Slotted Trailing Edge Flap at 100 M/sec Velocity

a. ABSOLUTE-LEVEL SPECTRA

b. VELOCITY-ADJUSTED SPECTRA

SYMBOL	FLAP	U, m/sec
+	SOLID	70.7
×	SOLID	100
△	PERFORATED	70.7
○	PERFORATED	100

Figure 20 Effect of Modifications to Aft Panel of Part Span Double Slotted Flap on Noise Radiation at 90° Microphone

56
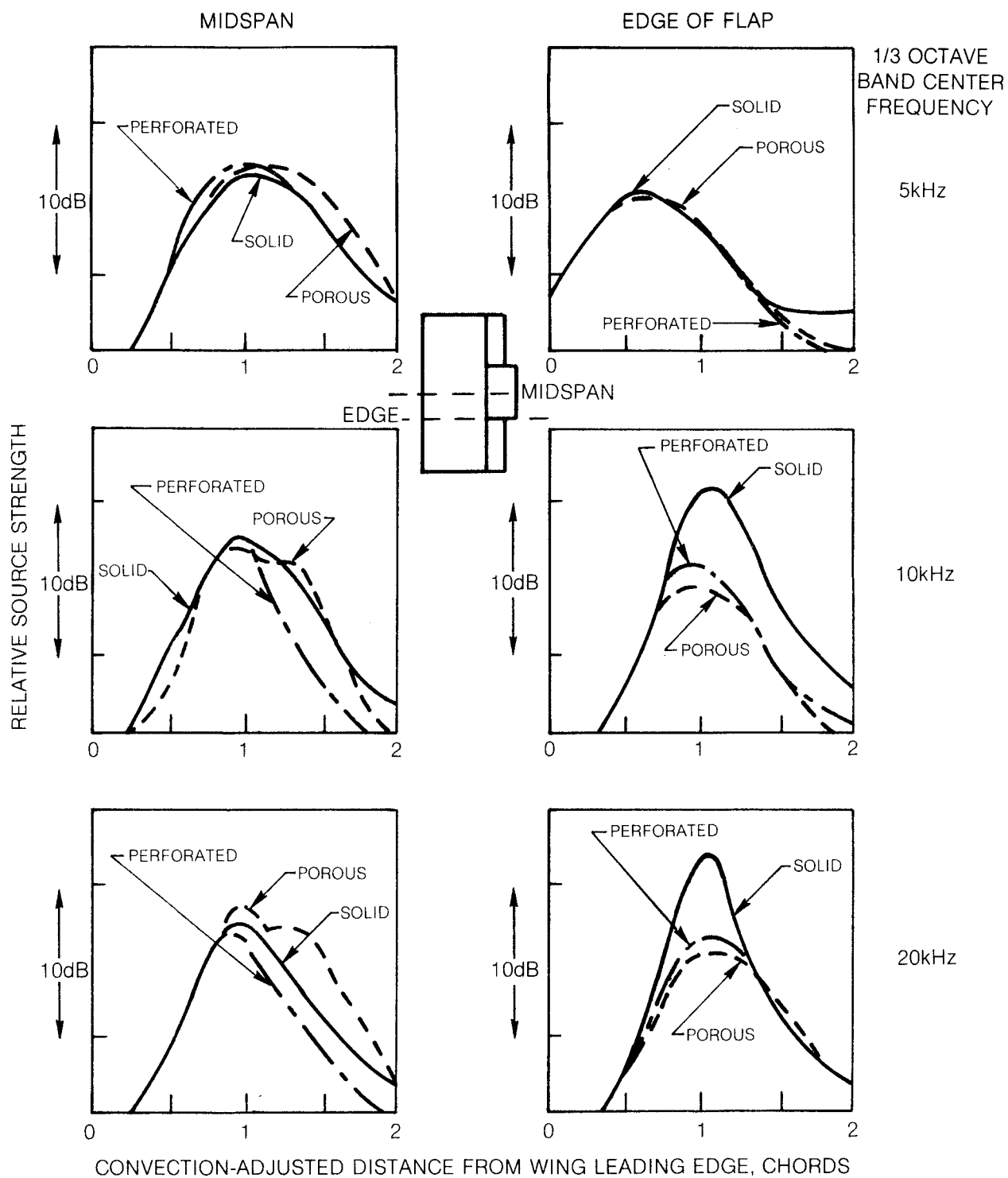
Figure 21 Effect of Modifications to Aft Panel of Part Span Double Slotted Flap on Noise Source Strength Distribution at 100 m/sec Velocity
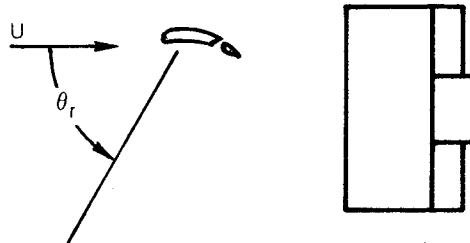
LINES ARE PREDICTED SHAPES FOR LIFT DIPOLE WITH
CONVECTIVE AMPLIFICATION, MATCHED TO DATA AT 90°

a. SINGLE SLOTTED 40° DEFLECTION PART SPAN TRAILING EDGE FLAP
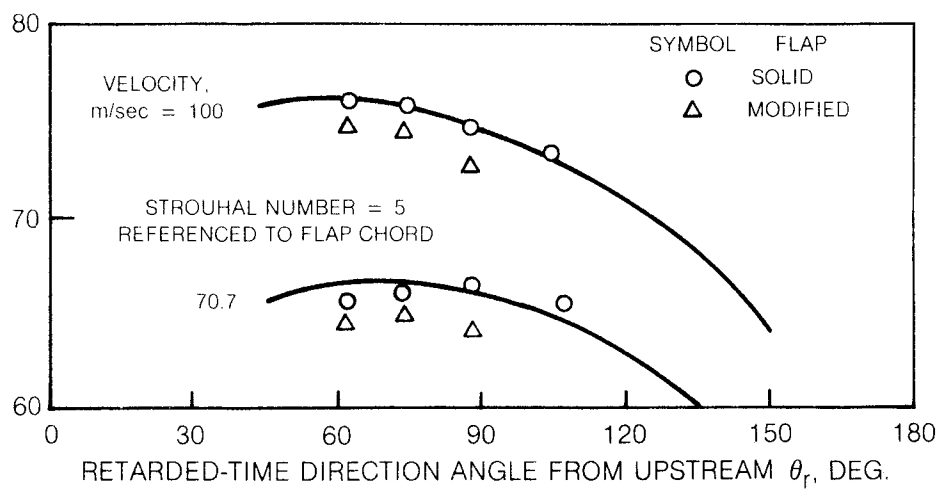
b. DOUBLE SLOTTED 40° DEFLECTION PART SPAN TRAILING EDGE FLAP
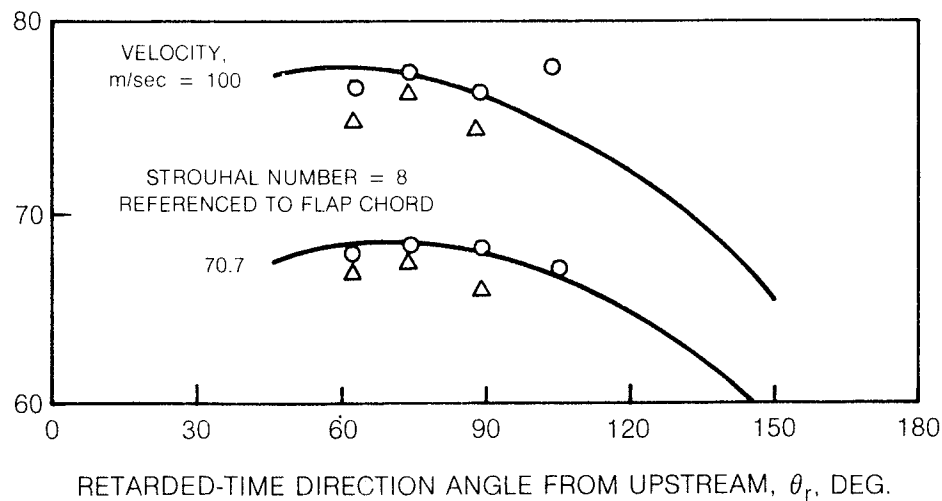
**Figure 22   Directivity of Wing With Single or Double Slotted Trailing Edge Flap Having
Solid or Modified Surfaces**

58

Figure 23 Effect of Modified Trailing Edge Flap on Noise Radiation Directly Below a
Leading Edge Flap, Trailing Edge Flap Configuration

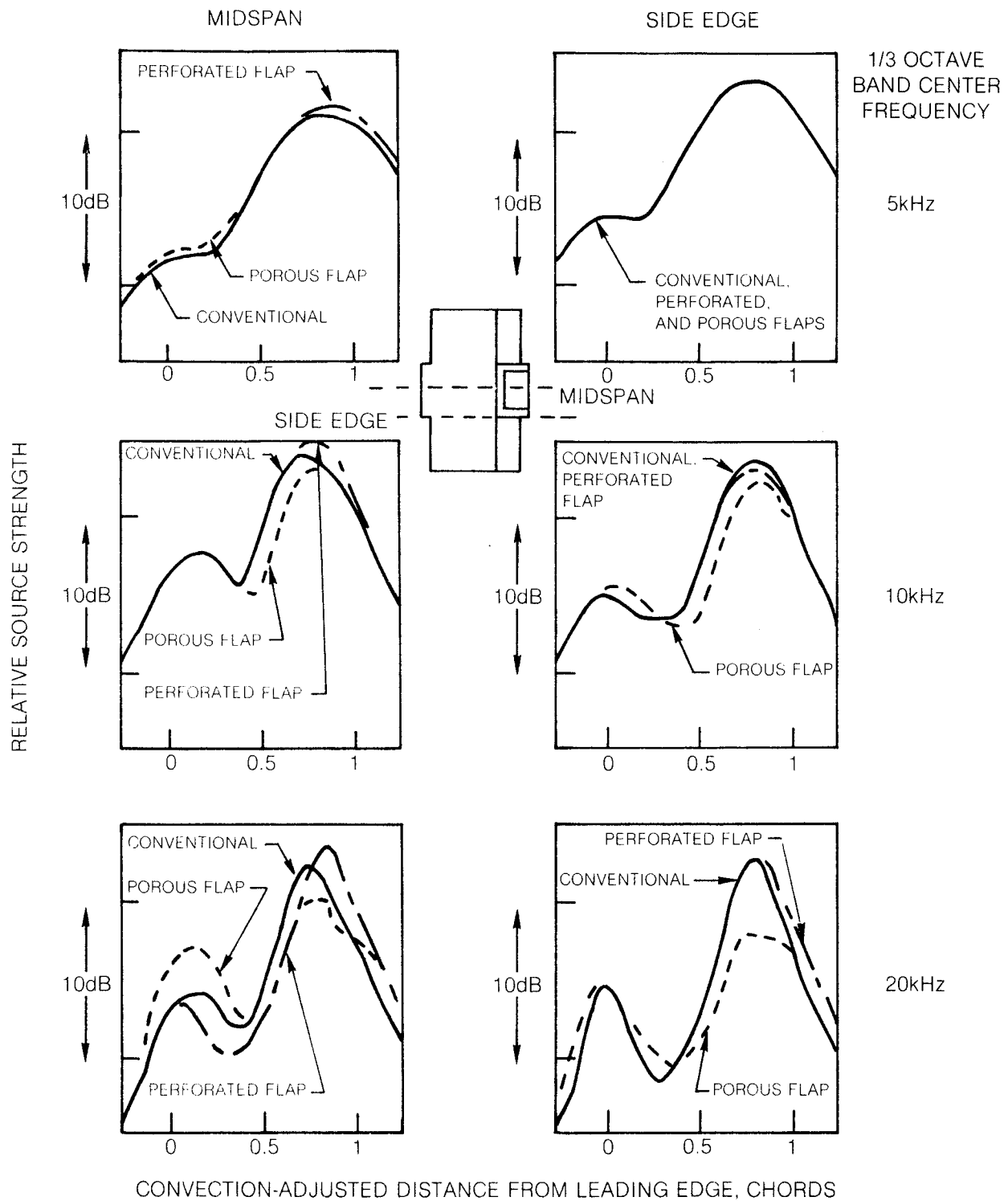MIDSPAN　　　　　　　　　　SIDE EDGE

1/3 OCTAVE
BAND CENTER
FREQUENCY

PERFORATED FLAP

10dB

POROUS FLAP

CONVENTIONAL

0   0.5   1

10dB

CONVENTIONAL,
PERFORATED,
AND POROUS FLAPS

0   0.5   1

5kHz

SIDE EDGE

MIDSPAN

CONVENTIONAL

10dB

POROUS FLAP

PERFORATED FLAP

0   0.5   1

CONVENTIONAL,
PERFORATED
FLAP

10dB

POROUS FLAP

0   0.5   1

10kHz

RELATIVE SOURCE STRENGTH

CONVENTIONAL

POROUS FLAP

10dB

PERFORATED FLAP

0   0.5   1

PERFORATED FLAP

CONVENTIONAL

10dB

POROUS FLAP

0   0.5   1

20kHz

CONVECTION-ADJUSTED DISTANCE FROM LEADING EDGE, CHORDS

**Figure 24   Effect of Modified Trailing Edge Flap on Noise Source Strength
Distribution for Leading Edge Flap, Trailing Edge Flap Combination at
70.7 m/sec Velocity**

60
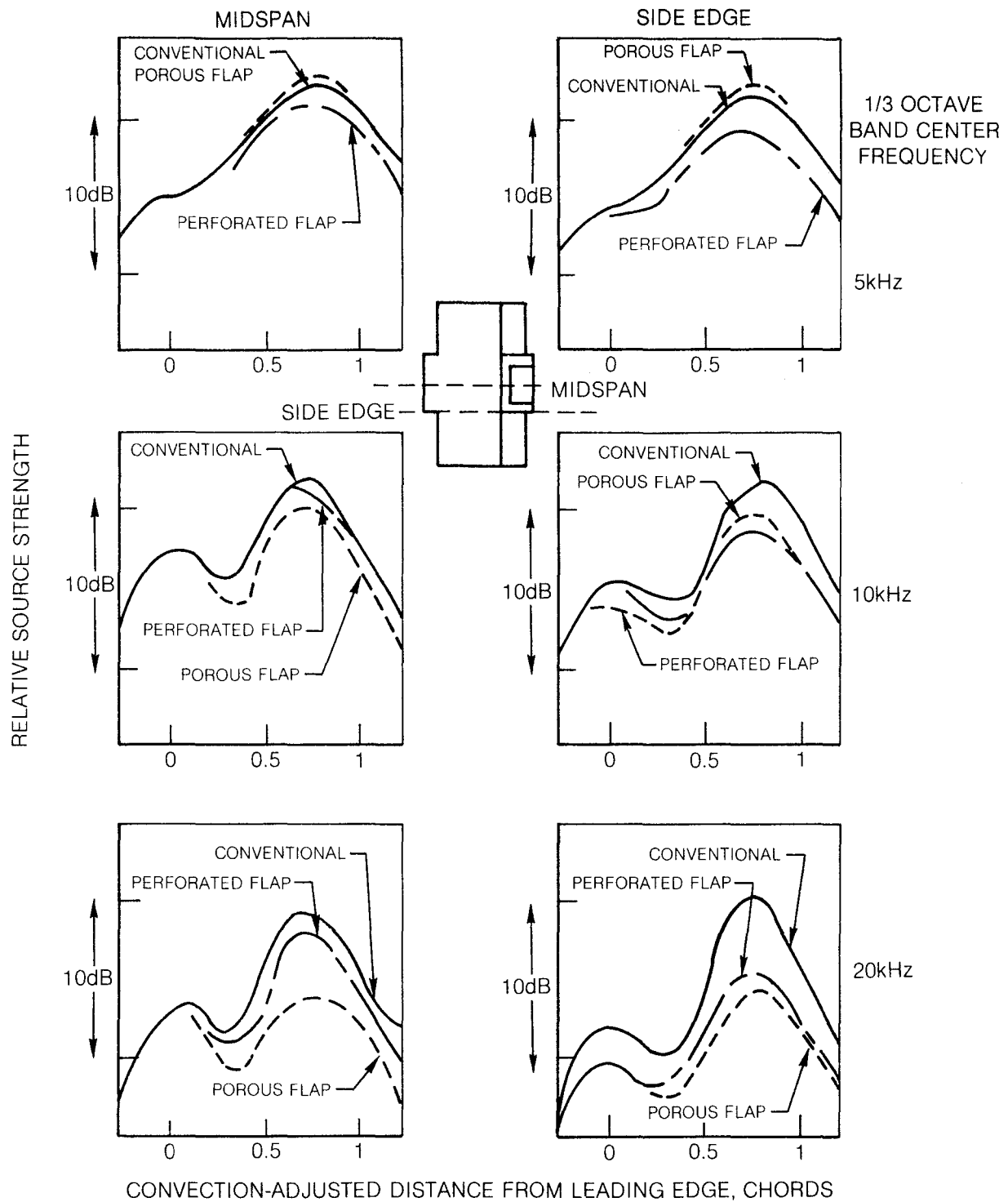
Figure 25 Effect of Modified Trailing Edge Flap on Noise Source Strength Distribution for Leading Edge Flap, Trailing Edge Flap Combination at 100 m/sec Velocity
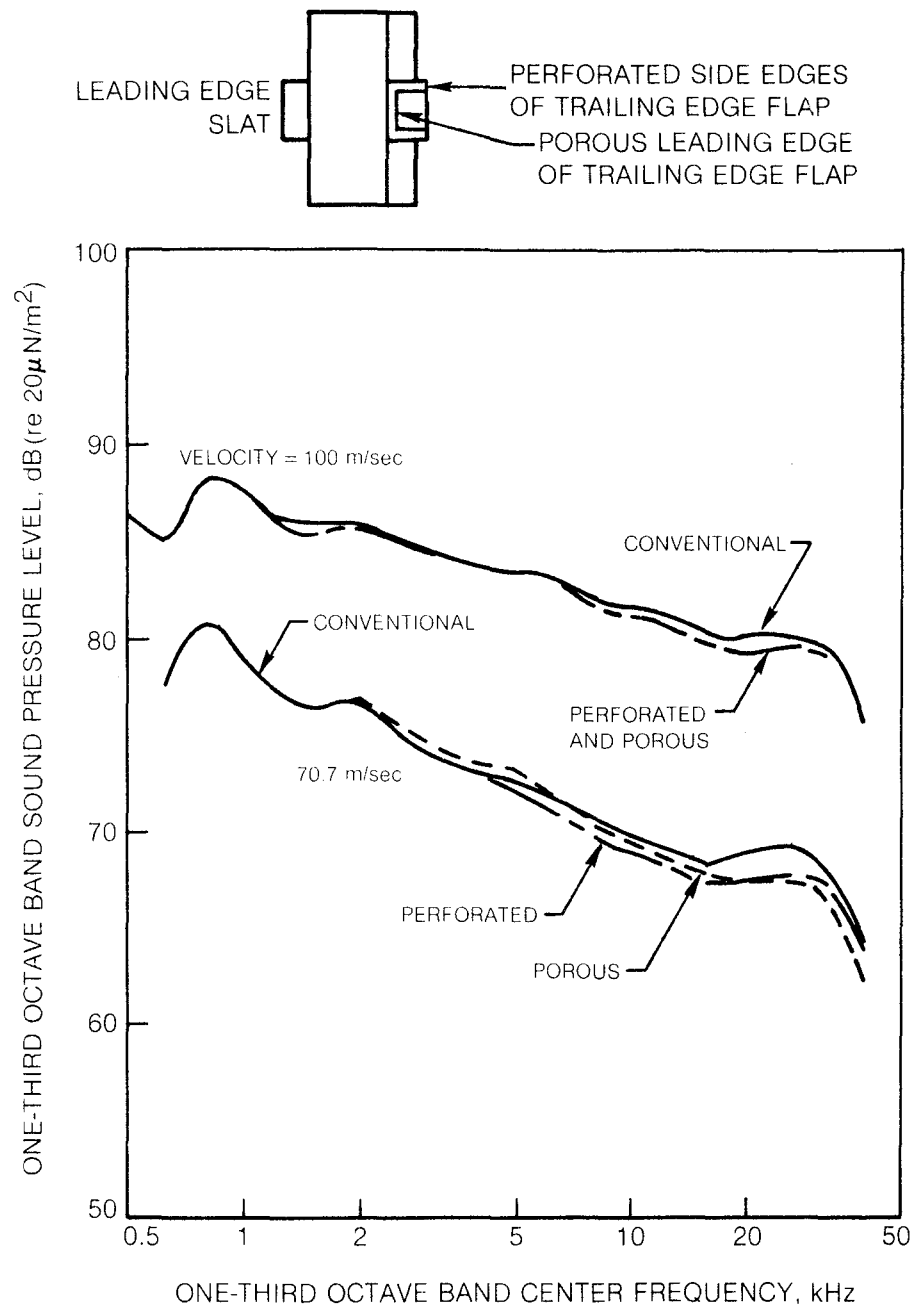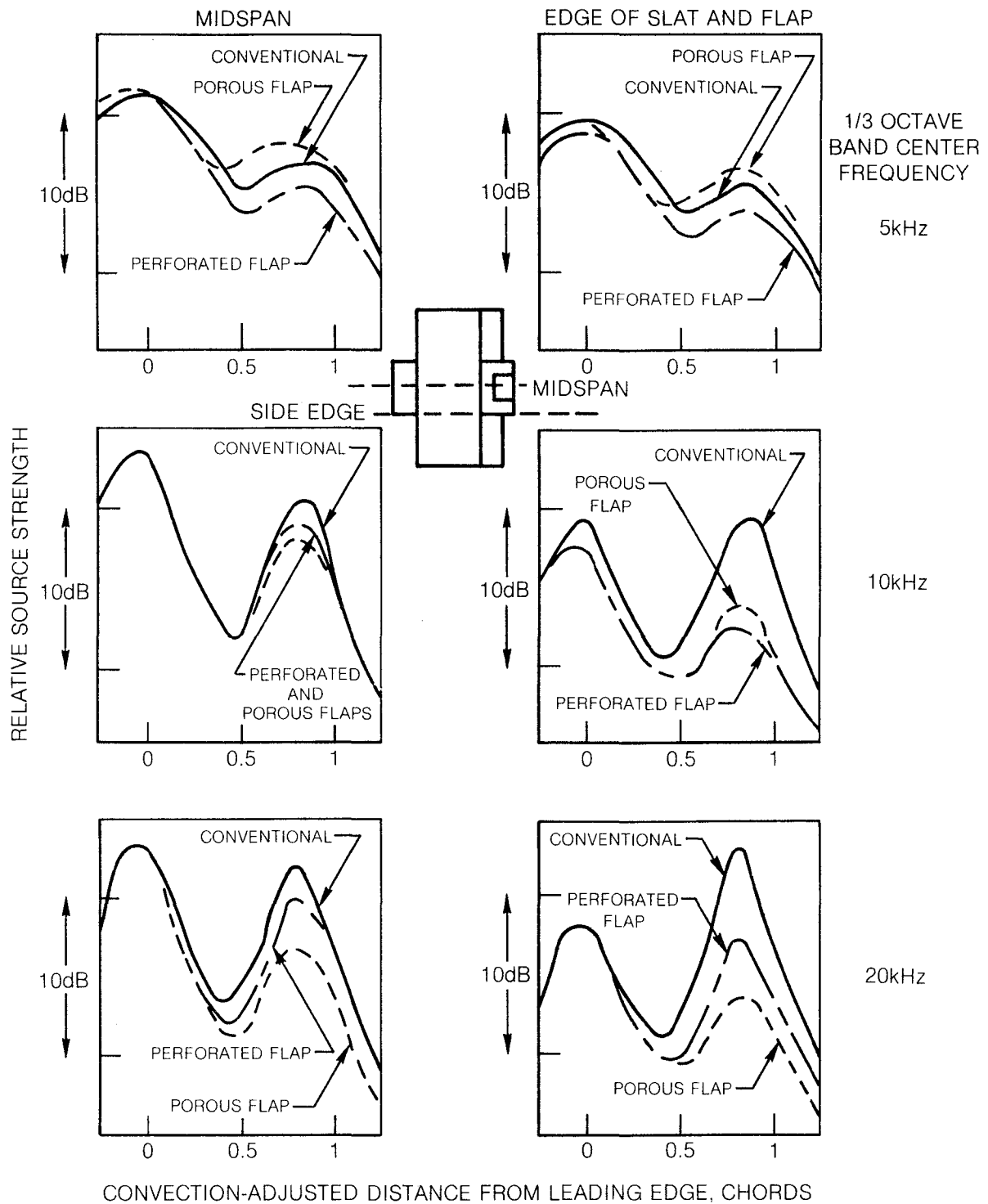
Figure 26 **Effect of Modified Trailing Edge Flap on Noise Radiation Directly Below a Leading Edge Slat, Trailing Edge Flap Configuration**

Figure 27 Effect of Modified Trailing Edge Flap on Noise Source Strength Distribution for Leading Edge Slat, Trailing Edge Flap Configuration at 70.7 m/sec Velocity
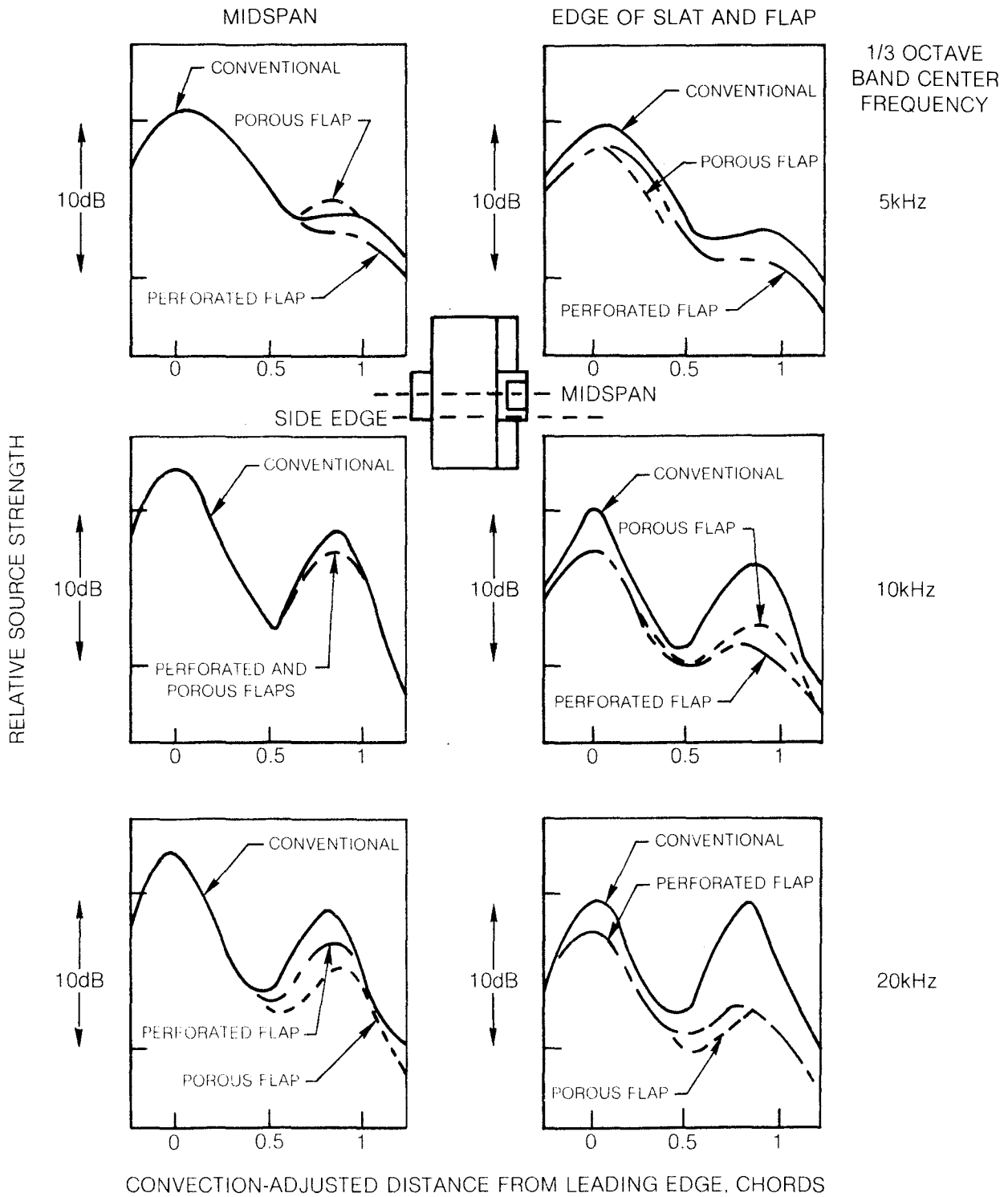
63

Figure 28 Effect of Modified Trailing Edge Flap on Noise Source Strength Distribution for Leading Edge Slat, Trailing Edge Flap Configuration at 100 m/sec Veocity
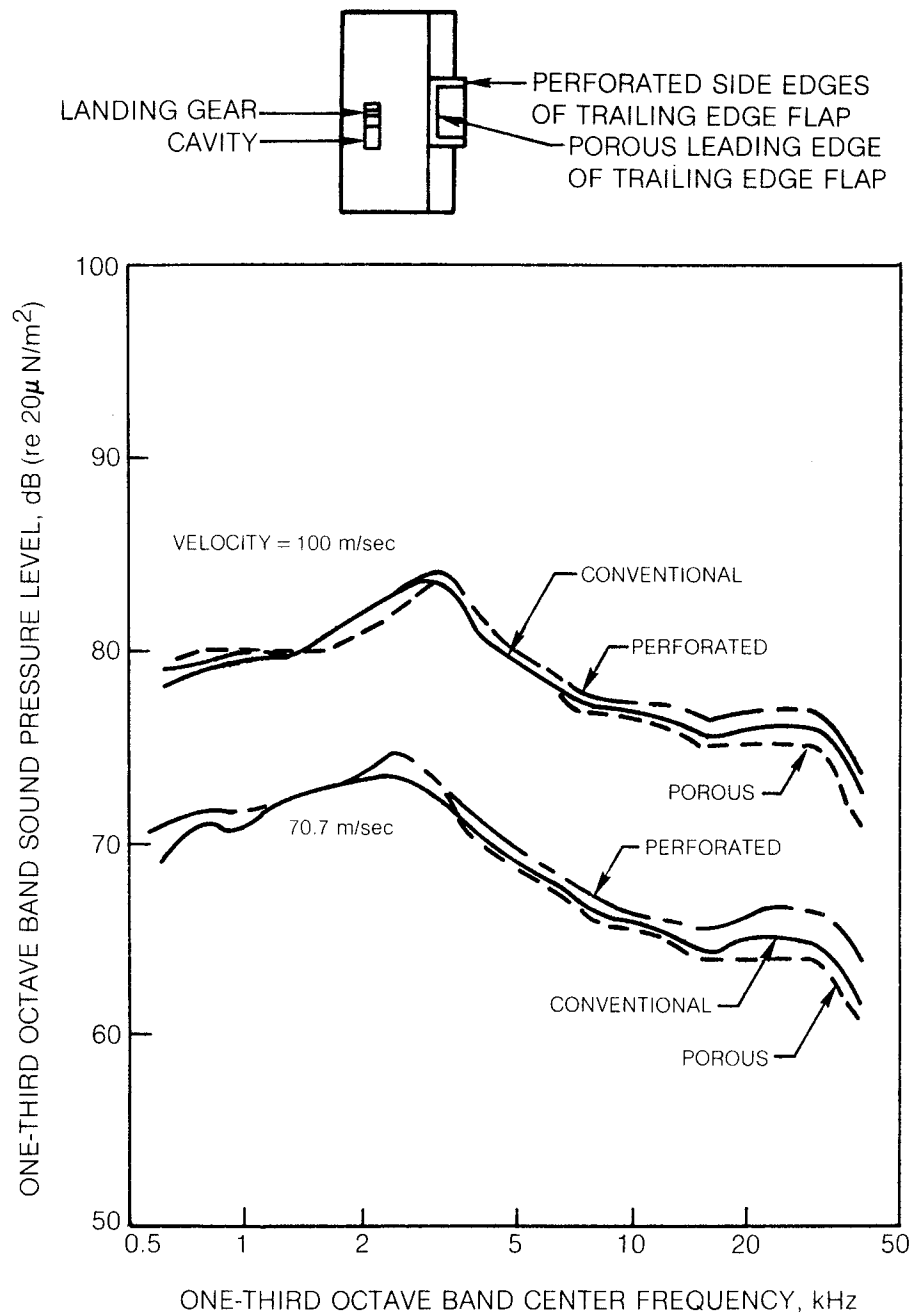
Figure 29 Effect of Modified Trailing Edge Flap on Noise Radiation Directly Below a Midspan Landing Gear, Trailing Edge Flap Configuration
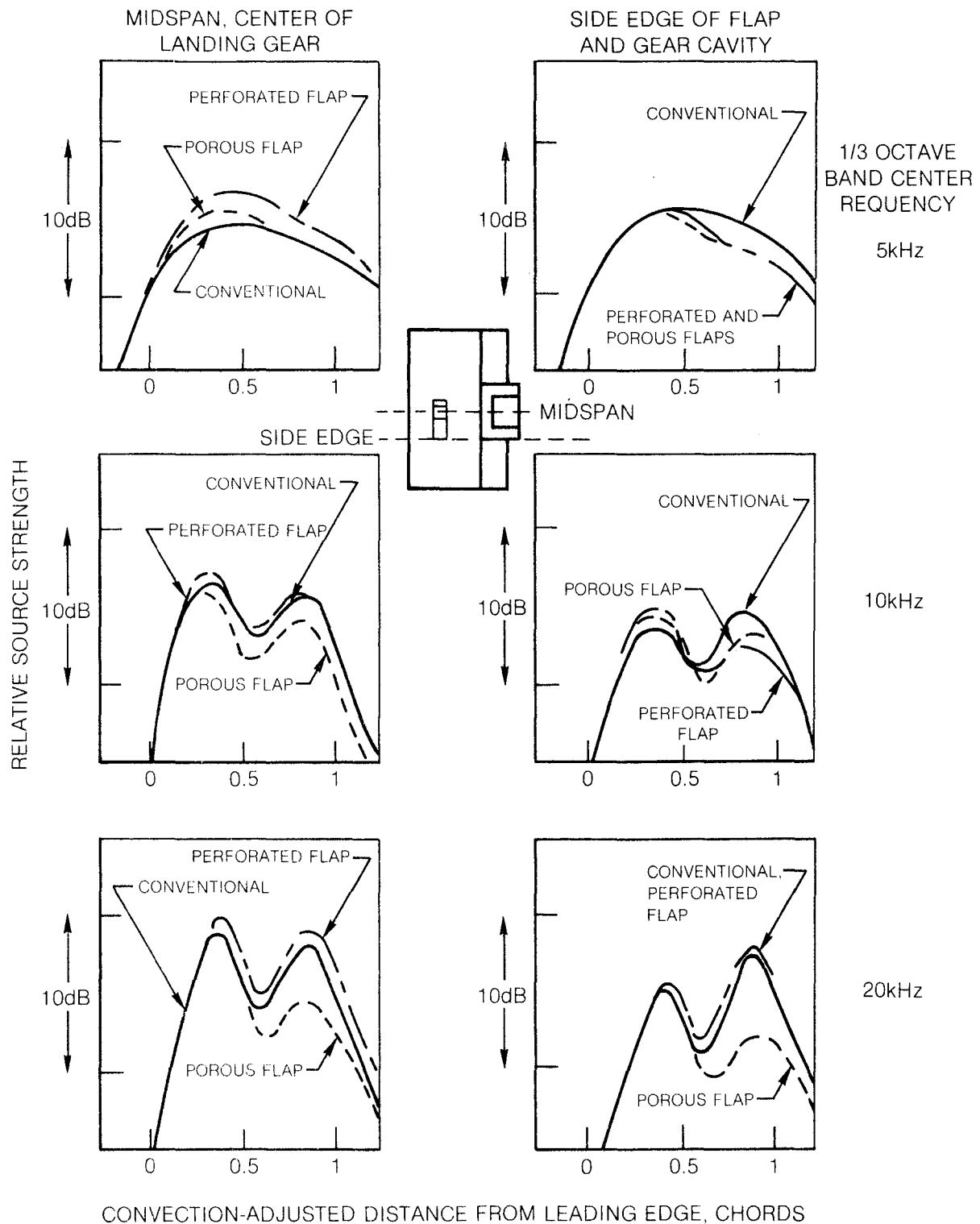
Figure 30 Effect of Modified Trailing Edge Flap on Noise Source Strength Distribution for Midspan Landing Gear, Trailing Edge Flap Configuration at 70.7 m/sec Velocity
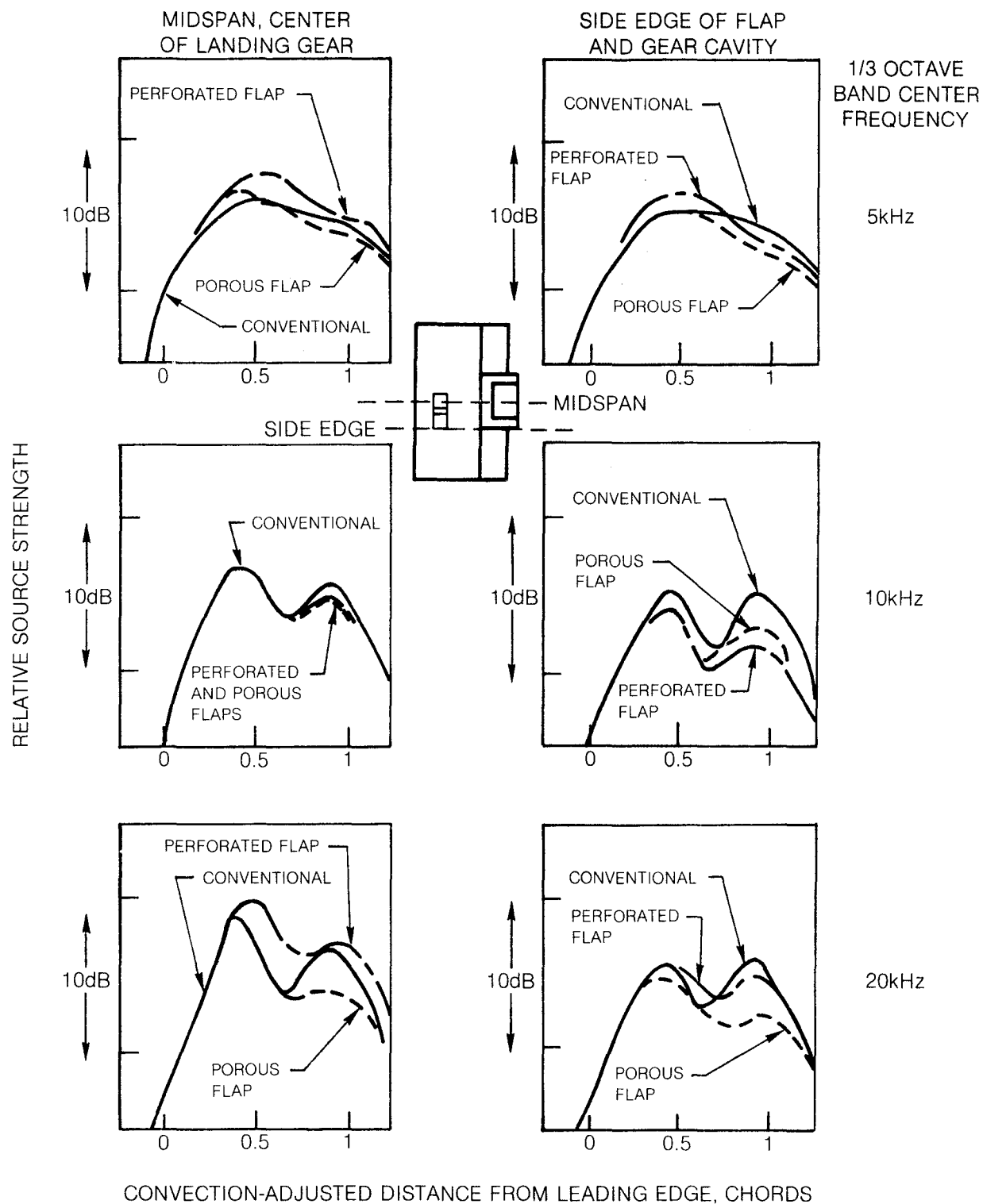
MIDSPAN, CENTER
OF LANDING GEAR

SIDE EDGE OF FLAP
AND GEAR CAVITY

1/3 OCTAVE
BAND CENTER
FREQUENCY

PERFORATED FLAP

CONVENTIONAL

PERFORATED
FLAP

5kHz

10dB

10dB

POROUS FLAP

CONVENTIONAL

POROUS FLAP

0   0.5   1

0   0.5   1

MIDSPAN

SIDE EDGE

CONVENTIONAL

CONVENTIONAL

POROUS
FLAP

10dB

10dB

10kHz

PERFORATED
AND POROUS
FLAPS

PERFORATED
FLAP

RELATIVE SOURCE STRENGTH

0   0.5   1

0   0.5   1

PERFORATED FLAP

CONVENTIONAL

CONVENTIONAL

PERFORATED
FLAP

10dB

10dB

20kHz

POROUS
FLAP

POROUS
FLAP

0   0.5   1

0   0.5   1

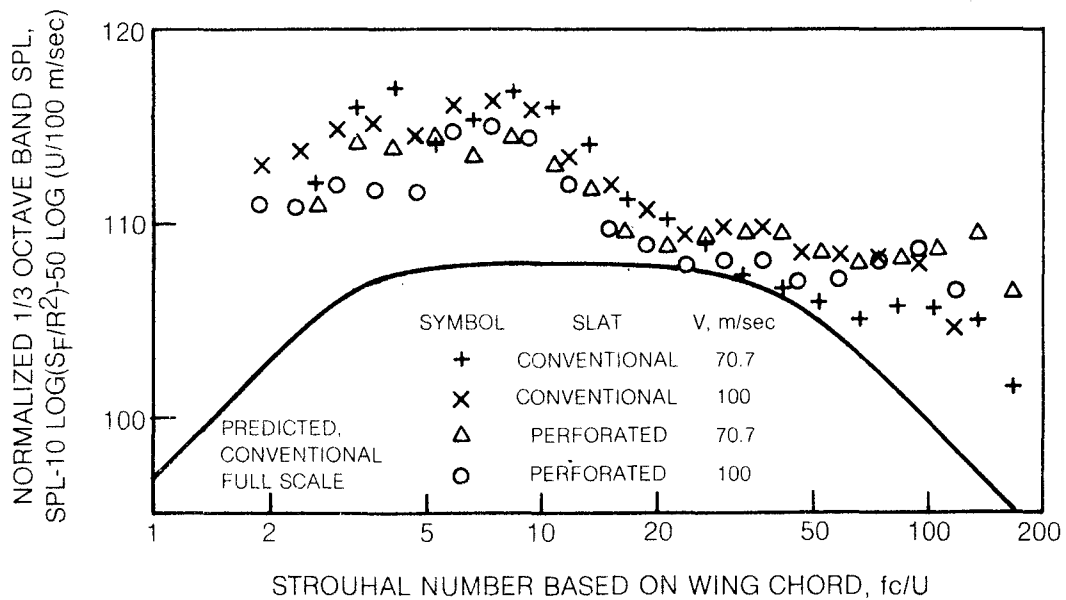CONVECTION-ADJUSTED DISTANCE FROM LEADING EDGE, CHORDS

**Figure 31 Effect of Modified Trailing Edge Flap on Noise Source Strength Distribution
for Midspan Landing Gear, Trailing Edge Flap Configuration at 100 m/sec
Velocity**

67
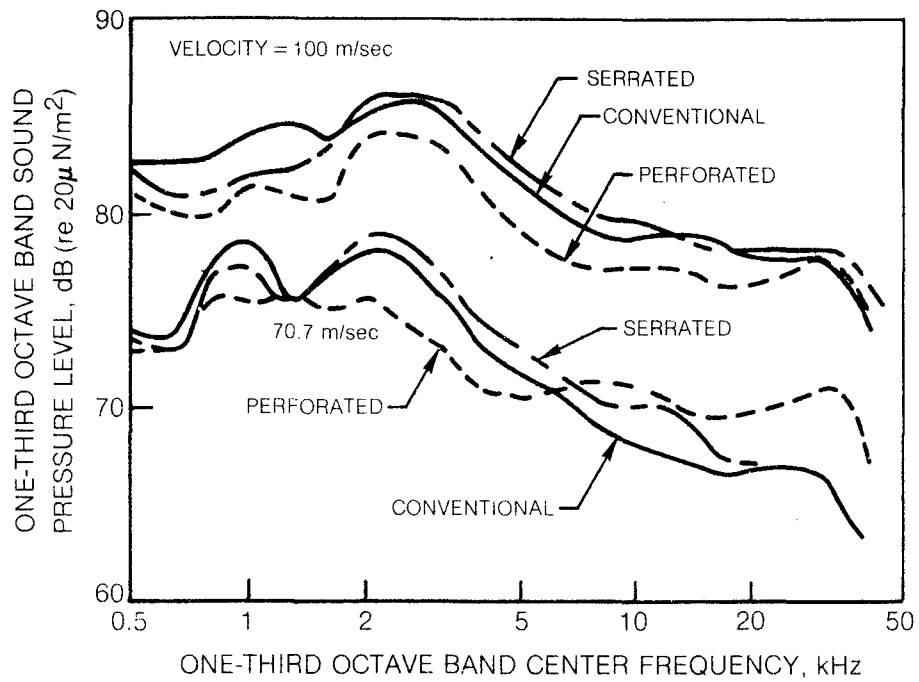
a) FAR-FIELD SPECTRA FOR WING WITH CONVENTIONAL AND MODIFIED LEADING EDGE SLATS

b) NORMALIZED FAR—FIELD SPECTRA FOR CONVENTIONAL AND PERFORATED SLAT

Figure 32 Effect of Slat Trailing Edge Modification on Far-Field Noise
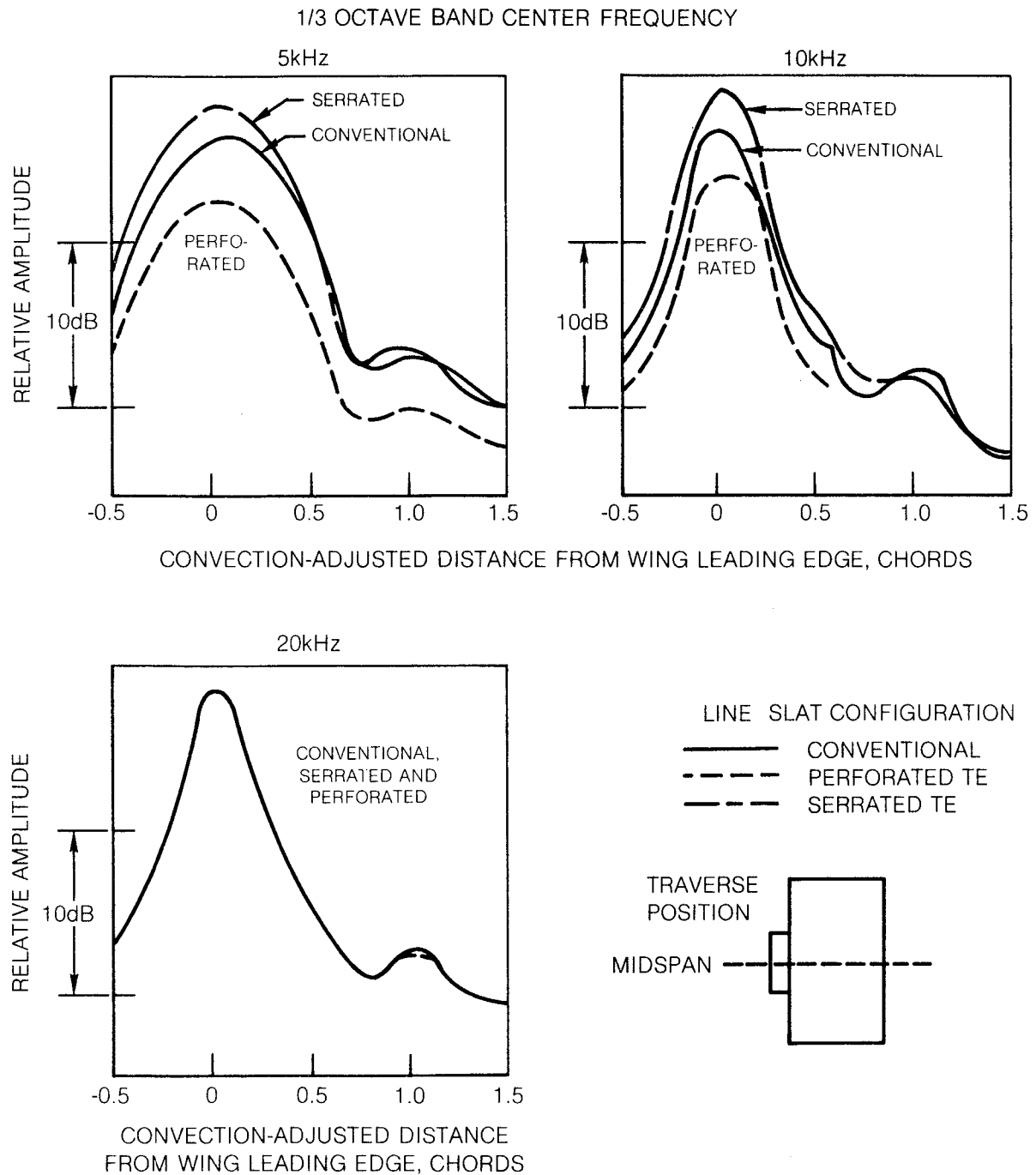
1/3 OCTAVE BAND CENTER FREQUENCY

Figure 33   Effect of Modified Trailing Edge Region of Leading Edge Slat on Noise
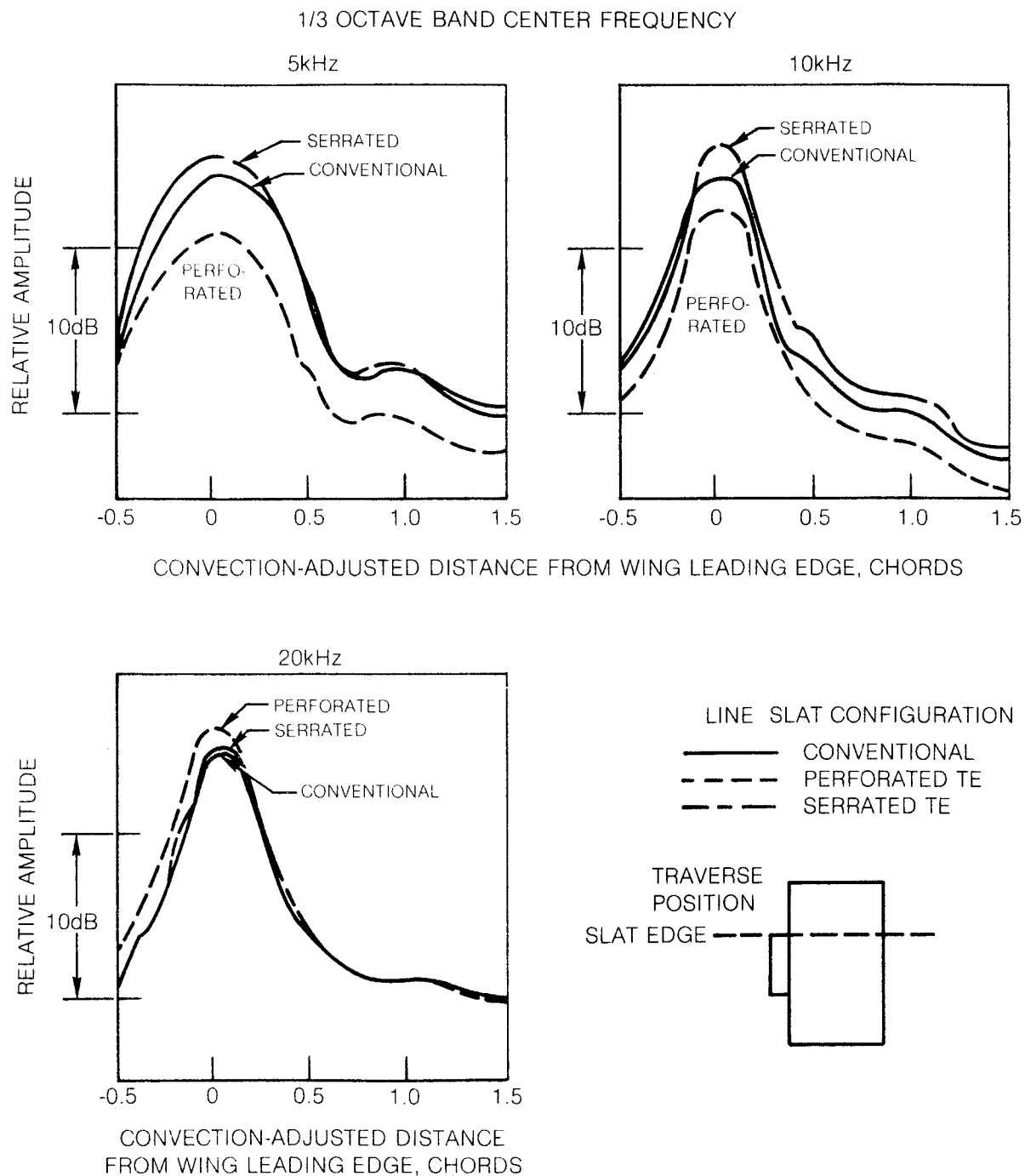Source Streamwise Distribution at Midspan for 70.7 m/sec Velocity

1/3 OCTAVE BAND CENTER FREQUENCY

5kHz

SERRATED
CONVENTIONAL

PERFO-
RATED

10dB

RELATIVE AMPLITUDE

-0.5   0   0.5   1.0   1.5

10kHz

SERRATED
CONVENTIONAL

PERFO-
RATED

10dB

-0.5   0   0.5   1.0   1.5

CONVECTION-ADJUSTED DISTANCE FROM WING LEADING EDGE, CHORDS

20kHz

PERFORATED
SERRATED

CONVENTIONAL

10dB

RELATIVE AMPLITUDE

-0.5   0   0.5   1.0   1.5

CONVECTION-ADJUSTED DISTANCE
FROM WING LEADING EDGE, CHORDS

LINE   SLAT CONFIGURATION

———————   CONVENTIONAL
— — — —   PERFORATED TE
— — —   SERRATED TE

TRAVERSE
POSITION
SLAT EDGE — — —

**Figure 34   Effect of Modified Trailing Edge Region of Leading Edge Slat on Noise
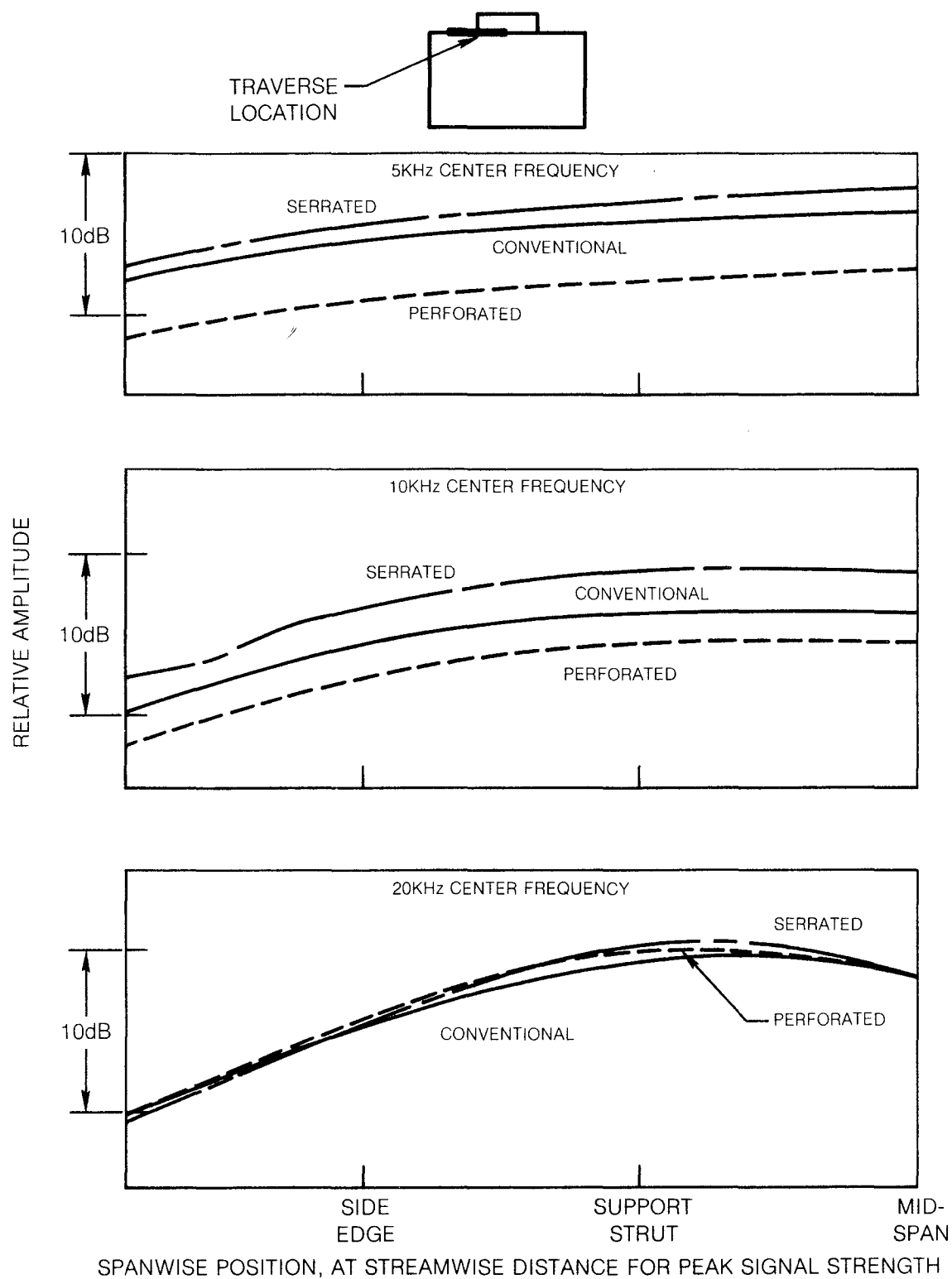Source Streamwise Distribution at Slat Edge for 70.7 m/sec Velocity**

70

Figure 35 Effect of Modified Trailing Edge Region of Leading Edge Slat on Noise Source Spanwise Distribution for 70.7 m/sec Velocity
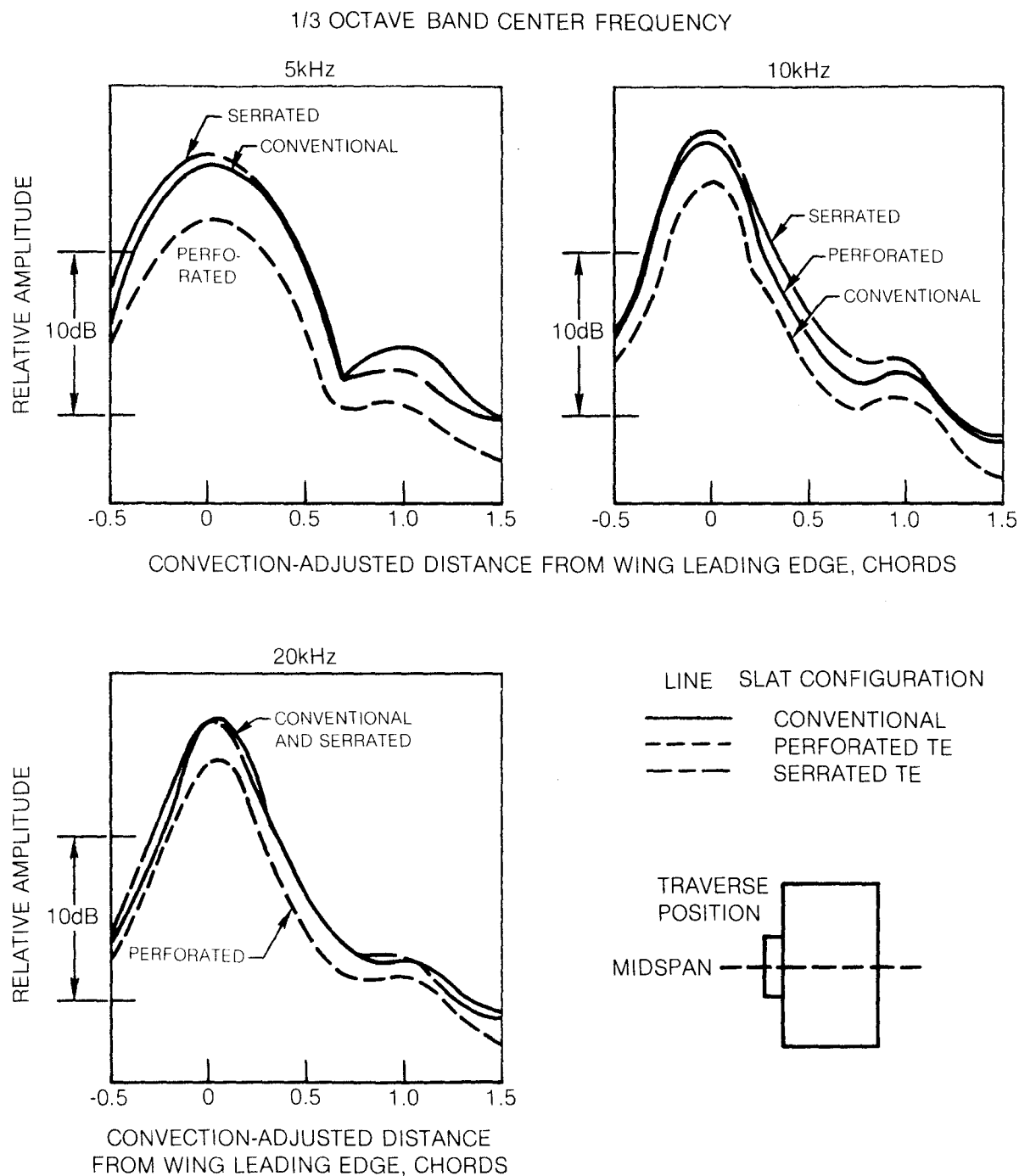
1/3 OCTAVE BAND CENTER FREQUENCY

Figure 36 Effect of Modified Trailing Edge Region of Leading Edge Slat on Noise
Source Streamwise Distribution at Midspan for 100 m/sec Velocity
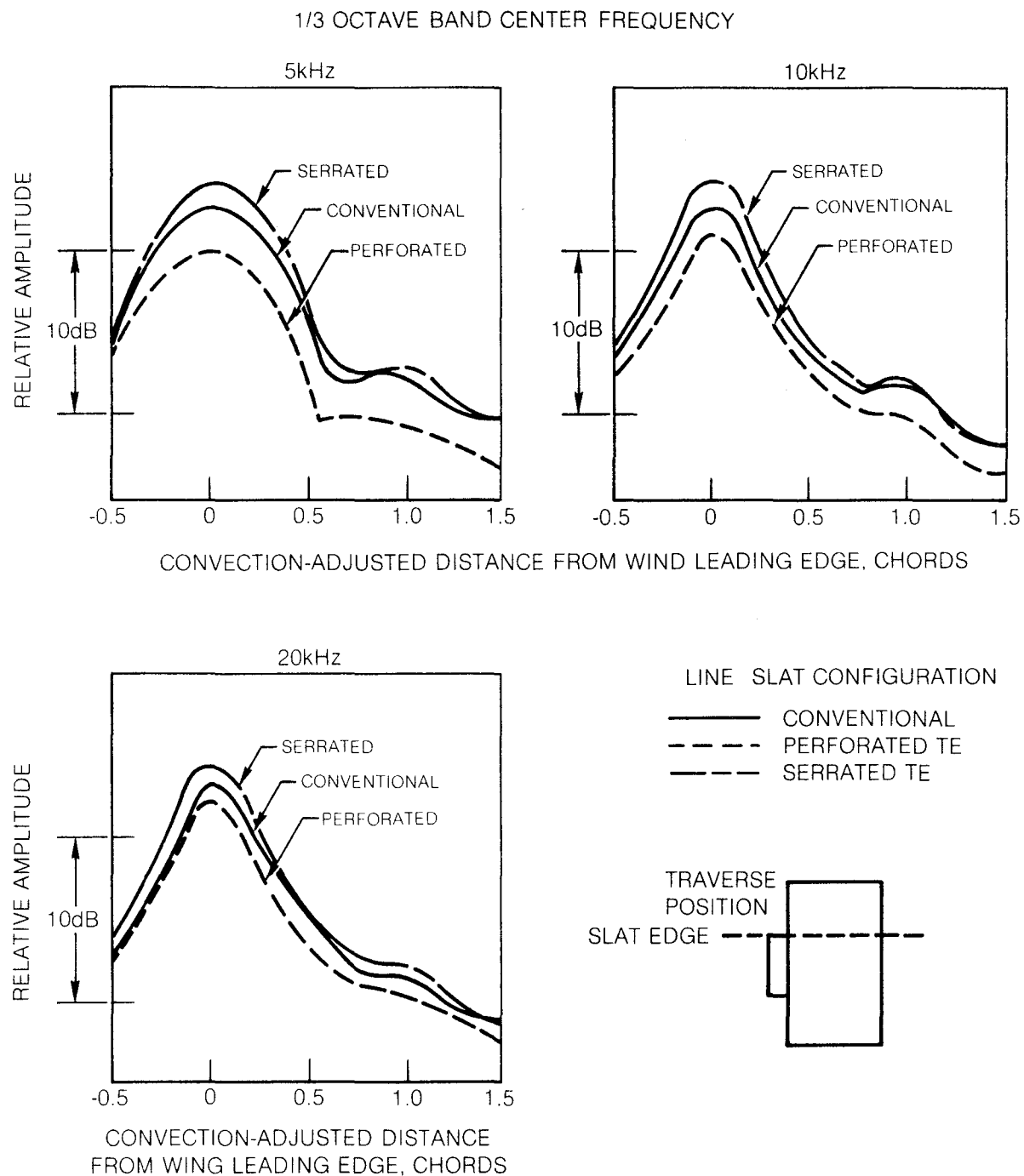
Figure 37 Effect of Modified Trailing Edge Region of Leading Edge Slat on Noise Source Streamwise Distribution at Slat Edge for 100 m/sec Velocity
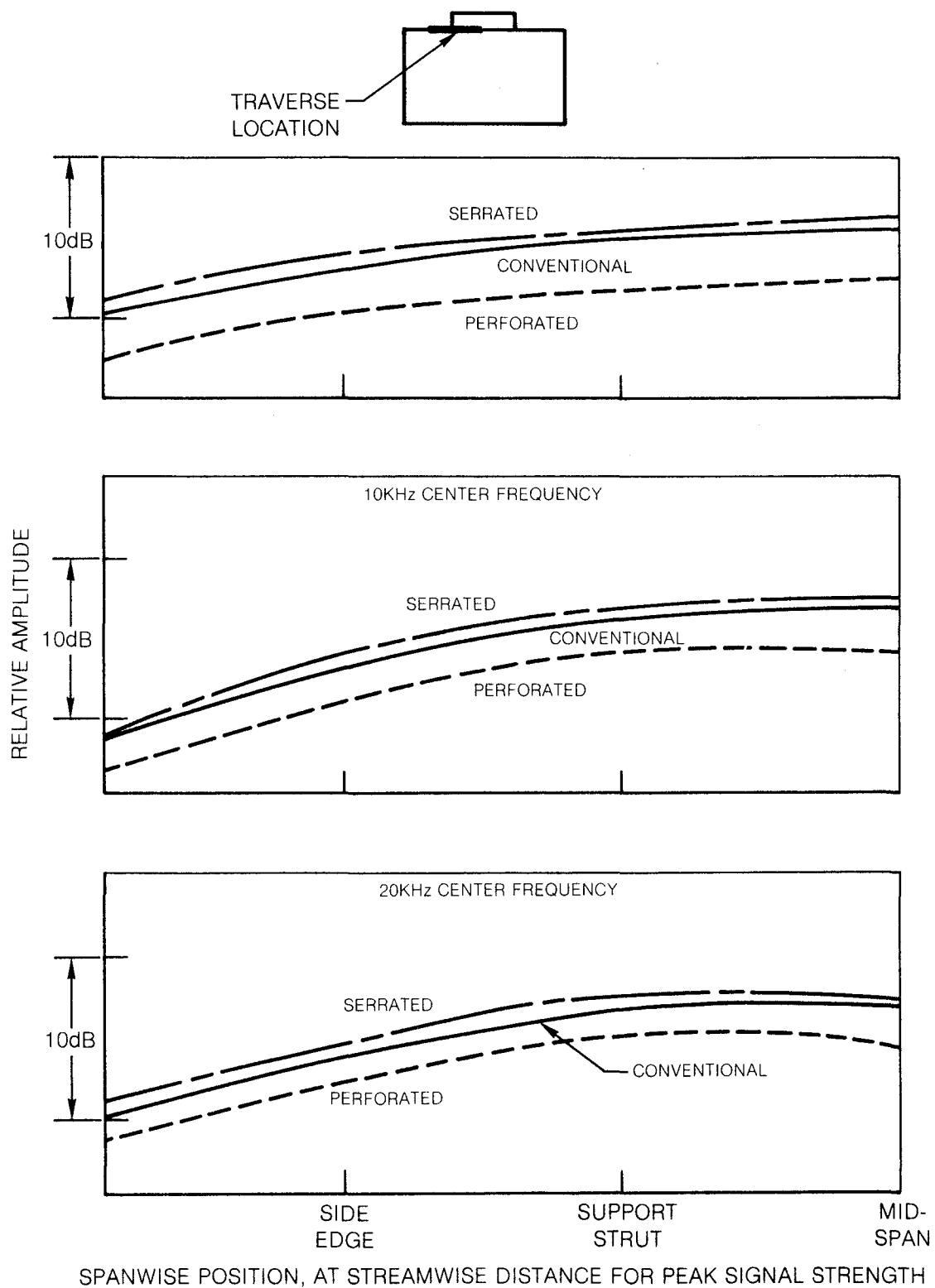
TRAVERSE LOCATION

SERRATED

CONVENTIONAL

PERFORATED

10dB

RELATIVE AMPLITUDE

10KHz CENTER FREQUENCY

SERRATED

CONVENTIONAL

PERFORATED

10dB

20KHz CENTER FREQUENCY

SERRATED

CONVENTIONAL

PERFORATED

10dB

SIDE EDGE

SUPPORT STRUT

MID-SPAN

SPANWISE POSITION, AT STREAMWISE DISTANCE FOR PEAK SIGNAL STRENGTH

Figure 38 Effect of Modified Trailing Edge Region of Leading Edge Slat on Noise Source Spanwise Distribution for 100 m/sec Velocity
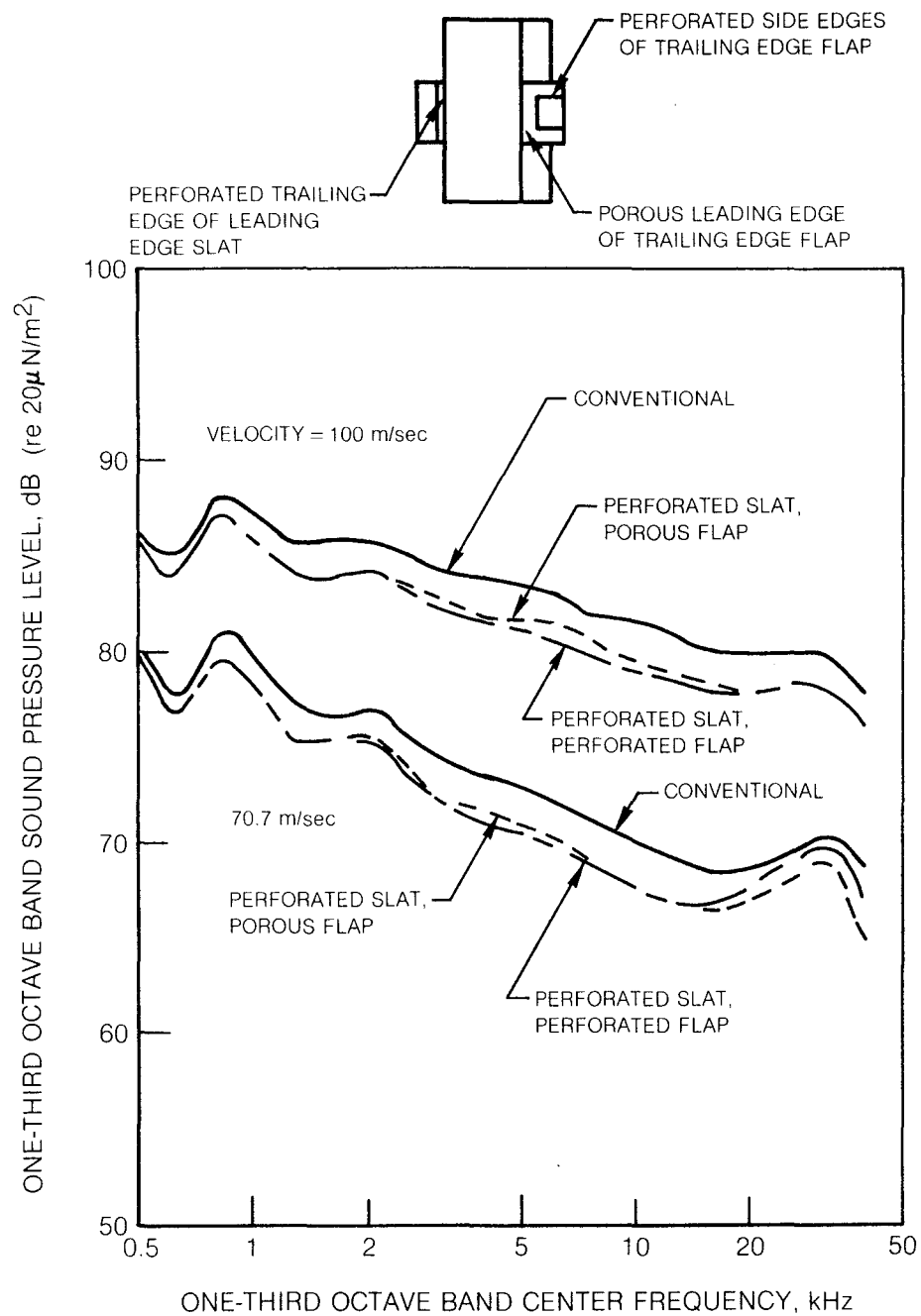
Figure 39 Effect of Modifications to Both the Leading Edge Slat and Trailing Edge Flap on Far Field Noise Radiation
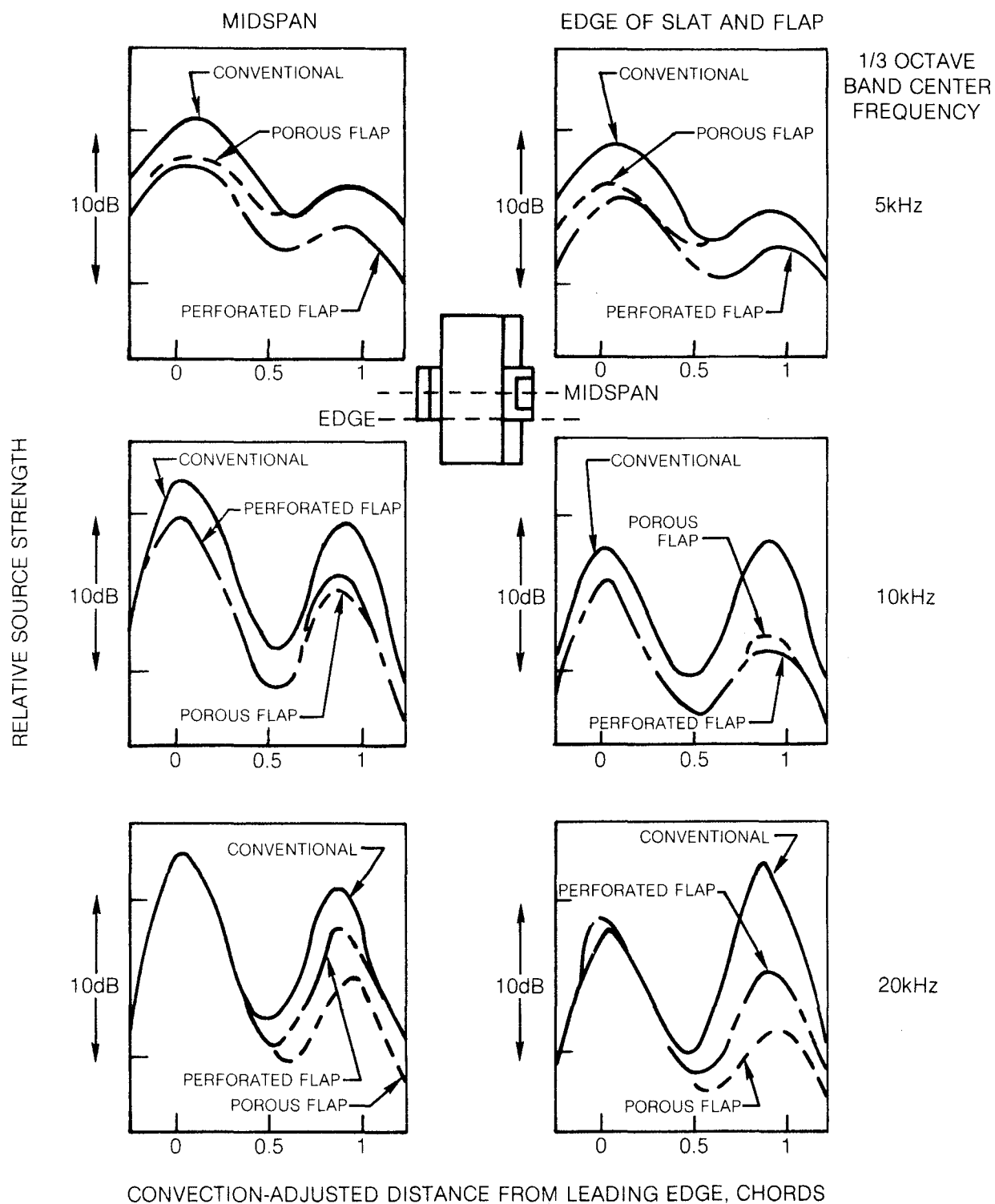
Figure 40   Effect of Perforated Leading Edge Slat and Porous or Perforated Trailing Edge Flap on Noise Source Strength Distribution at 70.7 m/sec Velocity

Figure 41 Effect of Perforated Leading Edge Slat and Porous or Perforated Trailing Edge Flap on Noise Source Strength Distribution at 100 m/sec Velocity

ONE-THIRD OCTAVE BAND
CENTER FREQUENCY = 10kHz
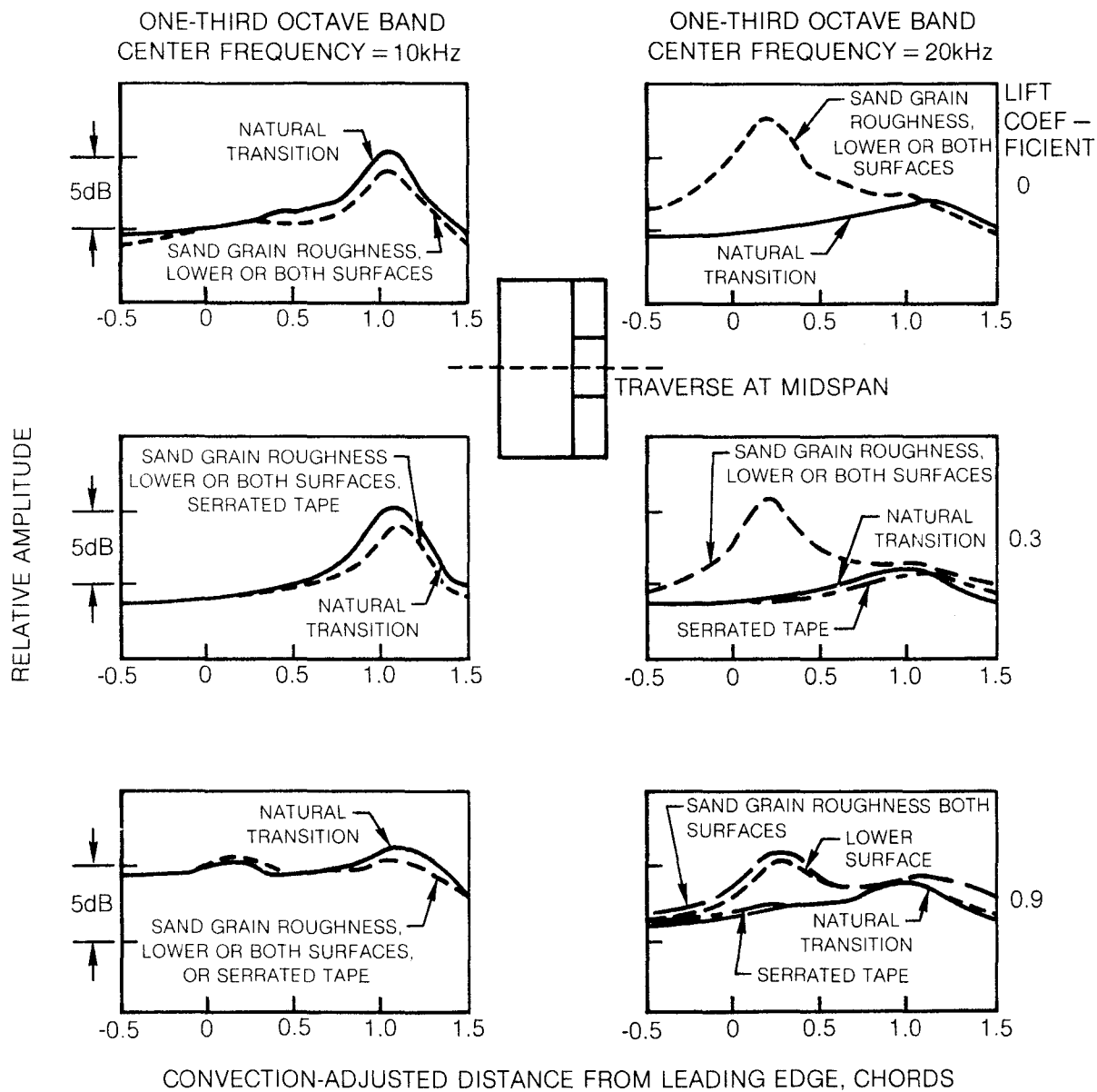
ONE-THIRD OCTAVE BAND
CENTER FREQUENCY = 20kHz

Figure 42 Effect of Fixed Boundary Layer Transition Location on Noise Signal Strength Distribution for NACA 23012 Airfoil at Lift Coefficients of 0, 0.3, and 0.9 at 100 m/sec Velocity
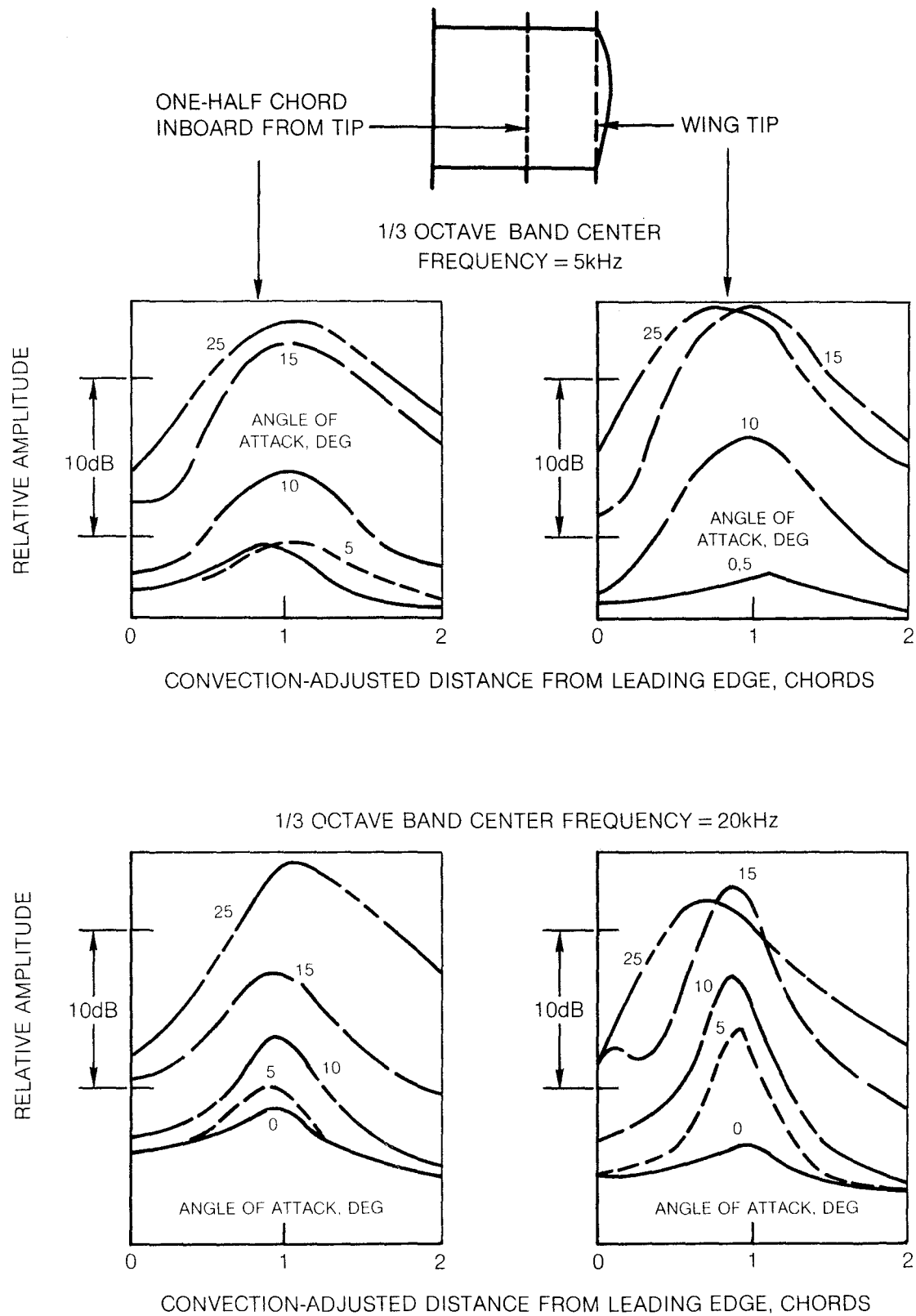
Figure 43 Effect of Wing Incidence on Chordwise Variation of Noise Source Strength for Two Spanwise Positions on Aspect Ratio 2.33 Rectangular Wing at 100 m/sec Velocity
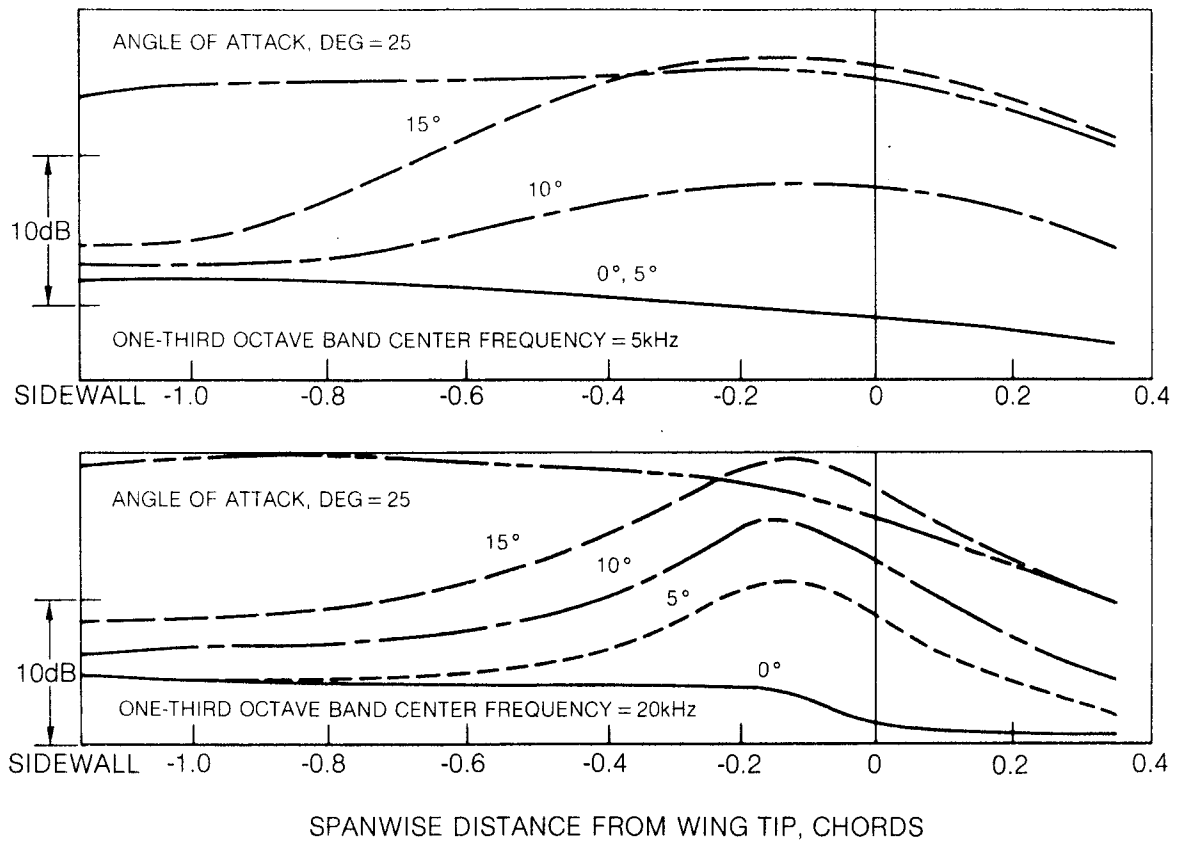
Figure 44 Effect of Wing Incidence on Spanwise Variation of Trailing Edge Noise for Aspect Ratio 2.33 Rectangular Wing at 100 m/sec Velocity

1. Report No. NASA CR- 159311	2. Government Accession No.	3. Recipient's Catalog No.
4. Title and Subtitle Airframe Noise Reduction Studies and Clean-Airframe Noise Investigation		5. Report Date May 1980
		6. Performing Organization Code
7. Author(s) Martin R. Fink and Douglas A. Bailey		8. Performing Organization Report No. R80-914626-12
		10. Work Unit No.
9. Performing Organization Name and Address United Technologies Research Center Silver Lane East Hartford, CT. 06108		11. Contract or Grant No. NAS1-15796
12. Sponsoring Agency Name and Address National Aeronautics and Space Administration Washington, D.C. 20546		13. Type of Report and Period Covered Contractor Report
		14. Sponsoring Agency Code

15. Supplementary Notes

Langley Technical Monitor: David Fratello

Final Report

16. Abstract   Acoustic wind tunnel tests were conducted of a wing model with modified leading-edge slat and trailing-edge flap. The modifications were intended to reduce the surface pressure response to convected turbulence and thereby reduce the airframe noise without changing the lift at constant incidence.   Tests were conducted at 70.7 and 100 m/sec airspeeds, with Reynolds numbers of 1.5×10^6 and 2.1×10^6. Considerable reduction of noise radiation from the side edges of a 40° deflection single-slotted flap was achieved by modification to the side-edge regions or the leading-edge region of the flap panel. Total far-field noise was reduced 2 to 3 dB over several octaves of frequency. When these panels were installed as the aft panel of a 40° deflection double-slotted flap, 2 dB noise reduction was achieved.

Use of a perforated trailing-edge region on a leading-edge slat achieved about 2 dB noise reduction.   The reductions of noise source strength obtained with a modified leading-edge slat and trailing-edge flap tested individually were retained when these components were installed together.

Artificially tripping the boundary layer of a wing model without high-lift devices at a Reynolds number of 2.1×10^6 had essentially no effect on noise radiation from the trailing edge.

Turbulence within a wing tip vortex viscous core was found to produce noise as it convects past the wing trailing edge.   Strength of this noise source increases with increasing lift coefficients below stall.

17. Key Words (Suggested by Author(s)) Noise, Noise Reduction, Airframe Noise, Wing Noise, Leading Edge Slat Noise, Trailing Edge Flap Noise.	18. Distribution Statement Unclassified-Unlimited

19. Security Classif. (of this report) Unclassified	20. Security Classif. (of this page) Unclassified	21. No. of Pages 80	22. Price*

*For sale by the National Technical Information Service, Springfield, Virginia 22151